



<https://theses.gla.ac.uk/>

Theses Digitisation:

<https://www.gla.ac.uk/myglasgow/research/enlighten/theses/digitisation/>

This is a digitised version of the original print thesis.

Copyright and moral rights for this work are retained by the author

A copy can be downloaded for personal non-commercial research or study,  
without prior permission or charge

This work cannot be reproduced or quoted extensively from without first  
obtaining permission in writing from the author

The content must not be changed in any way or sold commercially in any  
format or medium without the formal permission of the author

When referring to this work, full bibliographic details including the author,  
title, awarding institution and date of the thesis must be given

Enlighten: Theses

<https://theses.gla.ac.uk/>  
[research-enlighten@glasgow.ac.uk](mailto:research-enlighten@glasgow.ac.uk)

The Dehydration of Silicates and Studies in the  
Reactions of Salts of Strong Acids

by

NORMAN HENRY B.Sc., A.R.I.C.

A Thesis submitted to the University of Glasgow in fulfilment  
of the requirements for the Degree of Doctor of Philosophy.

September, 1965

ProQuest Number: 10647093

All rights reserved

INFORMATION TO ALL USERS

The quality of this reproduction is dependent upon the quality of the copy submitted.

In the unlikely event that the author did not send a complete manuscript and there are missing pages, these will be noted. Also, if material had to be removed, a note will indicate the deletion.



ProQuest 10647093

Published by ProQuest LLC (2017). Copyright of the Dissertation is held by the Author.

All rights reserved.

This work is protected against unauthorized copying under Title 17, United States Code  
Microform Edition © ProQuest LLC.

ProQuest LLC.  
789 East Eisenhower Parkway  
P.O. Box 1346  
Ann Arbor, MI 48106 – 1346

## ACKNOWLEDGEMENTS

The work described in this thesis was carried out in the Chemistry Department of the University of Strathclyde, Glasgow. The author wishes to thank Professor P.L. Pauson for providing the facilities for this project. Thanks are extended to my supervisors, Dr. R.A. Ross and Dr. D.W.A. Sharp, for their advice and encouragement during this work. Mr. T. Boyle is thanked for technical assistance. This work has benefited as a result of many helpful discussions with the staff and research students of the Inorganic Chemistry Department.

The award of a D.S.I.R. Research Studentship for the period 1962-65 is gratefully acknowledged.

September 1965

University of Strathclyde.

## CONTENTS

### ABSTRACT

### PART I

### The Dehydration of Silicates

Chapter 1	Introduction .. .. .	1
Chapter 2	Experimental .. .. .	1
Chapter 3	(1) The effect of sodium tungstate additions on the dehydration of silica gel.. .. .	2
	(ii) Mixed oxide systems .. .. .	5
	(iii) Effect of selected halides on the dehydration of silica xerogel..	7
Chapter 4	Discussion .. .. .	7
Appendix	Computer programmes .. .. .	9
References	.. .. .	10

### PART II

### Studies in the reactions of Salts of

### Strong Acids

Chapter 1	Introduction .. .. .	109
Chapter 2	Discussion .. .. .	116
Chapter 3	Experimental .. .. .	154
References	.. .. .	173

## ABSTRACT

### Part I

A kinetic study of the sintering of silica xerogel was made by following the dehydration of gel spheroids (2000-841  $\mu$  and 841-420  $\mu$ ) using a thermogravimetric balance. The scope of the work was extended to include the effects of small additions (usually 5 g. ion %) of mineralisers on the reaction rate. The additives used were  $\text{Na}_2\text{WO}_4$ ,  $\text{NaCl}$ ,  $\text{LiCl}$ ,  $\text{LiBr}$ ,  $\text{Li}_2\text{SO}_4$ ,  $\text{BaCl}_2$ ,  $\text{CaCl}_2$ ,  $\text{Al}_2\text{O}_3$ ,  $\text{NiO}$ ,  $\text{CdO}$ ,  $\text{ZnO}$ ,  $\text{Cr}_2\text{O}_3$  and  $\text{CuO}$ .

In most cases it was shown that the additives increase the rate of dehydration, this effect being purely catalytic below the Tamman temperature. However there was a marked tendency for solid-solid interaction to occur above this temperature. One of the important surface characteristics measured was surface area by low temperature gas adsorption ( $\text{N}_2$  at 90°K). This showed a feature characteristic of sintering viz. fall in surface area with increase in temperature. The method of Cranston and Inkley was used to calculate pore size distributions of the gel systems. Contrary to the normal method of calculating pore size distributions from the desorption branch of a B.E.T. isotherm, this method employs the adsorption branch as well

as leading to an independent determination of the surface area. The surface areas calculated in this fashion were within 2% of that calculated using the B.E.T. equation. An apparatus was designed to give a measure of the bulk or mercury density of the xerogel spheroids. The values derived showed an increase in density with temperature increase, which is a characteristic property of sintering reactions.

X-ray powder photographs were taken in an attempt to identify new phases formed by solid-solid interaction between the gel and the mineralizers.

## Part II

The object of the work was to make a general study of the preparation and physical properties of selected transition metal complexes in non-aqueous solvents. The metals examined were Cu(II), Co(II), Ni(II), and Zn(II) as either the bis-perchlorate, chloro-perchlorate, bis-tetrafluoroborate, or the chloro-tetrafluoroborate in ether solution. The method of preparation of the solution consisted of shaking the metal halide with silver perchlorate (tetrafluoroborate) in ether.

The ligands which were added to the above solutions were triphenyl-phosphine, triphenyl-arsine, triphenyl-stibine,

triphenyl-bismuthine, trimethyl phosphite, triethyl phosphite, triphenyl phosphite, triethyl amine and 4-methyl-2,6,7-trioxo-1-phosphabicyclo[2.2.2.] octane. In certain cases reaction took place between the ligand and the metal salt, but in the majority, normal complexes of the type  $M^{II}(L)_{1,2,3, \text{ or } 4} (ClO_4)_2$  or  $M^{II}(L)_{1,2,3 \text{ or } 4} ClClO_4$ , and the corresponding fluoroborates were formed.

The physical properties of the resulting complexes were then examined using infrared, ultraviolet (solution or reflectance spectra), far infrared and by the analysis of the compound. Using these data, possible structures are postulated.

PART I

## CHAPTER I

### Introduction

Very little work has been done on the thermal dehydration of silica gels, and no studies have been reported in which the effects of solid additives, or impurities, on the course of dehydration have been examined. No previous studies have been made of the chemistry of the thermal dehydration other than those which may be inferred from publications primarily concerned with sintering processes. For example, Goodman and Gregg<sup>1</sup> have shown that sintering of silica gel is consistent with dehydration and consequent loss of surface area and pore volume. Therefore, in the present studies, attention has to be given to the linked processes of chemical change due to dehydration-catalytic and non-catalytic - and physical change brought about by agglomeration or sintering.

Sintering is a broad term but may be considered as the adhesion of particles of a solid to form aggregates. It occurs most readily in "high temperature" regions and for metals and metallic oxides, this indicates a region from 0.4 to 0.5  $T_m$  where  $T_m$  = temperature of melting in °K. It involves a reduction of free energy

content along with a reduction in the specific surface of the solid.

The mechanism of sintering is extremely complex and may be influenced by various factors.<sup>2,3</sup> Huttig et al<sup>4,5</sup> were among the first to investigate the process systematically, and deduced a mechanism involving adhesion, surface diffusion and lattice diffusion. High temperature sintering has been investigated by a number of workers<sup>6,7,8,9,10,11</sup> because of the wide range of industrial importance regarding semi-conductors, ferrites and powder metallurgy, attached to the bulk movement of a solid, whether by surface diffusion, evaporation-condensation, volume diffusion, viscous or plastic flow. More recent investigators<sup>12,13</sup> have subdivided sintering processes into three stages, viz. (a) initial, (b) intermediate and (c) final. In the initial stage, neck growth commences between particles. In the intermediate stage there is a continuous pore phase and the pores are intersected by grain boundaries. When the pores are sealed the final stage sets in.

In contrast, however, to explanations of the sintering behaviour of metals<sup>10,11</sup> - which can be related purely to changes of surface free energy -

chemical interaction has to be considered in the case of silica xerogel and related hydrous oxide systems.

### Scope of present investigation

In the synthesis of minerals prepared by heat treatment or sintering reactions,<sup>14,15,16</sup> the rate of reaction may become large well below the fusion point of the reactants. Such processes may be completed some hundreds of degrees below the eutectic temperatures of the systems involved. However, no quantitative data is available as to the mechanism of this solid-state catalysis.

At the same time, silica and silica gels are often used in mixtures or as metal "supports" in many heterogeneous catalytic reactions. Hence, it is valuable to observe whether the properties of silica and silica gels may be influenced by the inclusion of catalytic agents such as oxide and halide additives.

Silica gel represents a relatively simple chemical system and its properties in the presence of such additives at temperatures above 240° are not known. Thus, information on (a) the energetics of dehydration, (b) chemical and (c) physical properties would be of considerable value in understanding the behaviour of

simple silica systems as these are applied in processes involving (i) hot gas-drying (ii) cracking catalysis and (iii) adiabatic dehumidification.

### Mineralizers

The use of crystallising agents or mineralizers ~~has~~ <sup>has</sup> been employed in order to accelerate crystal growth. The modes of action of such processes are diverse, and can best be understood by reference to specific examples which have been reviewed by Taylor<sup>15</sup> and Cohn<sup>16</sup>. In these reviews it has been shown that the sintering of amorphous alumina to give corundum is greatly accelerated by calcium fluoride. It is suggested that aluminium fluoride is formed



and that crystalline  $\text{Al}_2\text{O}_3$  then results from the reverse reaction, the mineralizer acting by forming an intermediate compound.

Barrer<sup>17</sup> has shown that a hydro-thermal synthesis of a zeolitic species has been observed in which alkaline-earth halides, viz. barium chloride or barium fluoride were specific mineralizers. The salts acted as space fillers to permit and stabilise the growth of

an open aluminosilicate framework. The barium chloride or barium fluoride may subsequently be extracted from solid solution throughout the interstices of the framework to leave the salt-free zeolite.

Not all mineralizers act by forming such intermediate compounds. Pyrolytic or pneumatolytic crystallisations are affected by water in two main ways<sup>19</sup> viz. (i) by lowering the viscosity of a magma with which it is associated and (ii) by lowering the fusion temperature of crystalline species in equilibrium with the magma. It might be anticipated that other volatile compounds such as hydrogen fluoride, hydrogen chloride, sulphur dioxide, hydrogen sulphide, ammonia or carbon dioxide would tend to give similar results to water.

The actual structure of silica gel has received much discussion. Vail<sup>19</sup> has pointed out that in silica gel the particles grow in size, become more anisotropic, and coagulate by aggregation; i.e. in the same volume of gel the individual particles may decrease in number and increase in size. Signer and Egli<sup>20</sup> concluded that the framework of silica gel was not made up of simple chains of Si—O—Si linkages. It is very likely that the network gel structure is composed

initially of polysilicic acid units containing an average of 3 to 5  $\text{SiO}_2$  units each, since as shown by Iler<sup>21</sup>, the silicic acid liberated from this silicate by acid is already polymerised at least to this degree. On the basis of the thermal ageing of silica gels, Shapiro and Kolthoff<sup>22</sup> confirmed that the structure of silica gel could best be visualised as being made up of discrete particles.

From the above considerations, along with the existing knowledge of gel formation, it is indicated that silica gels consist of three-dimensional networks of polymerised silicic acid, junction points of these silicic acid macromolecules consist of chains of micelles arranging themselves in lattice order.

On the basis of the concept that silica gel is composed of discrete particles, Plank and Drake<sup>23</sup> point out that, in view of the mechanical strength of dry gels, the particles must be firmly bonded together. These authors visualise that, at least initially, the "micelles" are bonded together in chains, probably by hydrogen bonding. However, in view of the fact that the surfaces of particles of colloidal silica is composed of  $\text{Si}(\text{OH})_x$  groups, it is

likely that, when these particles come together, condensation between silanol groups occurs and siloxane bonds are formed between the particles, as postulated by Carman.<sup>24</sup>

If the process of oxygen sharing is extended, so that each sheet is linked to the neighbouring sheets above and below, a three-dimensional network is obtained in which every oxygen atom is common to two tetrahedral  $\text{SiO}_4$  groups. The whole network then has the composition  $\text{SiO}_2$ , and represents one giant molecule of silica. The three principal crystalline forms of silica - cristobalite, tridymite and quartz - are based on this kind of structure.<sup>25</sup> Cristobalite and tridymite are built up in exactly the manner described, and differ in the way the cross-linking is achieved. In quartz, the regular arrangement is somewhat distorted, so that spirals of  $\text{O}-\text{Si}-\text{O}-\text{Si}-\text{O}-$  chains lie around trigonal screw axes of symmetry.

#### Outline of Experimental Approach

The effects of heat treatment<sup>22,26,27,28,29</sup> of silica gel has been investigated by a number of workers but these studies have been restricted almost entirely

to techniques based on physical adsorption of gases such as nitrogen.

Since it has been shown that foreign ions affect the sintering of active solids,<sup>30,31,32</sup> great care was taken to ensure that the silica gel was free from such impurities. Previous work on the thermal dehydration of silica gel has been carried out in these laboratories.<sup>33</sup> However, it was decided that an essential feature of the kinetic work was to have regular geometry of particles so that purely chemical effects might be separated from physical ones.

Besides studying the kinetics of dehydration by means of a thermal balance, the surface properties and pore structure of the gel were investigated using a number of techniques, viz. (i) mercury or bulk density to obtain pore volume data, (ii) surface area measurements from B.E.T. isotherms and (iii) X-ray powder photography.

The thermal balance was employed for several reasons: viz.,

- (1) it showed the quantity of volatile matter lost and the rate pattern of the loss,

- (2) it was used to follow sintering at steady temperatures,
- (3) it gave an easy and accessible method of following changes in the rate of sintering at different temperatures, with or without mineralizers.

Lump or mercury density was measured since the lump volume of a solid consists of the true volume of the solid phase together with the pore volume. This was of prime importance since bulk movement of a solid is consistent with a drastic reduction in pore volume, and immersion in mercury gives an indication of the temperature at which bulk movement commenced.

Low temperature gas adsorption has long been used for the evaluation of structural data, especially with respect to surface areas and pore structures.

Structural effects caused by heat treatment were examined by taking X-ray powder photographs and by photomicrographs. The X-ray technique was useful for identifying the formation of new solid phases, while photomicrographs supplied confirmatory evidence that the first stage of sintering had been reached. This point is defined by Coble.<sup>12</sup> (See page 2).

Details of the application of the above technique are given in the experimental section.

By an analysis of the results obtained from the above methods, it was hoped to elucidate the behaviour of silica gel on sintering and also to relate the importance of its surface characteristics in its applications to heterogeneous catalysis.

## CHAPTER II

### Experimental

A brief review of the general experimental approach has been given in Chapter I. In the present chapter the practical details involved, and the mode of interpretation of the results will be considered more fully.

#### (1) Preparation of silica xerogel

Microspheroids of silica gel were prepared by a method similar to that of Marisac.<sup>14</sup> This consisted of passing a fine jet of a mixture of sodium silicate (s.g. 1.10) and sulphuric acid (s.g. 1.10 - 1.15), at approximately the gelling pH (4.5) down a six foot column of oil (s.g. 0.75 - 1.00) at 60-70°.

The hydrogel formed into microspheroids in falling down the oil phase and then set in an underlying water layer containing a surface active agent.

Experiments were carried out with various types of cationic, anionic and non-ionic detergents to find the best surface active additive. Finally, the one chosen was a saturated solution of sodium dioctyl

sulphosuccinate dissolved in methylated spirits, as a 2% v/v solution in the water phase. On removal of the spheroids from the column - by downward flushing - the water was drained off and the hydrogel particles were allowed to synerise for 24 hours. The sulphate in the hydrogel was then removed by Soxhlet extraction with water for 20 hours. This was followed by extraction of any surface oil and sodium dioctyl sulphosuccinate with benzene for 16-24 hours. Finally, the spheroids were washed in acetone and dried slowly at 50°, before being separated into the required size ranges by sieving. The Soxhlet extraction times taken were shown to have removed the oil and detergent by the absence of " visible charring of the surface on heating in a crucible to around 400°C " .

## (2) Thermal balance

The rate of dehydration was examined on a T.R. model Stanton thermobalance equipped with a nichrome furnace; a chart speed of 12"/hour was used.

As in previous experiments,<sup>33</sup> the silica gel/additive charge was varied by a small amount in the

region of 0.9 - 1.1 g. Within these limits no real mass effect was observed on the dehydration rate results which were converted to a mg./g. basis as shown in Table 2.1.

Table 2.1. Loss in weight of 2000 - 841  $\mu$  spheroids of silica xerogel at 500°.

	<u>Wt. of sample A at 240° = 1.050 g.</u>		<u>Wt. of sample B at 240° = 0.905 g.</u>	
<u>Time (secs)</u>	<u>Wt. lost (mg)</u>	<u>Wt. lost (mg/g)</u>	<u>Wt. lost (mg/g)</u>	<u>Wt. lost (mg/g)</u>
75	5.77	5.50	5.07	5.60
100	7.24	6.90	6.20	6.85
150	11.97	11.40	10.36	11.45
200	16.80	16.00	14.48	16.00

In order to study the dehydration, the temperature was raised to 240° and held there until all physically adsorbed water from the gel spheroids had been driven off.<sup>54</sup> The sample was removed and kept over activated molecular sieves in a desiccator. The furnace was raised to the required temperature and held constant before quickly replacing the sample in the furnace. The weight loss was then recorded until a steady value was reached (i.e. less than 0.5 mg.<sub>CHANGE</sub> in 10 minutes).

In general, the time taken to reach the steady value was no more than 30 minutes.

(3) Low Temperature Gas Adsorption

(a) The adsorption of nitrogen at 90°K

At present, there is no method available by which the absolute value of surface area can be determined, though gas adsorption techniques give the most reproducible results for relative surface areas.

When a gas is admitted to an outgassed solid surface there is a charge attraction at the gas/solid interface which causes the gas to be retained, i.e. adsorbed. This process is always accompanied by a decrease in energy. By plotting the volume of gas adsorbed, at, or near its boiling point, for a series of relative pressures we obtain an adsorption isotherm. The first theoretical derivation of an equation to describe this phenomena was made by Langmuir<sup>35</sup> using kinetic theory. However, this equation is restricted in its application because of the assumptions made in its derivation. At present, the Brunauer, Emmett and Teller<sup>36</sup> (B.E.T.) theory of multimolecular adsorption,

though over-simplifying the problem, is generally agreed as the best method of obtaining surface areas.<sup>37,38,39,40</sup>

The B.E.T. equation is usually expressed in the form

$$\frac{p}{V(p_0-p)} = \frac{1}{V_m C} + \frac{(C-1)p}{V_m C p_0} \dots\dots (2.1)$$

where V = volume adsorbed at equilibrium pressure p

p<sub>0</sub> = saturated vapour pressure of adsorbate

V<sub>m</sub> = monolayer volume

C = constant depending on the heats of adsorption and liquefaction of the gas.

A plot of  $\frac{p}{V(p_0-p)}$  against  $\frac{p}{p_0}$  should give a straight line of slope  $\frac{C-1}{V_m C}$  and intercept  $\frac{1}{V_m C}$ , from whence V<sub>m</sub> and c may be obtained. This equation is found to hold experimentally in the range  $0.05 < \frac{p}{p_0} < 0.35$ . The surface area S is found from V<sub>m</sub> by means of the equation

$$S = V_m N A_0 \dots\dots\dots (2.2)$$

where N = Avogadro's number

A<sub>0</sub> = area occupied per molecule in the adsorbed phase.

Livingstone<sup>41</sup> proposes that A<sub>0</sub> may best be evaluated from the relationship

$$A_0 = F \left[ \frac{M}{N} \int_L \right]^{2/3} \dots \dots \dots (2.3)$$

where M = molecular weight

$\int_L$  = liquid density of the adsorbate

and F varies from 1.000-1.091, depending on the type of molecular packing.

Livingstone<sup>41</sup> suggests further that for nitrogen  $A_0 = 16.3 \text{ \AA}^2$  at 90.5°K and this value has been adopted in the present study.

In addition to surface areas, low temperature gas adsorption isotherms can provide data on pore size distributions. For this type of information the usual approach has been to apply the Kelvin equation (Equation 2.4) with various refinements to the desorption branch of the isotherm.<sup>26, 42, 43, 44, 45</sup>

$$\ln p/p_0 = - 2 \frac{V_m \gamma \cos \alpha}{r_k RT} \dots \dots (2.4)$$

where p = equilibrium pressure

$p_0$  = saturated vapour pressure

$\gamma$  = surface tension

$V_m$  = molar volume of the adsorbate

$\alpha$  = angle of contact of the adsorbate in liquid form with the adsorbent

R = gas constant

$T$  = absolute temperature

$r_k$  = value of a single pore radius.

However, Cranston and Inkley<sup>46</sup> have proposed an improved method of deriving pore-size distributions from the adsorption branch of the isotherm.

The method is a development of that by Barrett et al<sup>45</sup> but is more exact and provides an estimate of the total specific surface, which is almost independent of the B.E.T. value, and also leads to a comparison of pore volumes calculated in two ways. In terms of pore diameters the working equation becomes

$$V_{12} = R_{12} (v_{12} - k_{12} \sum_{d_2 + \frac{1}{2} \Delta d}^{d_{\max}} \frac{d - 2t_{12}}{d^2} v_d \Delta d) \dots (2.5)$$

where  $\Delta d$  = an increment of pore diameter

$v_d \Delta d$  = volume of pores having diameters between  $(d - \frac{1}{2} \Delta d)$  and  $(d + \frac{1}{2} \Delta d)$

$d_{\max}$  = diameter of largest pore

$V_{12}$  = volume of pores having radii between  $r_1$  and  $r_2$

Tables of values for  $R_{12}$ ,  $k_{12}$  and the factor  $(d-2t)/d^2$  are provided in the appendix.

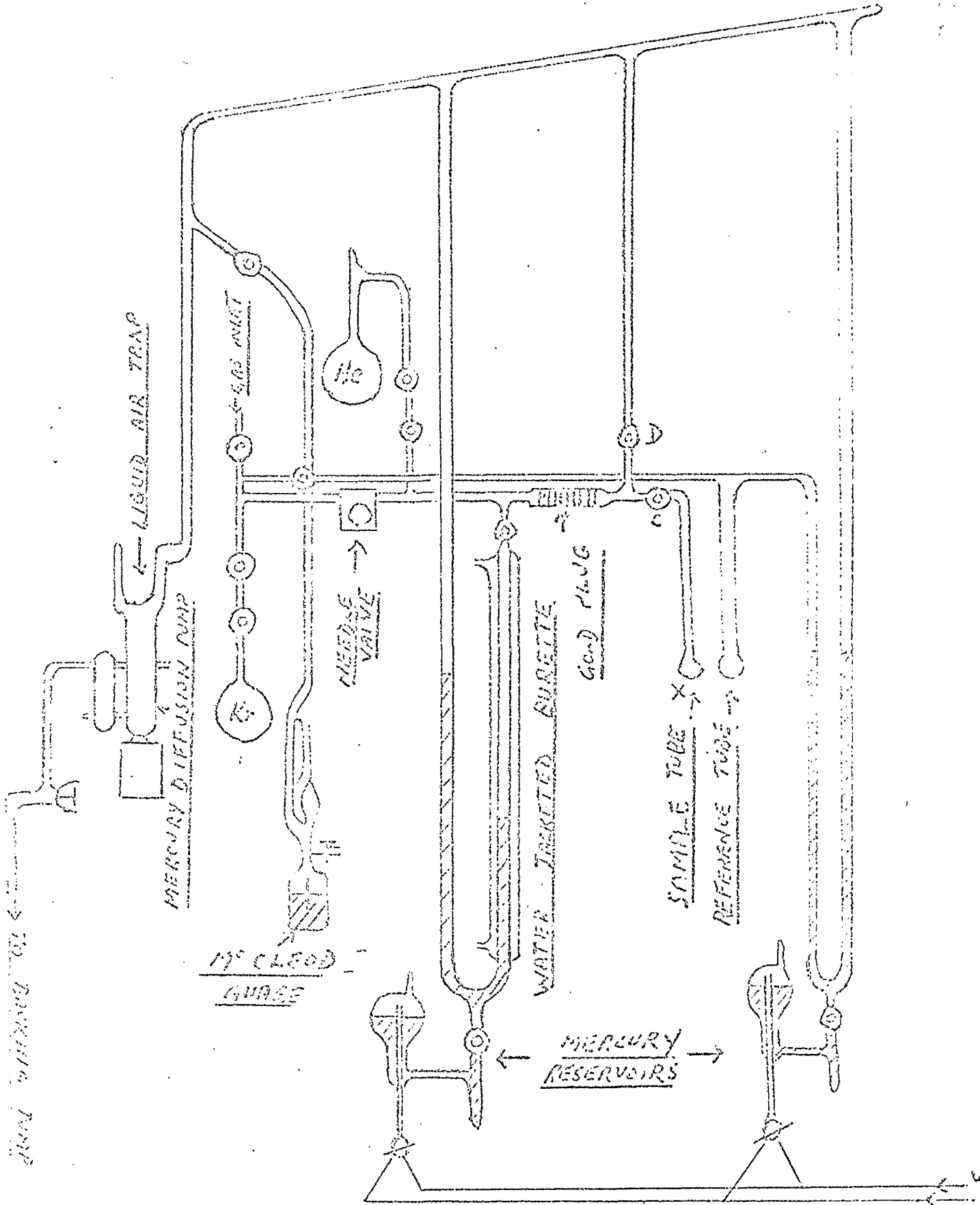


FIG. (1.1) GAS ADSORPTION APPARATUS

The values of pore statistics derived from the isotherms were computed using the English Electric KDF9 computer at Glasgow University.

(b) The measurement of adsorption isotherms

A constant volume apparatus similar to that of Joyner<sup>47</sup> was used for the measurement of the adsorption of nitrogen at low temperatures (Fig.2.1). Essential features included a small dead space, and a plug of gold foil to prevent mercury vapour contacting the adsorbate.

The sample was weighed into a bulb, X, and out-gassed for one hour at 200° and to a pressure of 10<sup>-6</sup> mm of mercury. Gas was then admitted slowly to the adsorption section via the fine control needle valve. Before any calculations can be made the dead space in the system was measured. This extended from the zero mark on the burette through all the interconnecting tubes between the needle valve and tap C, with tap D closed. This space plus the volume of the flask (i.e. with tap C open) was then calculated from the Ideal Gas Law, for room and liquid nitrogen temperatures. At the same time the average

temperature of the sample flask when immersed in liquid nitrogen was estimated. Application of the gas laws showed that the amount of gas adsorbed,  $V$  moles, was given by the equation

$$V = \frac{\sum pd Vd}{RT_r} - \frac{p}{R} \left[ \frac{V_a}{T_r} - \frac{V_c}{T_c} \right] \dots\dots\dots (2.6)$$

where  $\sum pd$  = sum of successive doser pressures (mm Hg)

$Vd$  = volume of doser (cc)

$p$  = equilibrium pressure (mm Hg)

$T_r$  = room temperature ( $^{\circ}K$ )

$V_a$  = dead space above liquid nitrogen (cc)

$T_c$  = temperature of cryostat ( $^{\circ}K$ )

$R$  = gas constant (cc mm  $^{\circ}K^{-1}$ )

A full description of the method employed is best understood by referring to table (2.2) which was employed for all measurements taken

Table (2.2). Calculation of Surface Areas

<u>Column</u>	<u>Heading</u>	<u>Description</u>
1	Pressure	The pressures measured at different points during the isotherm.
2	Volume	The volumes measured on the burette at the same points during the isotherm.

Table (2.2)(contd.). Calculation of Surface Areas.

<u>Column</u>	<u>Heading</u>	<u>Description</u>
3	Volume + dead space (Tr)	The volumes in column 2 + dead space with sample at liquid nitrogen temperature.
4	Volume + dead space (N.T.P.)	The volumes in column 3 corrected to N.T.P.
5	Pressure correction	The pressures in column 1 corrected for deviations from the ideal gas laws.
6	Flask volume	The flask volume at liquid nitrogen temperature corrected to N.T.P. from the average temperature of the flask at the various pressures in column 5.
7	Gas remaining	The volumes in columns 4 and 6.
8	Total admitted	The volume (top line in column 4) less the volume of the bottom line of the previous point. These volumes are added for adsorption curves and subtracted for desorption curves.
9	Volume adsorbed	Volume in column 8 (bottom line) less the volume in column 7.
10	$v/m$	The volumes in column 8 divided by the weight of the sample.
11	$p/p_0$	Pressures in column 1 divided by the saturation pressure.

#### (4) Measurement of Lump Density

Mercury has a high surface tension and a large contact angle and is thus unable to enter pores of radius below ca.  $50,000 \text{ \AA}$  when a pressure of one atmosphere exists across the meniscus.<sup>6,7</sup> The reciprocal of the mercury or lump density, viz. the lump volume includes the volume occupied by the crystal lattice, all the micropores and most of the macropores. It is customary to distinguish as micropores those pores which are so small as to become filled at  $p/p_0$  around 0.6; such pores usually have a diameter smaller than about  $50 \text{ \AA}$ .

The apparatus used for the lump density (fig. 2.2) was a modification of that designed by Jepsen.<sup>4,8</sup> The volume of the sample container was calibrated by finding the weight of mercury required to fill it. A known weight of silica gel was weighed into the sample holder and the system was outgassed for an hour at  $200^\circ$ . Freshly distilled mercury was then introduced until the level was above the etch mark on the capillary. After cooling, excess mercury was removed till the level was at the etch mark. The lump density  $\int L$  was

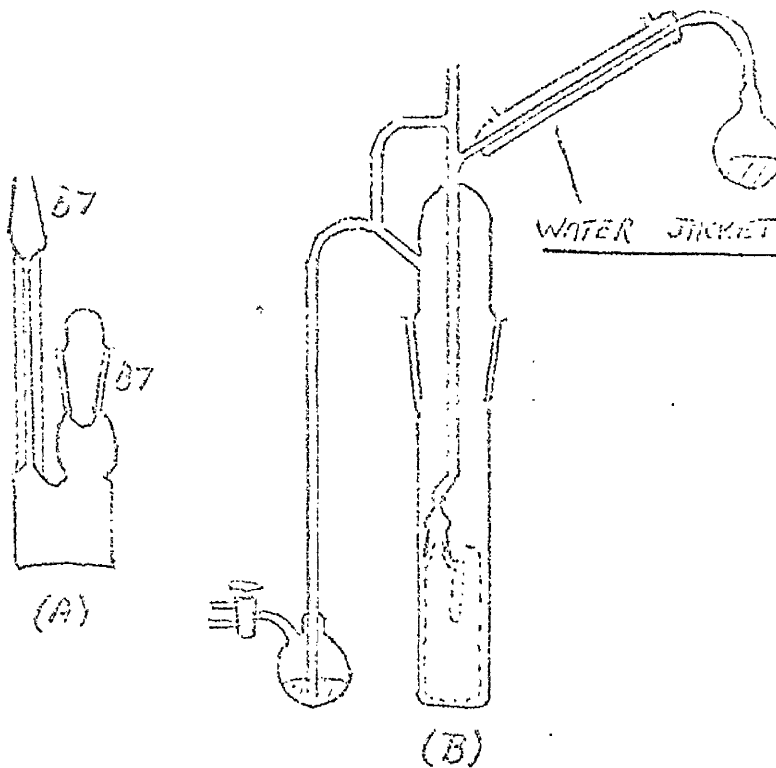


FIG. (2.2) BULK DENSITY APPARATUS

- A) SAMPLE HOLDER
- B) COMPLETE APPARATUS

calculated from the equation

$$\int L = \frac{w_1}{V - \frac{w_2}{d_H}} \dots\dots\dots (2.7)$$

where  $w_1$  = weight of gel

$w_2$  = weight of mercury in sample holder

$V$  = volume of sample holder

$d_H$  = density of mercury at room temperature

Duplicate determinations were within an experimental error of 1-2%.

#### (5) X-Ray Analysis

X-ray powder photographs were taken on a Phillips PW 1009 generator using Cu-K $\alpha$  radiation. The d-values of any new phases formed by the interaction of silica gel and additive were calculated using the Ferranti Sirius computer at the University of Strathclyde.

## CHAPTER III

### Section I

#### The Effect of Sodium Tungstate Additions

Before examining the effects of additives on the dehydration rate of silica gel, the first experiments were designed to study and elucidate the kinetics for the sintering of silica gel alone. For effective comparison, the surface properties measured in the latter case are included in that section dealing with the physical properties of gels as affected by the presence of additives.

#### Starting materials

Silica gel - the preparation of microspheroids was described in detail previously (Chapter II).

Irregular gel particles were prepared by allowing a mixture of sodium silicate and sulphuric acid to gel at pH = 4.5 in a large container. The gel was then broken up, and sieved to give particles of the same dimension range as the spheroids.

Analar sodium tungstate ( $\text{Na}_2\text{WO}_4 \cdot 2\text{H}_2\text{O}$ ). The sodium tungstate hydrate was heated to 120° on the thermal balance before each run, to drive off the water of crystallisation.

Three different methods of studying the effect of sodium tungstate (i.e.  $\text{Na}_2\text{WO}_4$ ) on the dehydration of silica xerogel were attempted. In all cases the amount of sodium tungstate was calculated as gram ion % of tungstate ion on the weight of  $\text{SiO}_2$  obtained from 1 g. silica gel activated at  $260^\circ$  and subsequently calcined at  $1500^\circ$  for several hours. This is shown in the following typical calculation.

Typical Calculation

Wt. of gel activated at  $240^\circ$  = 0.9868 g.

Wt. lost at  $1500^\circ$  = .0394 g.

∴ Volatile water content =  $\frac{.0394}{.9868} \times 100 = \underline{4\%}$

Since the volatile matter content = 4%

1 g. gel activated at  $240^\circ$  contains 0.96 g.  $\text{SiO}_2$

∴ 0.96 g.  $\text{SiO}_2 \equiv \frac{0.96 \times 28.06}{60.06}$  g. Silicon

$\equiv$  0.445 g. Silicon and

∴ 0.515 g. oxygen.

0.445 g. Si  $\equiv \frac{0.445}{28.06} \equiv$  0.0158 g. atoms Silicon

Similarly we have 0.0322 g. atoms oxygen.

Now 1 g.  $\text{Na}_2\text{WO}_4 \equiv$  0.0068 g. atoms  $\text{Na}^+$  and  
0.0034 g. ions  $\text{WO}_4^{2-}$

∴ g ion % for 1 g.  $\text{Na}_2\text{WO}_4 = \frac{.0034}{.048 + .0068 + .0034} \times 100$   
 $= \underline{5.84\%}$

This calculation was repeated for various weights of sodium tungstate and a plot of g. ion% tungstate ion against weight of sodium tungstate was drawn.

Thus depending on the starting weight of activated gel we can readily find the weight of sodium tungstate required for a definite g. ion % of tungstate ion.

Mixing in the principal series of experiments was by hand-stirring and shaking the gel and tungstate for about 5 minutes. (The amount of mixing was found to be of prime importance. At 500°C with efficient mixing, the rate of dehydration was 30.2 mg./g. after 200 secs., while at the same temperature, the rate of dehydration with poor mixing was 21.5 mg./g. and 25.7 mg./g. in two separate cases. It was concluded that continuous shaking and stirring for 5 minutes by hand, gave a degree of mixing which could not be improved on, as judged by the consistency achieved in the thermo-dehydration results.

In the second series of experiments, the xerogel spheroids were bedded carefully on a layer of sodium tungstate, and in the third, physical contact between gel and tungstate particles was excluded, so that the

effect of sodium tungstate vapour could be examined. This was carried out by suspending a fine mesh platinum container of sodium tungstate in the furnace, just below the level of the crucible containing the xerogel spheroids.

#### Thermal dehydration of silica xerogel

The pattern of weight losses for silica xerogel was examined from 400-800° with spheroidal and irregular particles of size ranges 2000 - 841 $\mu$  and 841 - 420 $\mu$ . Figs. (3.1) and (3.2) show the variation of weight loss with temperature for spheroidal and irregular xerogel of size range 841-420 $\mu$ . As shown, there is a tendency for the irregular form to achieve a higher degree of dehydration, at each temperature, than that of the spheroidal form of the same size range. Thus the steady weight loss for microspheroids at 750° was 40.33 mg./g. at a temperature 50° lower. This feature is also illustrated in table (3.1), which shows the weight loss achieved at three different temperatures with the large size range. The results show an increasing degree of dehydration with temperature for both particle shapes.

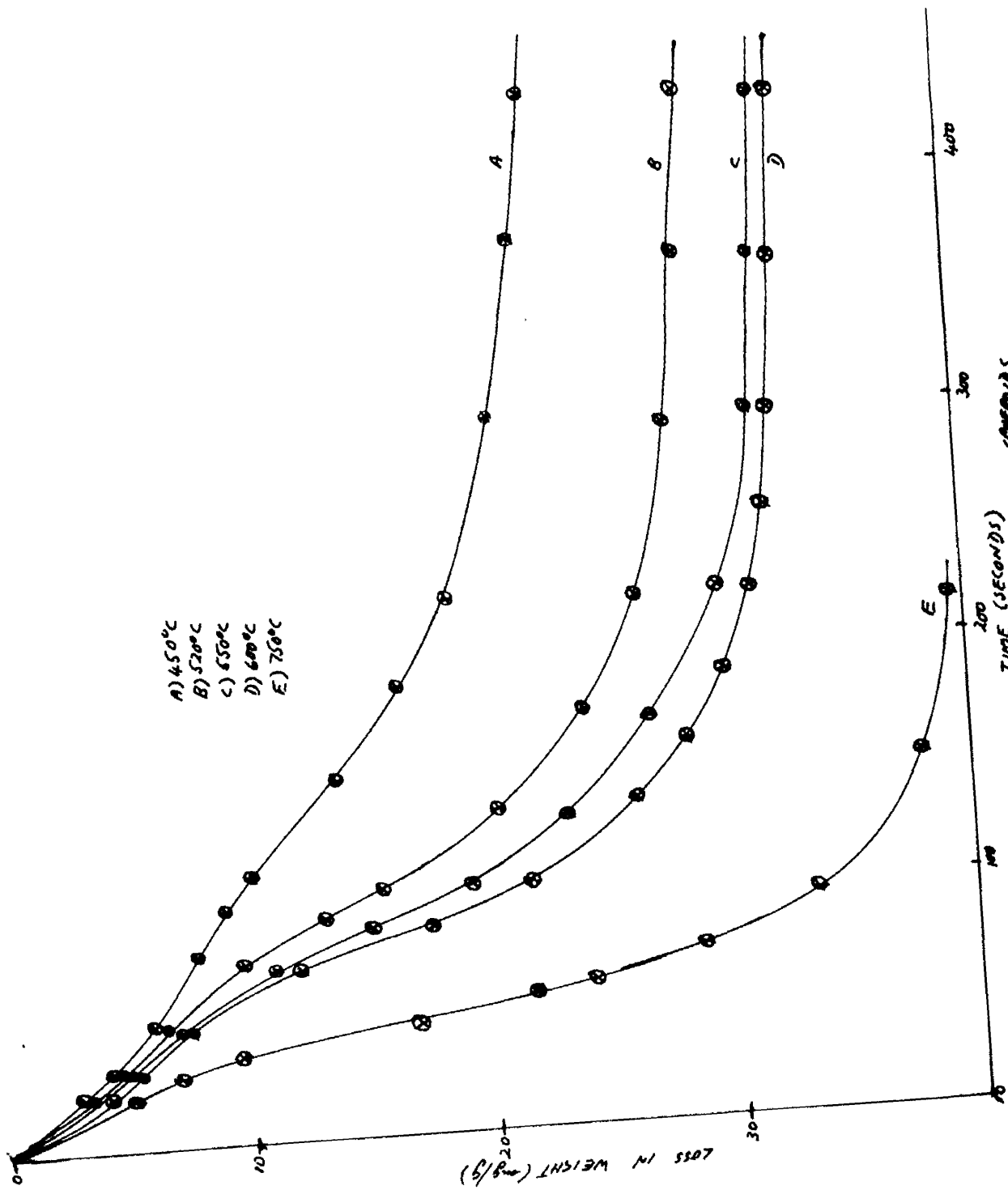


FIG. (3-1) DEHYDRATION CURVES FOR 8μ-420μ SPERMID.

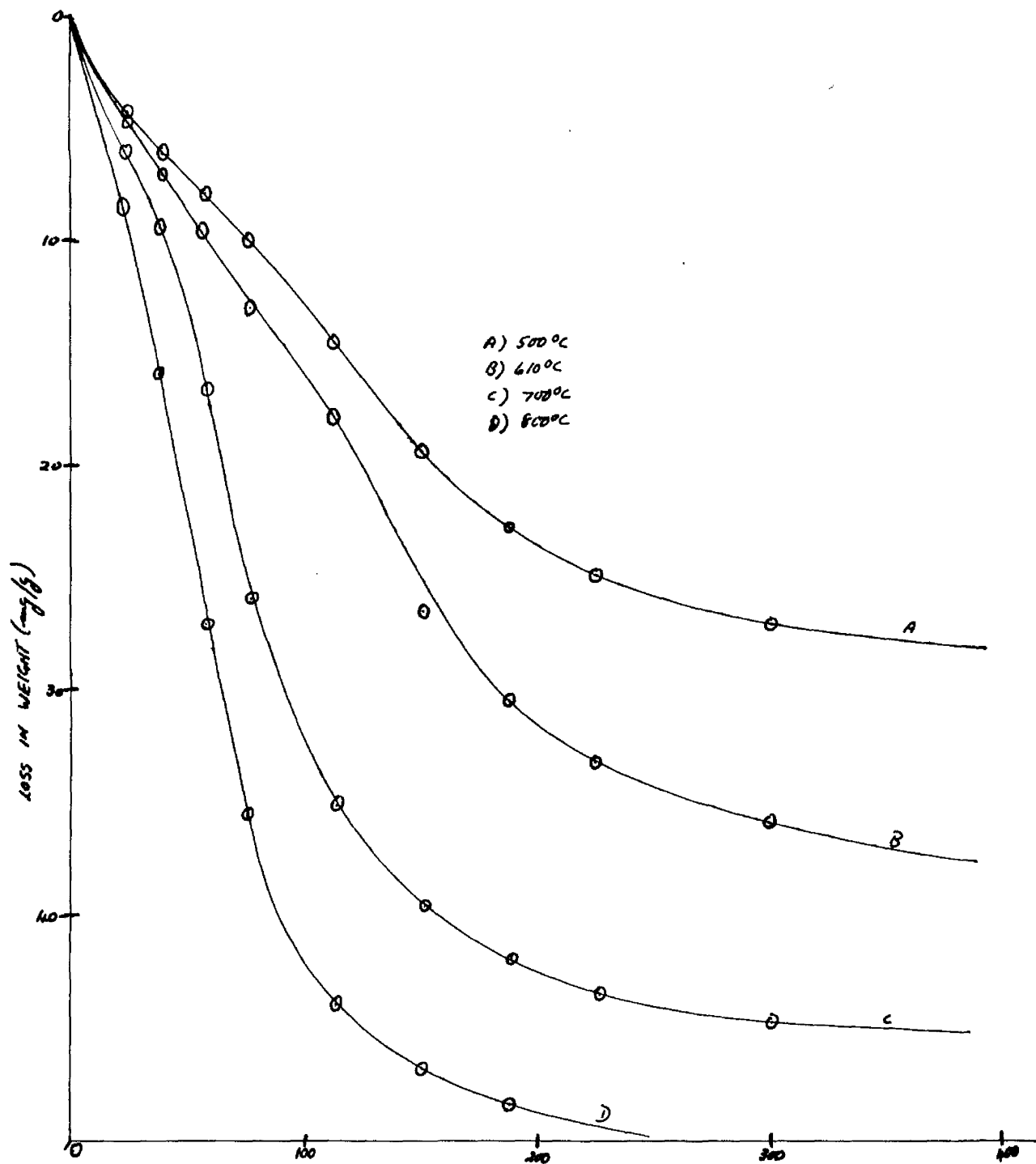
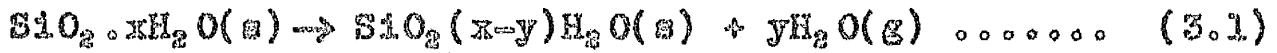


FIG. (3.2) DEHYDRATION CURVES FOR 841-420 μ IRREGULAR GEL PARTICLES

Table (3.1). Loss in weight of spheroidal and irregular particles of silica gel at different temperatures.

<u>Temp. (°C)</u>	<u>Time (secs.)</u>	<u>Wt. loss (mg./g)</u>	
		<u>2000-841<math>\mu</math> spherical</u>	<u>2000-841<math>\mu</math> irregular</u>
500	75	5.50	9.20
	100	6.90	12.60
	150	11.40	18.85
	200	16.00	22.70
700	75	16.40	26.60
	100	19.85	33.30
	150	23.40	40.20
	200	24.65	43.00
800	75	23.20	39.70
	100	25.60	44.40
	150	28.20	48.85
	200	29.00	51.40

For spheroidal xerogel, a plot of dehydration rate against weight of volatile component (i.e. H<sub>2</sub>O) retained by the gel showed that the dehydration behaviour could be represented by a first order kinetic expression. On this basis, reaction rate data were evaluated from the following representation of the dehydration reaction:



where the silica gel activated at 240° is represented by  $\text{SiO}_2 \cdot x\text{H}_2\text{O}$ . The rate of dehydration to  $\text{SiO}_2 \cdot (x-y)\text{H}_2\text{O}$  was then followed experimentally by determining the rate at which water molecules were lost by the reactant.

In order to establish a value for rate constants in this type of dehydration reaction, use was made of the generalised equation of Erofojev<sup>49</sup> and Avrami<sup>50</sup> for nucleation and growth, viz.

$$\alpha = 1 - \exp\left(-\int_0^t p dt\right) \dots\dots\dots (3.2)$$

where  $\alpha$  = reacted fraction of the sample.

Erofojev<sup>51</sup> has shown the generalised equation<sup>49</sup> to be applicable in determining the kinetics of decomposition of potassium permanganate and ammonium dichromate. This was then adapted for the case of a monomolecular reaction, i.e.,

$$-\left[\log\left(1-\frac{x}{y}\right)\right]^{1/n} = kt \dots\dots\dots (3.3)$$

where  $n = 1$  and  $x/y$  = fraction dehydrated.

This is same form of the equation which Jacobs<sup>52</sup> et al

used for investigating the kinetics of thermal decomposition of nickel oxalate, and which was applicable over the range  $0.04 < x/y < 0.85$ . These limits of applicability were used for all the experiments in the following studies.

The rate constants evaluated from this adapted equation are listed in table (3.2).

Table (3.2). Rate constants for the dehydration of (a) 2000-841  $\mu$  and (b) 841-420  $\mu$  silica gel spheroids.

<u>Size range (<math>\mu</math>)</u>	<u>Temp. (<math>^{\circ}</math>C)</u>	<u>k (sec.<math>^{-1}</math>) <math>\times 10^8</math></u>
2000-841	500	2.77
	700	8.00
	750	10.60
	800	13.00
841-420	450	3.63
	520	5.00
	550	5.45
	600	6.73
	750	11.17

Plots of these rate constants (fig. 3.3) in the Arrhenius manner led to an activation energy of  $9.4 \text{ k cal.mole}^{-1}$  for the 2000-841  $\mu$  xerogel spheroids.

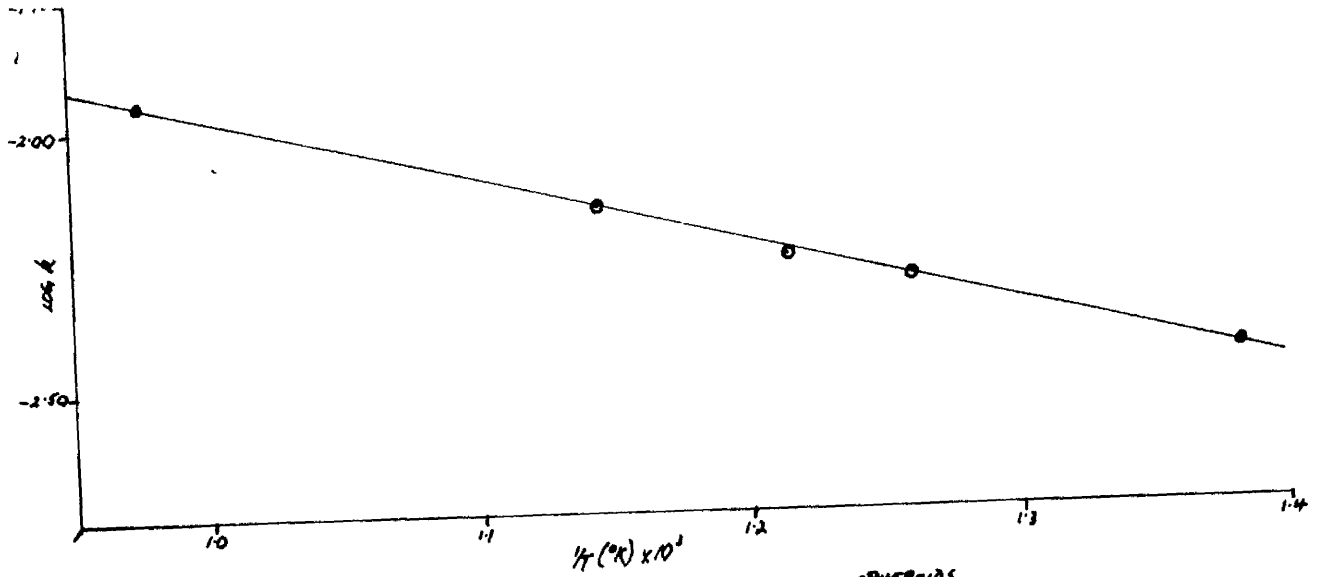


FIG. (3.3) ARRHENIUS PLOT FOR 841-420  $\mu$  SPHEROIDS

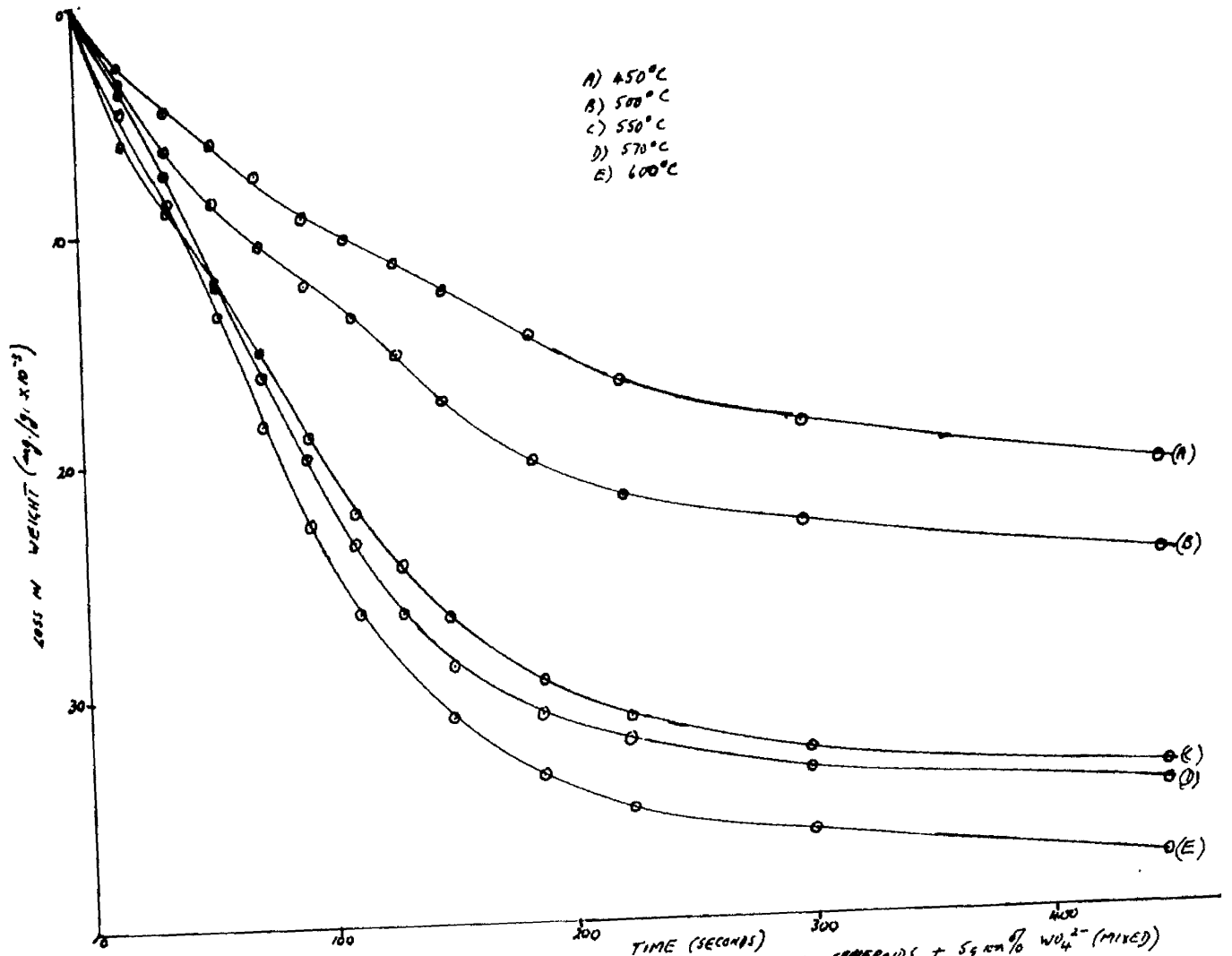


FIG. (3.4) DEHYDRATION CURVES FOR 2,000-841  $\mu$  SPHEROIDS + 5% w/w  $\text{WO}_4^{2-}$  (MIXED)

Fig.(3.3) showed that the value of the activation energy was however, dependent on particle size, and for the 841-420  $\mu$  spheroids,  $E_A$  was 5.6 k cal mole<sup>-1</sup>.

Thermal dehydration of silica gel in the presence of sodium tungstate.

The next step was to investigate the effect of a selected transition metal anion (viz. in the form of sodium tungstate) on the dehydration rate of silica gel. In this series of experiments the size range of the spheroids was restricted to 2000-841  $\mu$  .

(a) Silica gel + Na<sub>2</sub>WO<sub>4</sub> : mixed.

Analysis of the thermal balance experiments led to a pattern of weight losses as shown in fig.(3.4), for the addition of 5 g.ion % WO<sub>4</sub><sup>2-</sup>. Fig.(3.5) now showed that the dehydration rate was proportional to the half power of the weight content of volatile water retained by the gel at any instant.

Thus in order to establish rate constants for this reaction, the Avrami-Erofeyev<sup>50,49</sup> equation was modified as shown below:-

$$-\log\left[1 - \frac{x}{y}\right]^{1/n} = kt \quad \dots \dots \dots (3.4)$$

where n = 2.

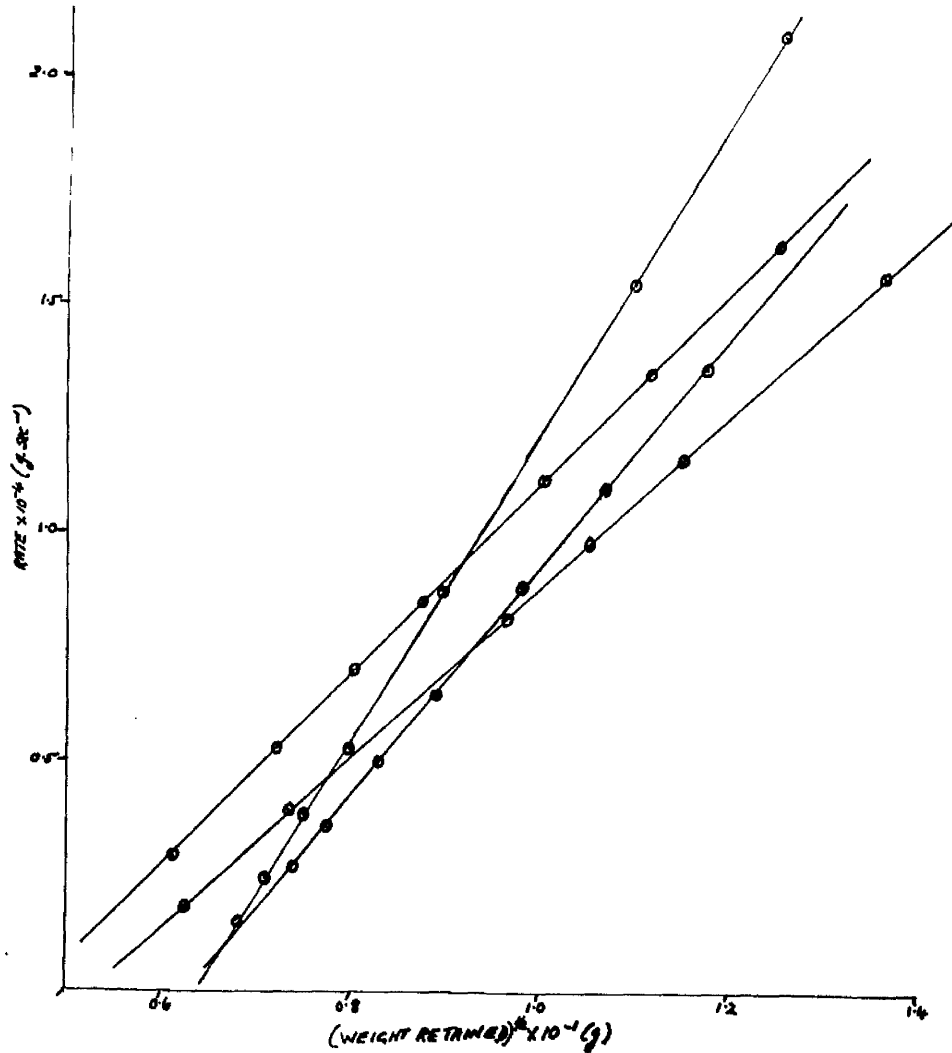


FIG. (3.5) PLOT OF RATE OF DEHYDRATION AGAINST HALF POWER OF WEIGHT CONTENT RETAINED BY THE GEL AT VARYING TEMPERATURES.

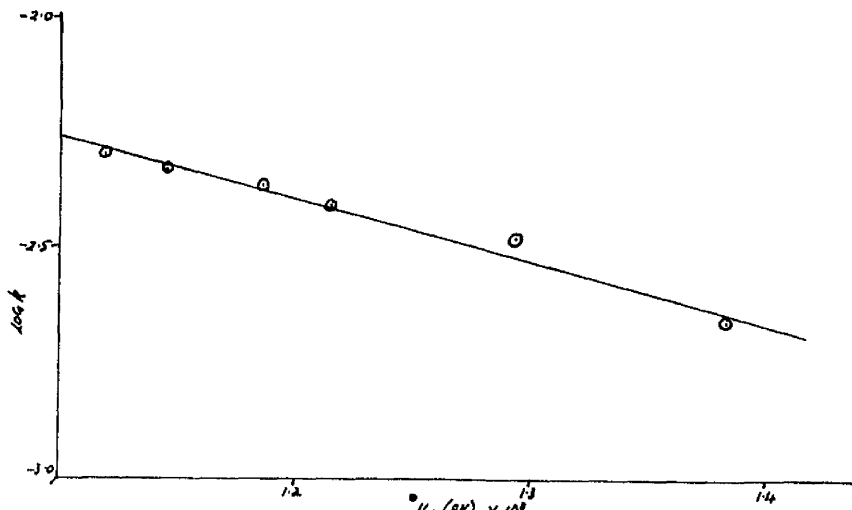


FIG. (3.6) ARRHENIUS PLOT FOR 2000-861 M SPHEROIDS + 5 g m % W/O<sub>4</sub> (MIXED)

The values of the rate constants derived are given in Table (3.3), and when plotted in the Arrhenius fashion led to an activation energy of 6.3 k cal.mole<sup>-1</sup>, fig.(3.6).

Table (3.3). Rate constants for the dehydration of silica xerogel in the presence of 5 g.10n % WO<sub>4</sub><sup>2-</sup>.

<u>Temp. (°C)</u>	<u>k(mole <sup>1</sup>/<sub>4</sub> sec.<sup>-1</sup>) x 10<sup>5</sup></u>
450	2.08
500	3.82
550	4.06
570	4.68
600	4.55
620	5.00

Experiments were carried out in which the amount of additive mixed with the gel was varied. In fig.(3.7) the reaction rate at 500°C was plotted against the percentage of sodium tungstate added for 15, 20, 25 and 30 mg. g. loss in weight from the hydrogel. In all cases the rate climbs initially to a maximum value which lies at approximately 2-3 g.10n % WO<sub>4</sub><sup>2-</sup>. The rate then falls off with increasing % WO<sub>4</sub><sup>2-</sup> and starts to level out at 10 g.10n %.

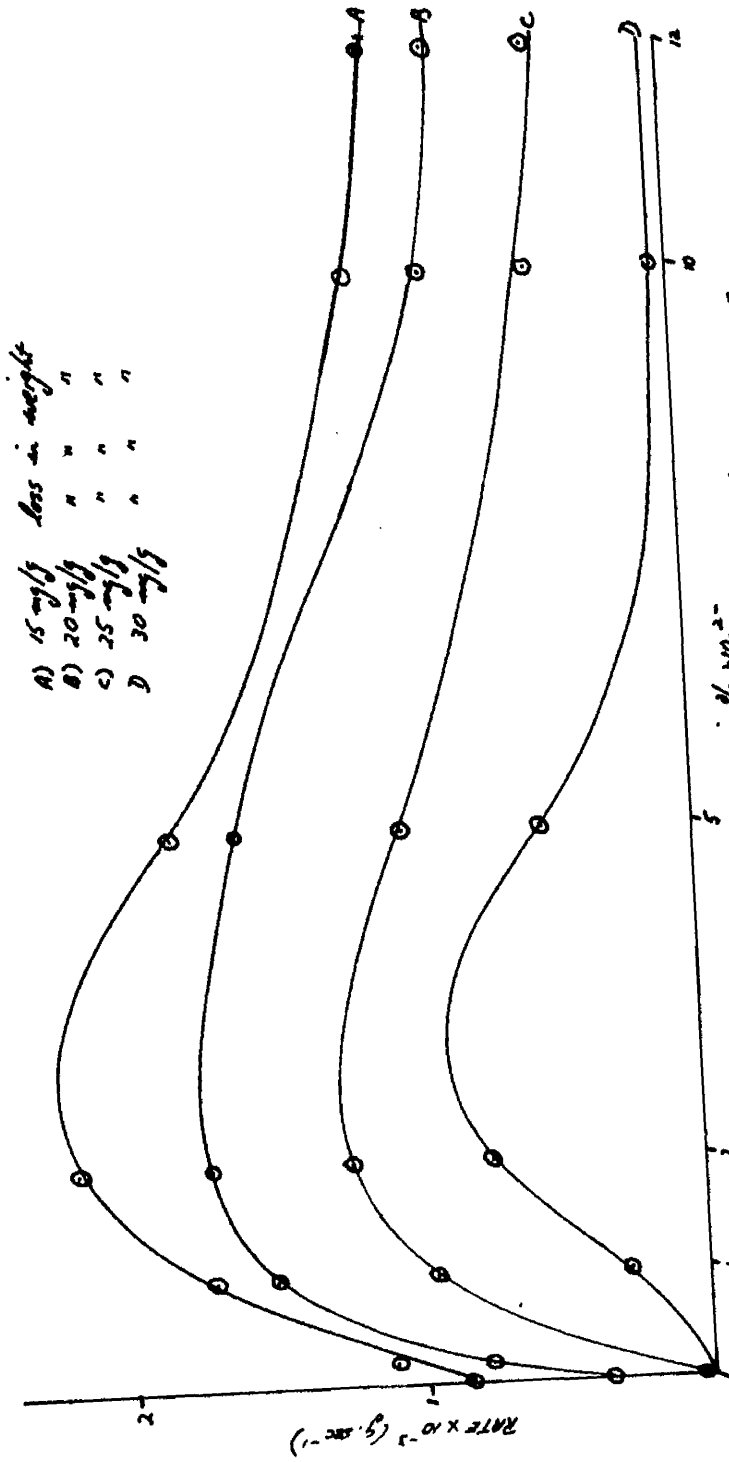


FIG. (3.7) RATE CURVES AT 5000 SHOWING DEPENDENCE ON % OF ADDITIVE

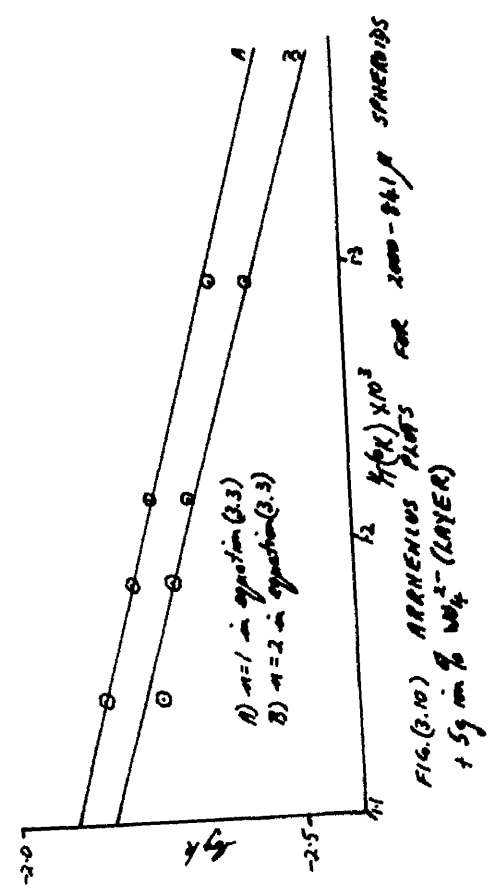


FIG. (3.10) ARRHENIUS PLOTS FOR 2000-261A SPHERES + 5g in. % W<sub>4</sub> (LAYER)

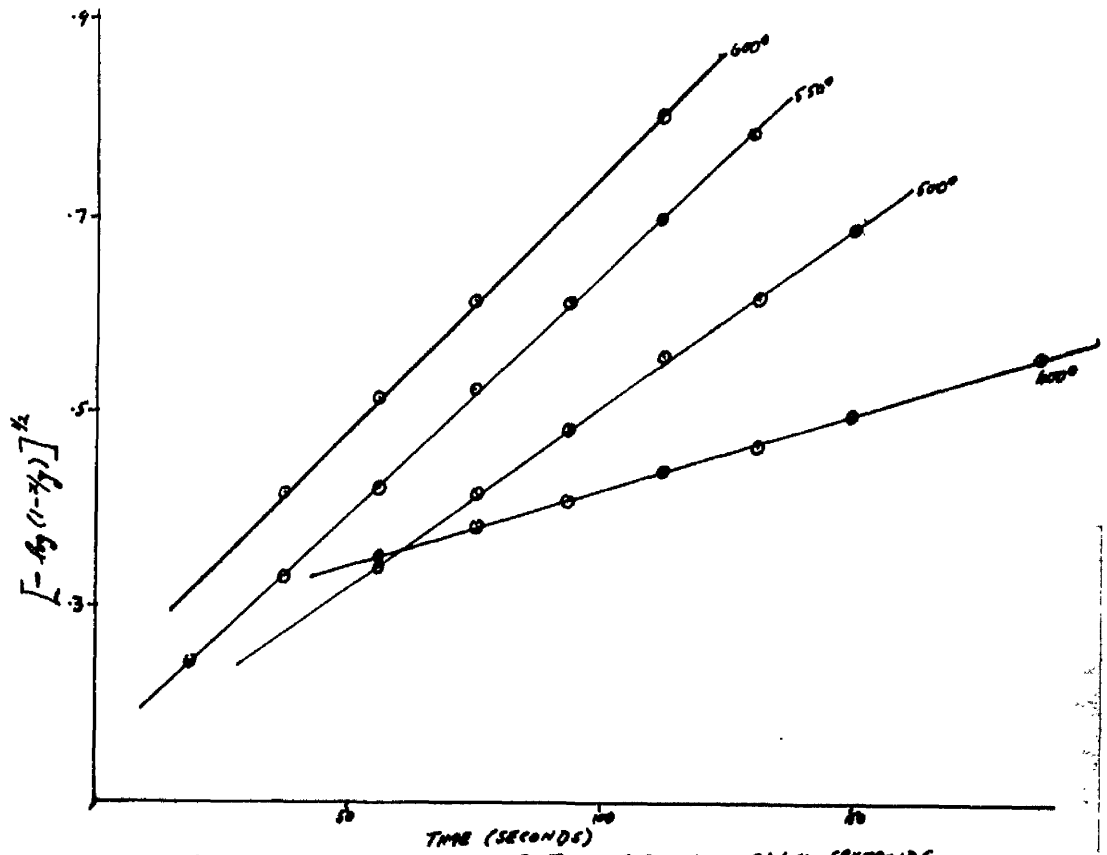


FIG. (3.8) AVRAMI-EROFYEV PLOTS FOR 2000-841M SPHEROIDS + 5g mm<sup>3</sup> % W<sub>0</sub><sup>2-</sup> (LAYER) WHERE n=2

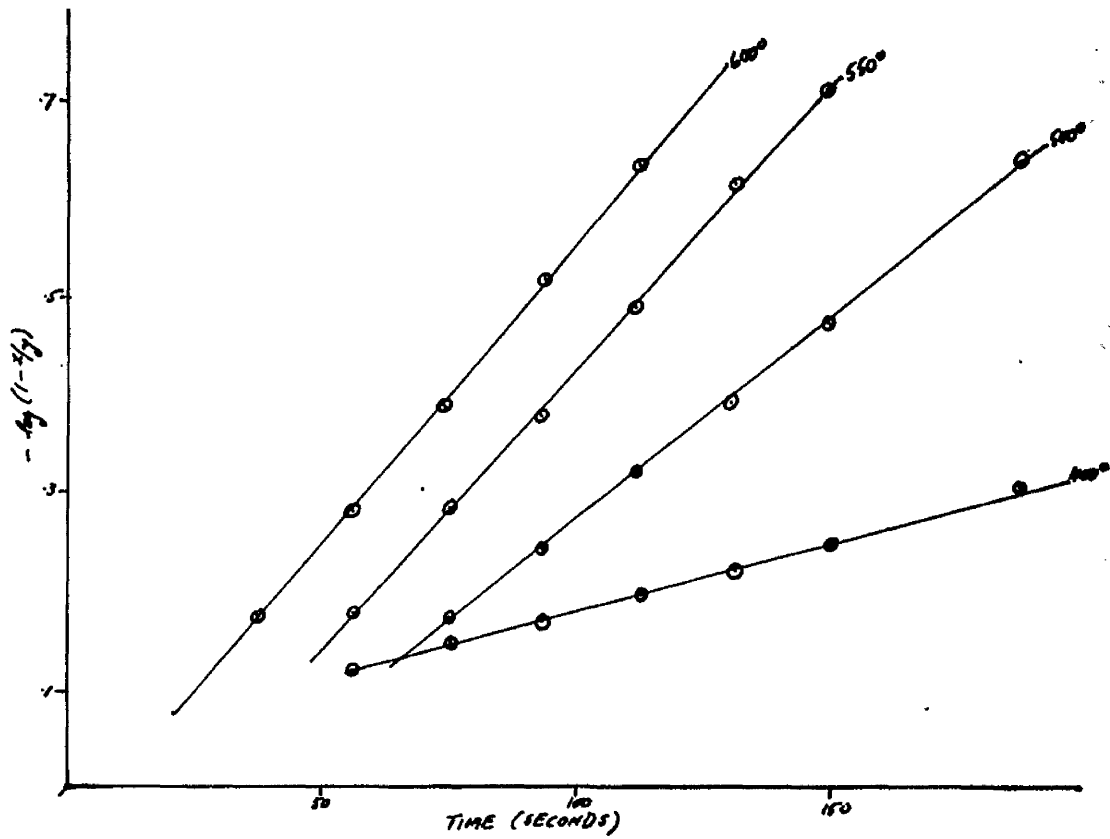


FIG. (3.9) AVRAMI-EROFYEV PLOTS FOR 2000-841M SPHEROIDS + 5g mm<sup>3</sup> % W<sub>0</sub><sup>2-</sup> (LAYER) WHERE n=1

In each case this level lies slightly above the dehydration rate found in the absence of tungstate.

(b) Silica gel + Na<sub>2</sub>WO<sub>4</sub> : layer.

This layer technique was carried out to illustrate clearly, the extent to which physical contact between the xerogel and additive affects the dehydration. The results showed that the rate of dehydration increased, but to a lesser extent than that found in experiments with thorough mixing of the gel and additive. Thus, a plot of rate against weight retained by the gel seemed to show that an apparent half order rate relationship was again applicable. However, further calculations showed that in this case, the rate of dehydration could equally well be interpreted by a first power relationship. This is clearly shown in figs. (3.8) and (3.9) for Avrami-Erofeyev plots where  $n = 2$ , and  $n = 1$  respectively. The calculated values of the rate constants are listed in table (3.4).

Table (3.4). Rate constants for the dehydration of silica xerogel in the presence of 5 g. ion %  $WO_4^{2-}$  (layer).

<u>Temp. (°C)</u>	<u>1st order</u> <u><math>k(\text{sec.}^{-1}) \times 10^3</math></u>	<u><math>\frac{1}{2}</math> order</u> <u><math>k(\text{mole}^{\frac{1}{2}} \text{sec.}^{-1}) \times 10^3</math></u>
500	4.10	3.71
550	5.73	4.90
570	6.12	5.23
600	6.91	5.42

The Arrhenius plots derived from these values are shown in fig.(3.10) and led to activation energies of 6.2 k cal.mole<sup>-1</sup> for the 1st power relationship and 6.4 k cal.mole<sup>-1</sup> for the  $\frac{1}{2}$  power relationship.

Interpretation of such results presented difficulties, but it may be concluded that the extent of contact between the gel and the additive, could affect the formation and stability of possible intermediate phases formed during the reaction.

Thus the anomaly of two possible power relationships may arise, simply from geometric factors.

(c) Silica gel +  $Na_2WO_4$  : (vapour)

(c) Silica gel +  $Na_2WO_4$  : (vapour)

Finally the rate of dehydration of the xerogel spheroids was examined in the presence of " sodium

tungstate vapour" i.e. the solid additive was removed from the melt. Once again the rate of dehydration had increased but to a lesser extent than in the previous two cases. Analysis of the results again showed that the dehydration obeyed a half-order power law. The values of the rate constants are shown in table (3.5).

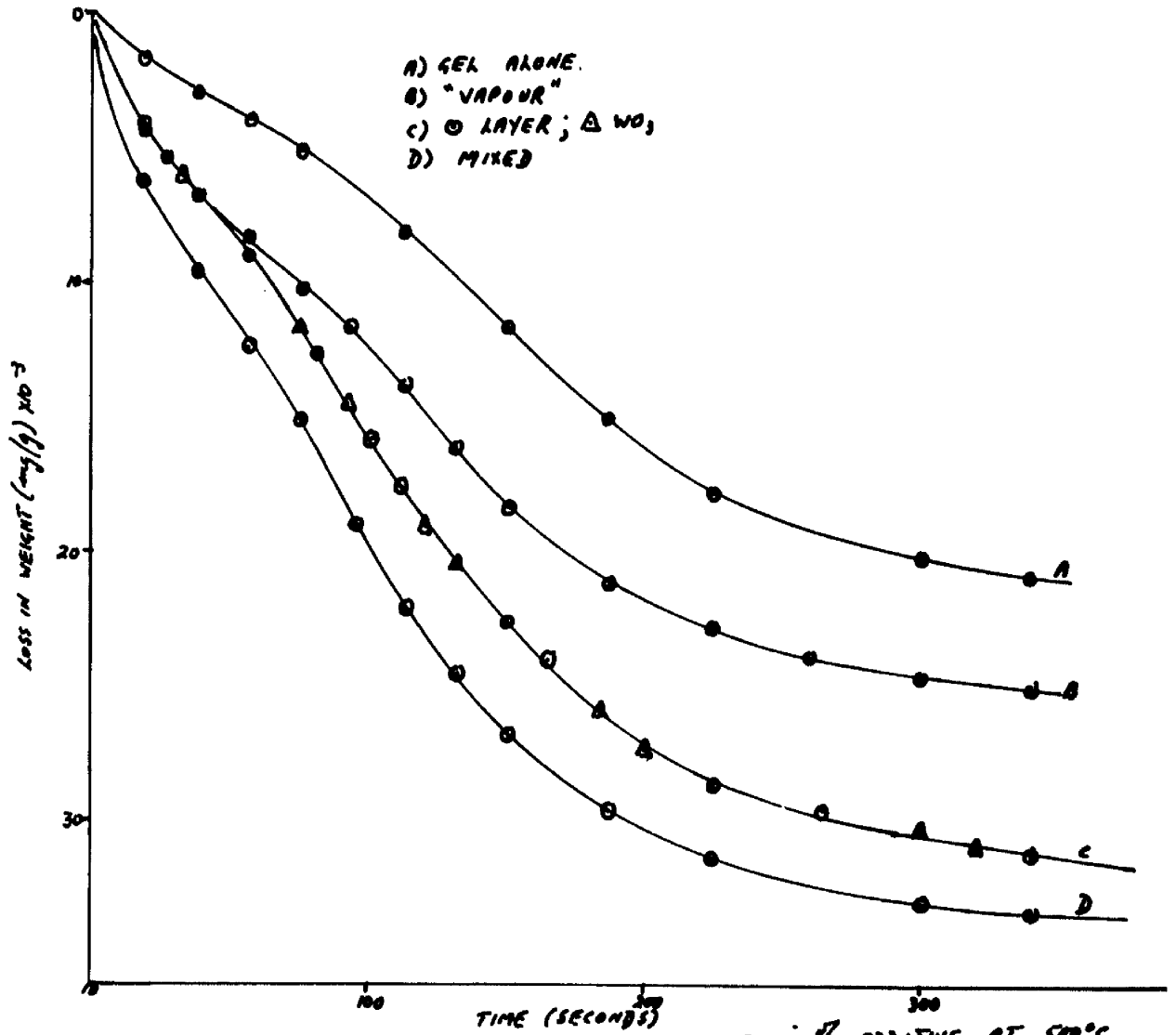
Table (3.5). Rate constants for xerogel dehydration in which the sodium tungstate was removed from the melt.

<u>Temp (°C)</u>	<u>k(mole <sup>1/2</sup> sec.<sup>-1</sup>) x 10<sup>3</sup></u>
500	3.33
550	4.37
570	4.72
600	4.90

Fig.(3.11) illustrates the comparative rates of dehydration for the different methods of tungstate addition at 500°. It is clearly shown that the amount of dehydration achieved by sodium tungstate decreased in the experimental series : mixed > layer > vapour > no additive.

(d) Silica gel + tungstic oxide (mixed).

Two experiments were carried out, in which the



effect of 5 g. ion %  $WO_3$  on the dehydration of the gel was examined. Fig.(3.11) shows that the weight loss in this case virtually coincided with the 'layer' curve for sodium tungstate at the same temperature. This was again shown for a dehydration experiment at  $570^\circ$ .

These results indicate that in the experiments with sodium tungstate, acceleration of dehydration was not achieved simply by the action of tungstic oxide arising from the decomposition of sodium tungstate.

(e) Analytical observations

X-ray powder photographs were taken for a large range of samples. These showed that there was no apparent long-range interaction between the gel and tungstate, as judged by the absence of lines.

The gel and the tungstate were separated by sieving before taking the photographs. This separation was possible since the sodium tungstate particles were of a smaller size range than the gel spheroids.

It should be noted that at  $650^\circ$  for a thoroughly mixed sample, the resulting X-ray photograph yielded d-values shown in table (3.6) from the lines of

greatest intensity. Those indicated the formation of  $\alpha$ -tridymite at a somewhat lower temperature than that quoted by Peyronel.<sup>83</sup>

Table (3.6).     d-values for  $\alpha$ -tridymite.

<u>Experimental (650°)</u>	<u>Standard</u>
4.083	4.30, 4.08
3.244	3.81, 3.25
2.770	2.96, 2.47
2.108	2.37, 2.29, 2.07, 2.03
1.870	1.97, 1.87
1.760	1.76, 1.68
1.616	1.61, 1.58
1.539	1.53, 1.52
1.395	1.39, 1.37, 1.33, 1.29

The recovery of sodium tungstate from the mixed solids was examined after separate dehydration runs at 500°, 550° and 600° with 5g. ion %  $\text{WO}_4^{2-}$  additions. The mixture was shaken up with water, boiled and the filtrate evaporated to dryness.

The results all showed a 99-100% recovery of tungstate. These results were confirmed by the oxine method and indicate that the increase in dehydration rate in the tungstate experiments was primarily of a catalytic nature.

Table (3.7). Percentage recovery of tungstate from dehydrated samples of 2000-841// xerogel.

<u>Temp. (°C)</u>	<u>% recovery of tungstate</u>	
	<u>Oxine</u>	<u>Evaporation</u>
500	99.5	99.7
550	99.7	99.7
600	99.1	99.5

Physical Properties of Silica Gel

Physical Properties of Silica Gel

(a) Surface area and bulk density. 2000-841//  
gel spheroids over a wide range of temperature as shown in fig.(3.12). The values of surface area derived from this type of isotherm are listed in table (3.8) along with the values of the bulk density. The trend of these values is better illustrated by fig.(3.13). Also listed in table (3.8) are the values of the surface area (S') calculated by the method of Cranston and Inkley.<sup>46</sup> The values for 841-420// spheroids, though not covering such a wide temperature range are also listed in table (3.8).

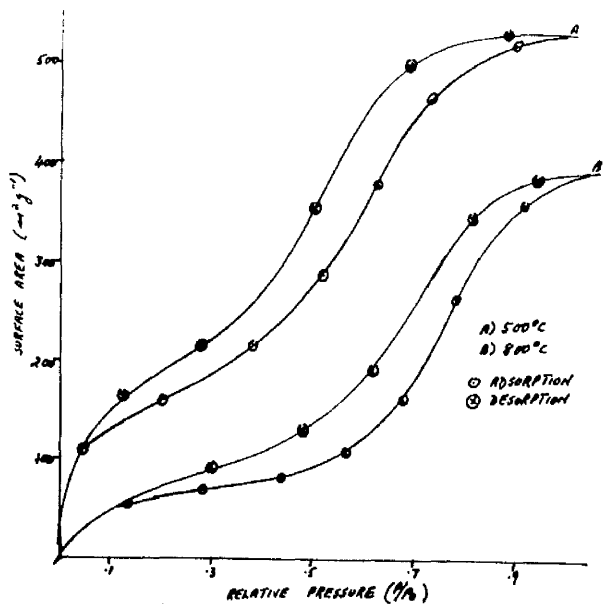


FIG. (3.12) B.E.T. ISOTHERMS FOR 2000-84μ SPHEROIDS

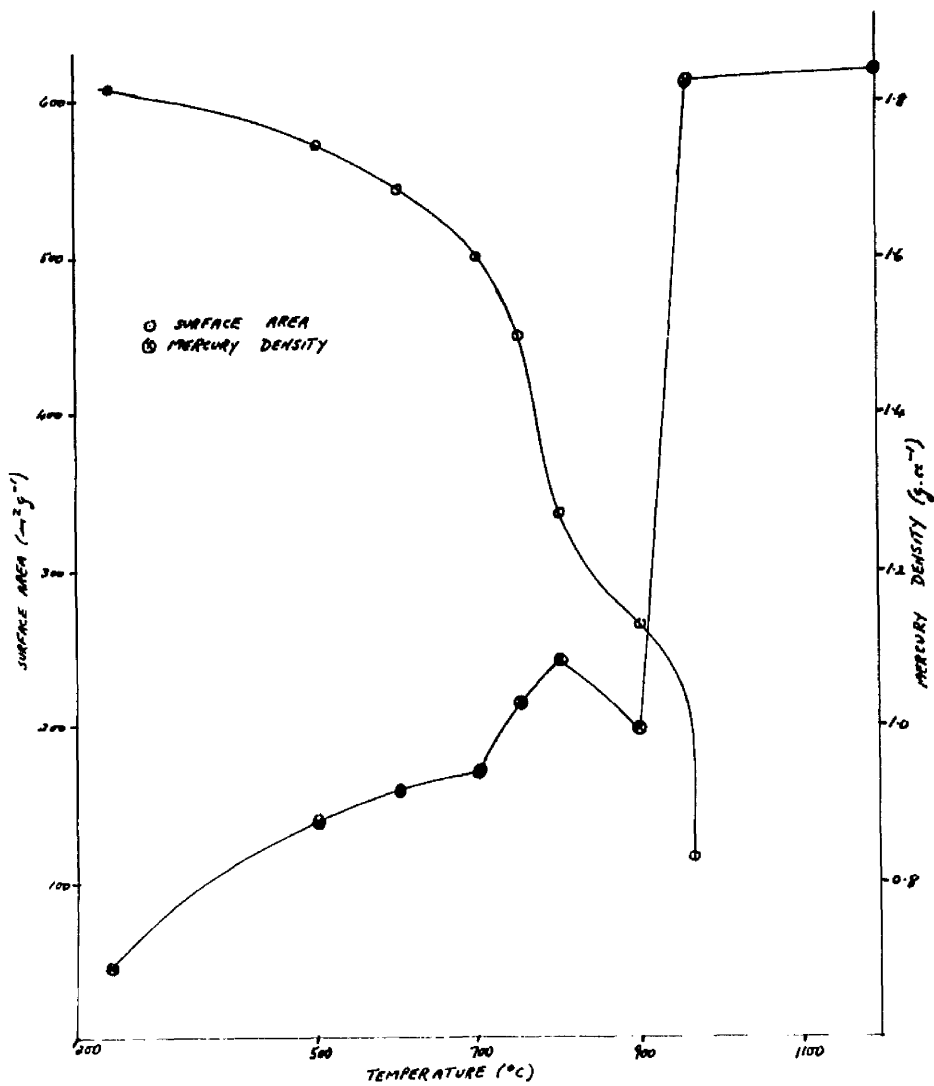


FIG. (3.13) PHYSICAL PROPERTIES OF 2000-84μ SPHEROIDS

Table (3.8). Surface area and bulk density values for xerogel spheres of size ranges 2000-841 $\mu$  and 841-420 $\mu$ .

<u>Temp. (°C)</u>	<u>Size range</u>					
	<u>2000-841(<math>\mu</math>)</u>			<u>841-420(<math>\mu</math>)</u>		
	<u>Surface area (m<sup>2</sup>/g)</u>	<u>S'</u>	<u>Mercury density (g/cc)</u>	<u>Surface area (m<sup>2</sup>/g)</u>	<u>S'</u>	<u>Mercury density (g/cc)</u>
240	612	598	0.690	-	-	-
450	-	-	-	565	569	0.882
500	574	566	0.886	550	543	0.905
520	-	-	-	531	518	0.922
550	-	-	-	502	491	0.940
600	546	531	0.926	-	-	-
700	503	500	0.942	-	-	-
750	451	467	1.035	401	417	1.055
800	336	318	1.086	290	299	1.140
900	271	265	1.049	-	-	-
960	120	105	1.825	-	-	-
1200	-	-	1.840	-	-	-

Fig.(3.13) illustrates the fall in surface area with temperature for 2000-841 $\mu$  xerogel spheroids, there being a gradual decrease in surface area and then a very marked decrease around 750-800°.

The melting point of the xerogel is not known, since

there is a transformation at around 1150°C before melting; but for approximate purposes, it has been assumed to be the same as that of cristobalite viz. 1996°K.<sup>84</sup> In agreement with the results of Goodman and Gregg<sup>2</sup> for precipitated silica, the density shows a sharp increase around 750-800°. The bulk Tammann temperature ( $\alpha = 0.5$ ) of the gel will be around 750°. At about 750° the pore volume of the gel falls sharply, showing that bulk movement of the solid starts at this temperature, so that the rapid reduction in surface area coincides with this bulk movement of the solid. Above the Tammann temperature there was a rapid increase in density at 900° and greater. This was expected from the x-ray data which showed that there was conversion to cristobalite and also from the elimination of pores as indicated by gas adsorption.

Table (3.9) shows the values of surface area and mercury density of the xerogel for the four different types of additive experiments. As expected, there was a fall in surface area and increase in lump density, with increase in temperature for all four sets of experiments.

Table (3.9). Physical measurements of xerogel samples in the presence of sodium tungstate and tungsten oxide.

<u>Condition</u>	<u>Temp. (°C)</u>	<u>Surface Area (m<sup>2</sup>/g)</u>	<u>S'</u>	<u>Mercury ∫ (g/cc)</u>
Gel + 5g.10n% WO <sub>4</sub> <sup>2-</sup> MIXED	450	514	519	.797
	500	489	499	.819
	550	450	463	.834
	570	431	422	.862
	600	421	413	.881
	620	395	390	.912
Gel + 5g.10n % WO <sub>4</sub> <sup>2-</sup> LAYER	400	563	573	.820
	500	536	524	.837
	550	518	510	.842
	570	501	489	.859
	600	438	436	.875
	645	408	400	.896
Gel + "vapour" of Na <sub>2</sub> WO <sub>4</sub>	500	552	560	.821
	550	532	520	.834
	570	514	501	.846
	610	454	462	.871
Gel + 5g. 10n % WO <sub>3</sub>	500	531	527	.834
	570	501	509	.853

The decrease in surface area is greatest in the mixed and least in the "non-contact" experiments. This might be anticipated, since the rate of dehydration decreases in the order mixed > layer = tungstic oxide mixed > vapour.

In the experiments in which the percentage of tungstate ion was varied from 0.2-12.0 g.ion %, at 500°, the surface area did increase slightly with increasing concentration of tungstate ion, but the mercury density remained substantially constant at 0.81-0.82 g./c.c.

Pore size distribution curves were calculated from the adsorption branch of the B.E.T. isotherms by the method of Cranston and Inkley.<sup>46</sup> The xerogel spheroids showed a maximum pore diameter around 60 Å and a secondary maxima at 35-40 Å. Fig.(3.14) shows the pore size distribution curve for spheroids of size range 2000-841 μ dehydrated at 600°. The inset in fig.(3.14) shows the pore size distribution curves over the narrower range 30-100 Å, for xerogel particles treated at 240°, 500°, 600°, 750°, 800° and 960°.

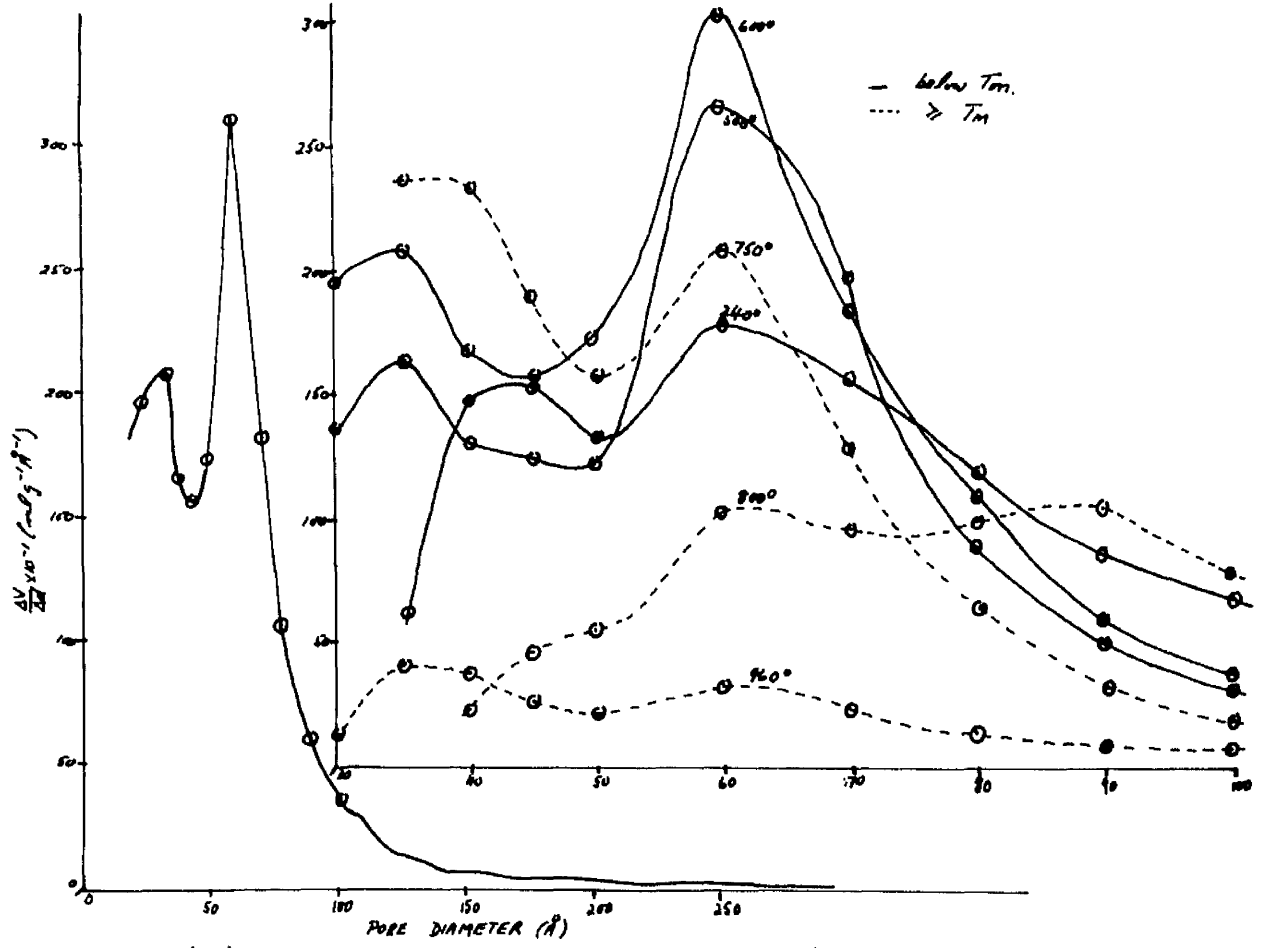


FIG. (3.14) PORE SIZE DISTRIBUTION CURVES FOR 2000-841  $\mu$  SPHERULIDS.

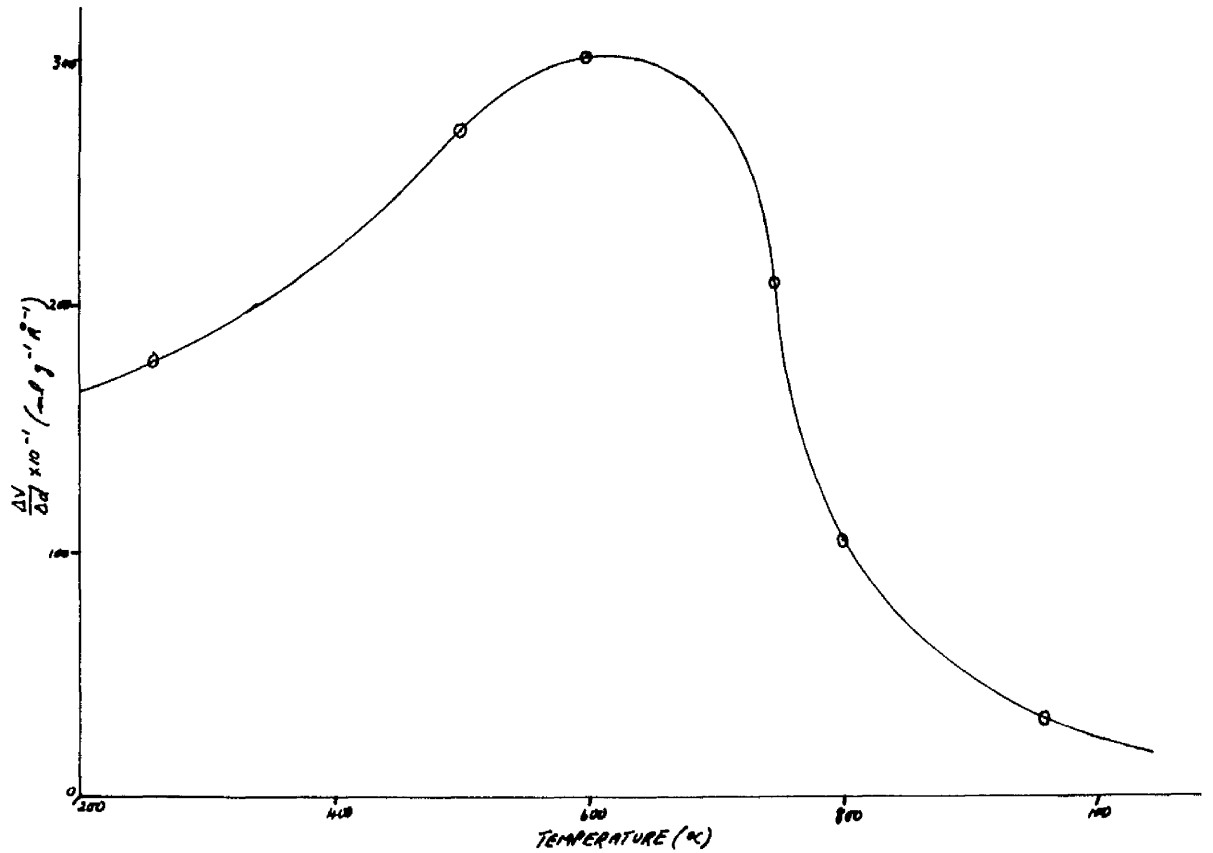


FIG. (3.15) PORE VOLUME AGAINST TEMPERATURE FOR PORES 60  $\text{\AA}$  DIAMETER

The height of the peak at  $60 \text{ \AA}$  tended to increase with increase of temperature of sample initially, but began to fall very rapidly at  $750^\circ$ , i.e. around the bulk Tammann temperature ( $0.5 T_m$ ). Above  $750^\circ$ , the distribution peaks become broader, consistent with collapse of the gel framework and with the decreased surface area and high mercury density already found. Ultimately, samples treated at  $960^\circ$  give a near-flat distribution curve from  $30\text{-}100 \text{ \AA}$ .

For samples activated by the presence of sodium tungstate, the strongest peak was also at  $60 \text{ \AA}$ . A similar pattern of behaviour to that of the simple xerogel was found with increase in temperature. The height of the peaks in distribution curves for samples treated at  $500^\circ$  in presence of varying concentrations of sodium tungstate, did not follow any specific pattern. These curves may be taken to emphasise the difficulty of efficient mixing and the possibility of having localised concentrations of additive.

Fig.(3.15) of the derivative  $\Delta v/\Delta d$  against temperature for a concentration of pores of 60 Å shows the steady rise of the pore volume to a maximum at 600-700°, the rapid fall setting in above 700° and the ultimate near-zero value at 960°.

## Section II

## Section II

### Mixed Oxide Systems

~~It has been shown~~ in these laboratories that for small additions of alkaline earth halides to silica xerogel,<sup>55</sup> ~~that~~ a temperature demarcation zone exists, at which transition from catalytic to solid-solid interaction takes place. It would seem to be valuable if these studies were extended to other inorganic compounds such as oxides to see if any general behaviour pattern could be established.

Previous work on solid state investigations of mixed oxide systems has been very much of an empirical nature. Huttig<sup>55</sup> proposed that the following six stages existed in the life time of an oxide mixture, e.g. for ZnO + Cr<sub>2</sub>O<sub>3</sub> :-

- (a) This is denoted by the term "covering" stage in which the oxides are mixed at room temperature,

and is mainly distinguished by having intimate surface contact of the two compounds.

- (b) This is the activation stage and is due to the formation of Zwitter-molecules and to molecular covering of surfaces. The molecules of the mobile component ( $\text{Cr}_2\text{O}_3$ ) diffuse over the surface of the less mobile component ( $\text{ZnO}$ ).
- (c) This comprises a stage of deactivation of the Zwitter-molecules and of molecules covering the surface. This process may be regarded as similar to Taylor's<sup>56</sup> switch from van der Waal's adsorption to activated adsorption.
- (d) This is a stage due to internal diffusion. Increase in temperature causes diffusion of the mobile oxide into the crystal lattice of the less mobile oxide. This is the first stage in which the molecules of the less mobile oxide actually contribute to the catalytic activity of a mixture.
- (e) This stage is the formation of less ordered crystalline aggregates of the addition compound.
- (f) This occurs with the filling of crystal defects.

In order to examine such oxide systems, the effect of addition of selected oxides on the dehydration of silica xerogel was investigated.

### Starting materials

Silica xerogel:- 2000-841 // spheroids of silica gel were prepared as described previously (p.11).

Nickel oxide:- Green nickel oxide (NiO) was prepared by roasting nickel nitrate ( $\text{Ni}(\text{NO}_3)_2 \cdot 6\text{H}_2\text{O}$ ) to  $1000^\circ$ .

Zinc oxide:- The zinc oxide (ZnO) used was supplied by Hopkin and Williams.

Cadmium oxide:- The cadmium oxide was anhydrous grade supplied by B.D.H.

Cupric oxide:- The cupric oxide (CuO) was A.R. grade supplied by Hopkin and Williams.

Beryllium oxide:- The beryllium oxide was prepared by heating the basic carbonate to  $600^\circ$ .

Alumium oxide:- The alumina ( $\text{Al}_2\text{O}_3$ ) used was Grade H supplied by Spence.

Chromic oxide:- The green chromic oxide ( $\text{Cr}_2\text{O}_3$ ) was prepared by heating B.D.H. chromic hydroxide to ca.  $900^\circ$ .

The above oxides were all of a particle size  $< 300\mu$ . The choice of the oxides used was made primarily to examine if valency or ionisation effects were important. Another feature of the selection of oxides was to distinguish between transition metal oxides with free d-orbitals, viz.  $\text{Cr}_2\text{O}_3$ ,  $\text{NiO}$  and  $\text{CuO}$ , and non-transition metal oxides, viz.  $\text{Al}_2\text{O}_3$ ,  $\text{ZnO}$  and  $\text{BeO}$ .

In all cases the amount of oxide added was calculated as g. ion % of metal ion (5 g. ion %) on the weight of  $\text{SiO}_2$  obtained from 1 g. silica gel activated at  $240^\circ$  and subsequently calcined at  $1500^\circ$  for several hours. As for the tungstate experiments, mixing was by hand-stirring and shaking for 5 minutes. The methods of investigation were identical to the tungstate experiments. One significant difference was that pore size distributions were omitted, since B.E.T. isotherms were measured only to a relative pressure value of ca. 0.3.

#### Silica gel spheroids

Plots of rate of loss in weight with time [fig.(3.16)], again showed an increasing degree of dehydration with time over the four temperatures

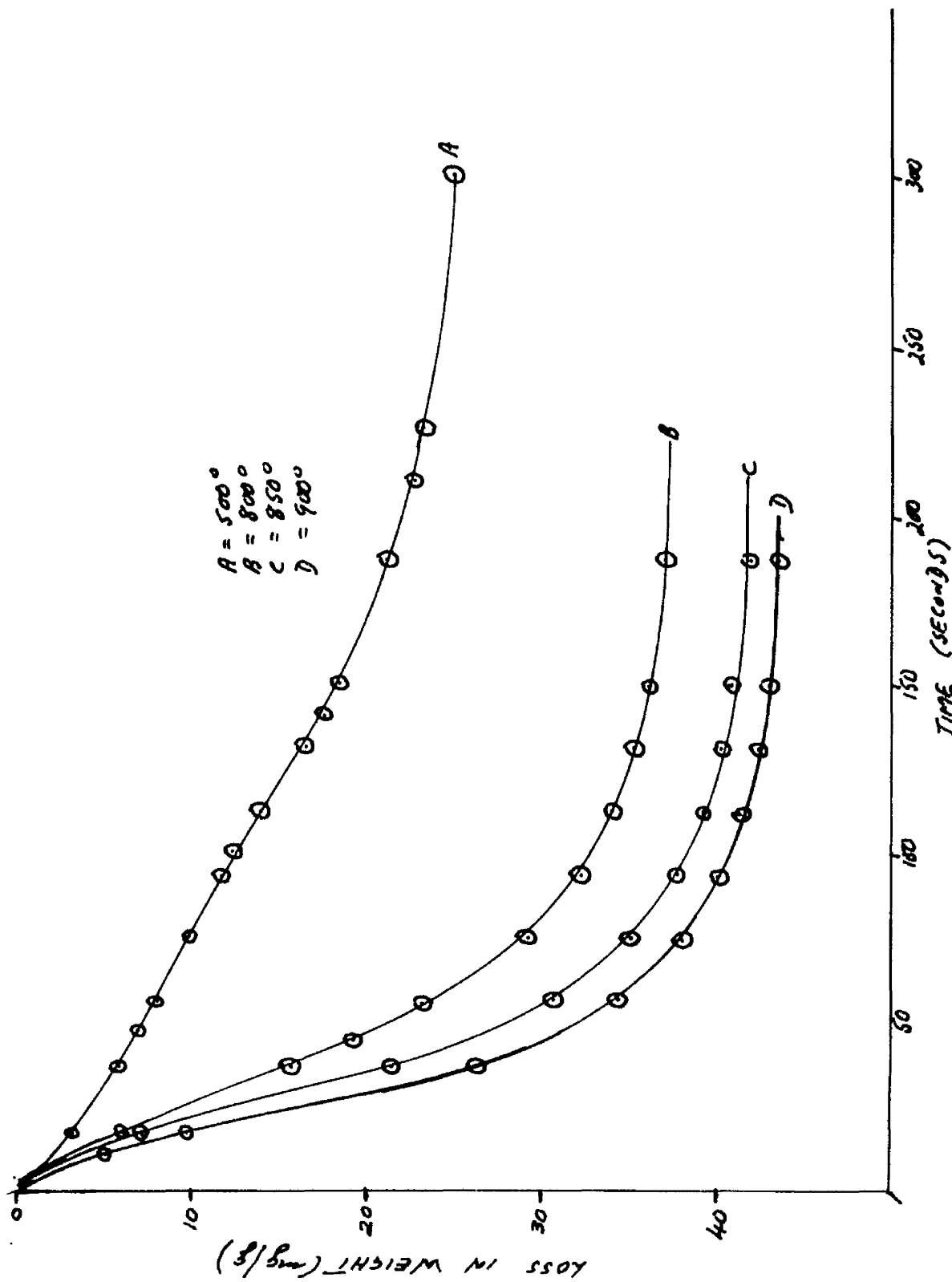


FIG. (3.16) DEHYDRATION CURVES FOR 2000-841 μ XEROGEL SPHEROIDS AT DIFFERENT TEMPERATURES.

examined, viz. 500°, 800°, 850° and 900°.

It has been shown that the Avrami-Erofojev<sup>50,49</sup> equation was applied successfully for the silica gel/sodium tungstate system. For the oxide experiments, calculations of rate constants were carried out using classical kinetic expressions and these results compared with Avrami-Erofojev constants.

The classical differential expression for 1st order kinetics is:-

$$-\frac{dw}{dt} = kw \dots\dots\dots (3.5)$$

where  $w$  = weight retained by the gel

and  $t$  = time

Integration of equation (3.5) between  $w_0$  to  $w_t$  and time  $t = 0$  to  $t = t$  gives

$$\log w_t = \log w_0 - kt \dots\dots\dots (3.6)$$

where  $w_t$  = weight retained at time  $t$ .

Therefore a plot of  $\log w_t$  against  $t$  should give a straight line of slope  $-k$ .

The results obtained by this method were in very good agreement to those obtained using the Avrami-Erofojev equation as can be seen in tables (3.10) and (3.12).

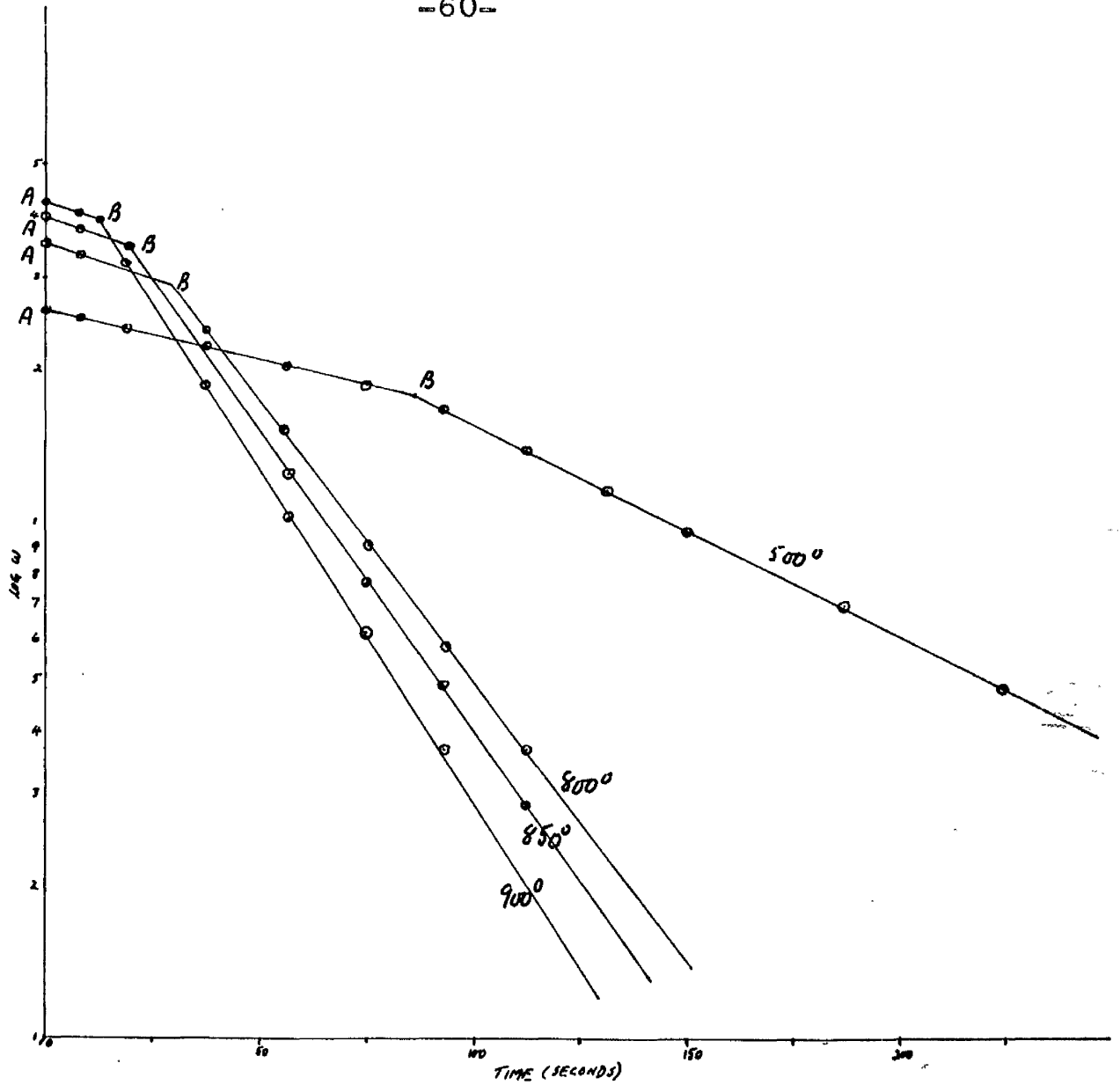


FIG. (3.17) PLOT OF WEIGHT RETAINED BY GEL AGAINST TIME

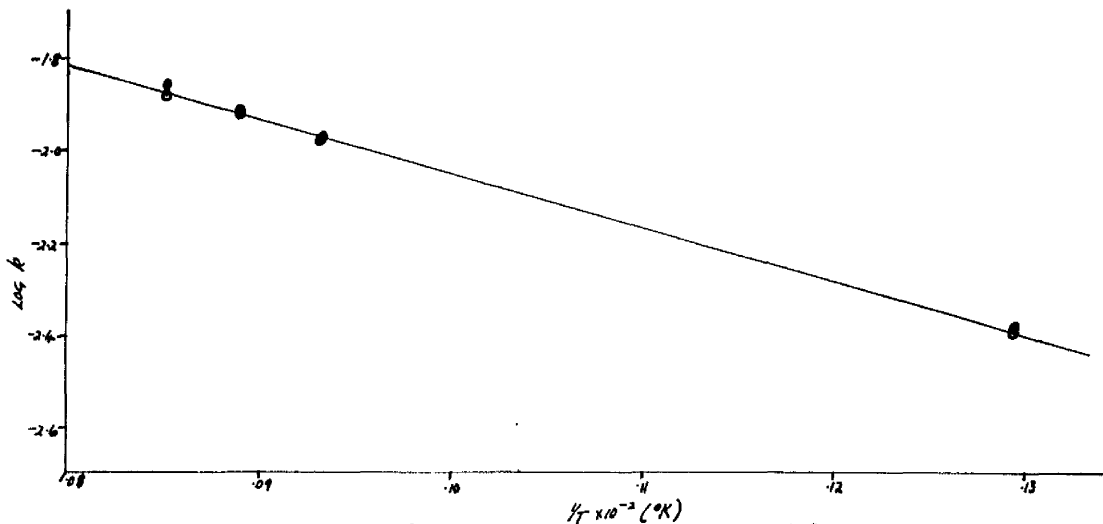


FIG. (3.18) ARRHENIUS PLOT FOR 2000- $\mu$  XEROGEL SPHEROIDS

A plot of  $\log w_t$  against  $t$  is shown in fig.(3.17) for 2000-841 // gel spheroids.

The sections of the graph labelled AB indicate possibly that there might be two consecutive first order reactions taking place which result in a common product. However, further study leads to the conclusion that this feature is probably inherent in the system and is maybe an induction period.

The rate constants calculated by both methods are listed in table (3.10).

Table (3.10). Rate constants for the dehydration of 2000-841 // gel spheroids.

<u>Temp. (°C)</u>	<u><math>k(\text{sec.}^{-1}) \times 10^3</math> classical</u>	<u><math>k(\text{sec.}^{-1}) \times 10^3</math> Avrami-Erofojev</u>
500	4.12	4.15
800	10.91	10.47
850	11.65	11.72
900	12.92	13.81

The above values when plotted in the Arrhenius manner (fig.3.18) gave a best straight line which showed the activation energy to be  $5.3 \text{ k cal.mole}^{-1}$ .

The decrease in activation energy from the earlier batch results, was supported by surface area

and bulk density measurements. This phenomenon was assumed to be due to differences arising in the preparation, such as volatile matter content.

A comparison of the two batches of gel are given in table (3.11).

Table (3.11).      Comparison of properties of different gel batches.

Temp. (°C)	k(sec. <sup>-1</sup> ) x 10 <sup>3</sup>	<u>Batch 1</u>		<u>Batch 2</u>		
		Surface area (m <sup>2</sup> /g)	Mercury density (g/cc)	k(sec. <sup>-1</sup> ) x 10 <sup>3</sup>	Surface area (m <sup>2</sup> /g)	Mercury density (g/cc)
500	2.77	574	0.886	4.12	632	1.021
750	10.60	451	1.035	-	-	-
800	13.00	336	1.086	10.91	444	1.200
850	-	-	-	11.65	394	1.314
900	-	271	1.049	12.92	276	1.474

Silica gel + selected oxides

Curves of loss in weight against time showed that in general, the addition of an oxide increased the total amount of dehydration; the increase was of the order of 3-11 mg./g. at 900°, depending on the additive.

Rate constants evaluated in the manners described are shown in table (3.12), using a first power rate law.

Table (3.12). Rate constants for 2000-841 # gel spheroids in presence of 5 g.ion % oxide additives.

<u>Oxide</u>	<u>Temp. (°C)</u>	<u>k(sec.<sup>-1</sup>) x 10<sup>3</sup> classical</u>	<u>k(sec.<sup>-1</sup>) x 10<sup>3</sup> Avrami-Erofovey</u>
	500	4.20	4.35
CuO	800	9.69	9.58
	850	11.15	11.00
	900	12.54	12.91
	500	4.40	4.48
Al <sub>2</sub> O <sub>3</sub>	800	10.71	10.91
	850	11.72	11.91
	900	12.75	12.68
BeO	500	3.83	3.70
	800	10.21	9.89
	850	11.37	11.72
	900	11.91	12.65
Cr <sub>2</sub> O <sub>3</sub>	500	4.00	4.10
	800	12.25	12.78
	850	13.19	13.31
	900	14.72	14.75
ZnO	500	3.62	3.82
	800	9.90	9.86
	850	10.49	11.04
	900	11.66	12.03

Table (3.12), (contd.). Rate constants for  
2000-841  $\mu$  gel spheroids in presence of 5 g. ion %  
oxide additives.

<u>Oxide</u>	<u>Temp. (°C)</u>	<u>k(sec.<sup>-1</sup>) x 10<sup>3</sup></u> <u>classical</u>	<u>k(sec.<sup>-1</sup>) x 10<sup>3</sup></u> <u>Avrami-Erofeyev</u>
	500	3.35	3.28
NiO	800	12.59	12.27
	850	13.50	13.95
	900	17.24	17.99

The best straight lines from the Arrhenius plots of the k values in table (3.12) led to the following activation energies, viz. CuO,  $4.8 \pm 0.1$ ; NiO,  $7.2 \pm 0.1$ ; Cr<sub>2</sub>O<sub>3</sub>,  $5.8 \pm 0.1$ ; BeO,  $5.4 \pm 0.2$ ; ZnO,  $5.2 \pm 0.1$ ; and Al<sub>2</sub>O<sub>3</sub>,  $4.8 \pm 0.1$ ; k cal.mole<sup>-1</sup>. Table (3.12) shows that rate constants calculated by the two methods are numerically close. Hence it is not surprising that the activation energies obtained from Arrhenius plots of classical rate constants and Avrami rate constants were invariably of the same value. This point is illustrated in fig. (3.19) for CuO, Cr<sub>2</sub>O<sub>3</sub>, ZnO and NiO, in which both classical and Avrami-Erofeyev rate constants are plotted against  $1/T$  °K.

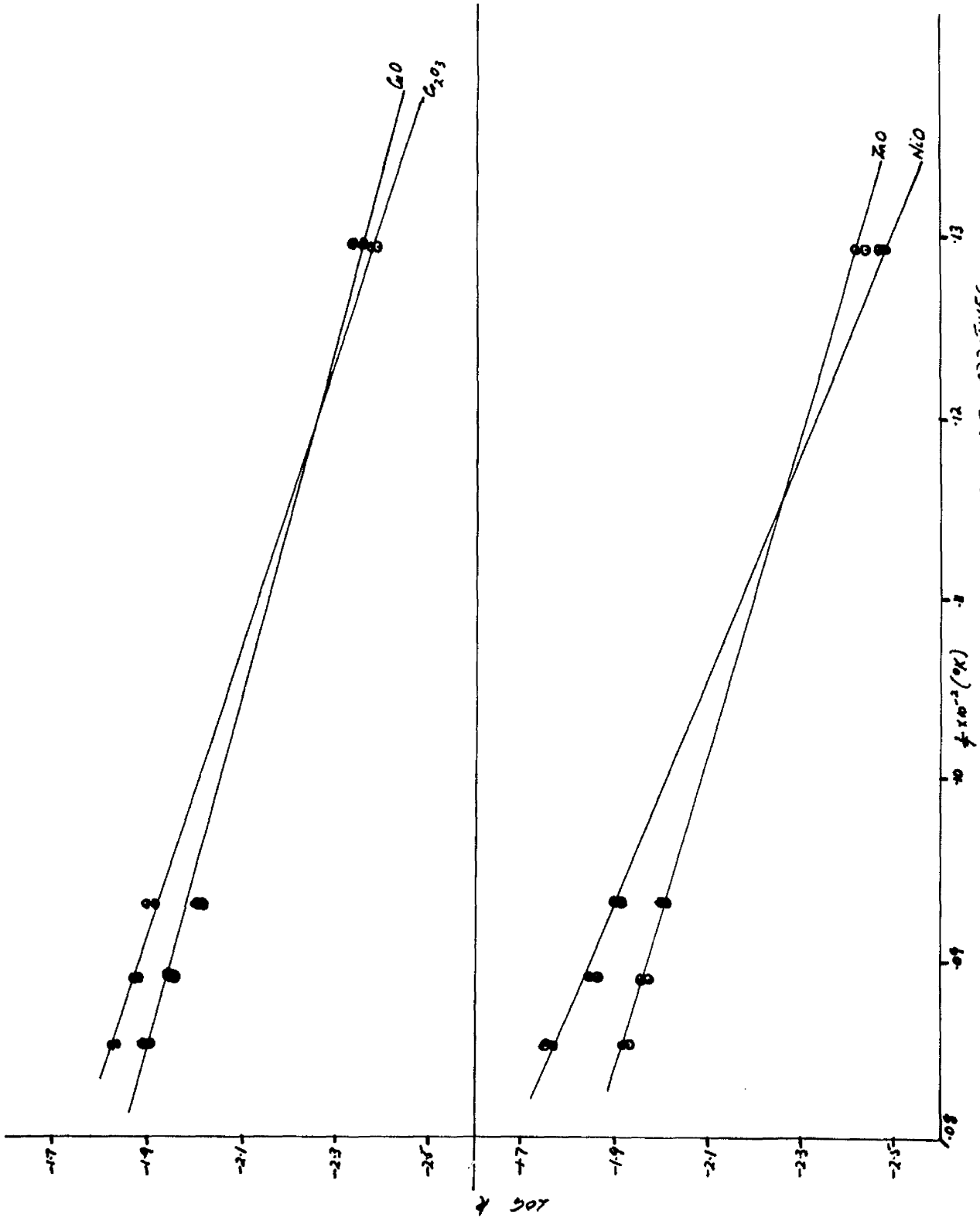


FIG (3.19) ARRHENIUS PLOTS FOR A SELECTION OF OXIDE ADDITIVES.

At the end of each experiment, the remaining oxide was separated from the xerogel by sieving. For the three high temperature examinations, i.e. 800, 850 and 900° for all additive systems, sieving revealed that shrinkage of the xerogel particles had occurred. Although those observations were purely empirical and secondary, the degree of shrinkage seemed to be connected with the extent of crystallisation of the spheroids, this being greatest for additions of  $Al_2O_3$  and  $Cr_2O_3$  at 900°. X-Ray powder photographs showed that there was no interaction between the gel and oxides at 500°, and in fact, the patterns were very weak below 900°, (ca. 8% w/w of material required before detection by X-rays). It has been shown in this department over the past two years that in general, our X-ray equipment will only show a material diffraction pattern when 8% or more of that material is present. However, at 900° a reproducible pattern of lines was obtained. It was interesting to note that the d-values obtained did not exactly conform to listed values for the silicates which are likely to be formed.

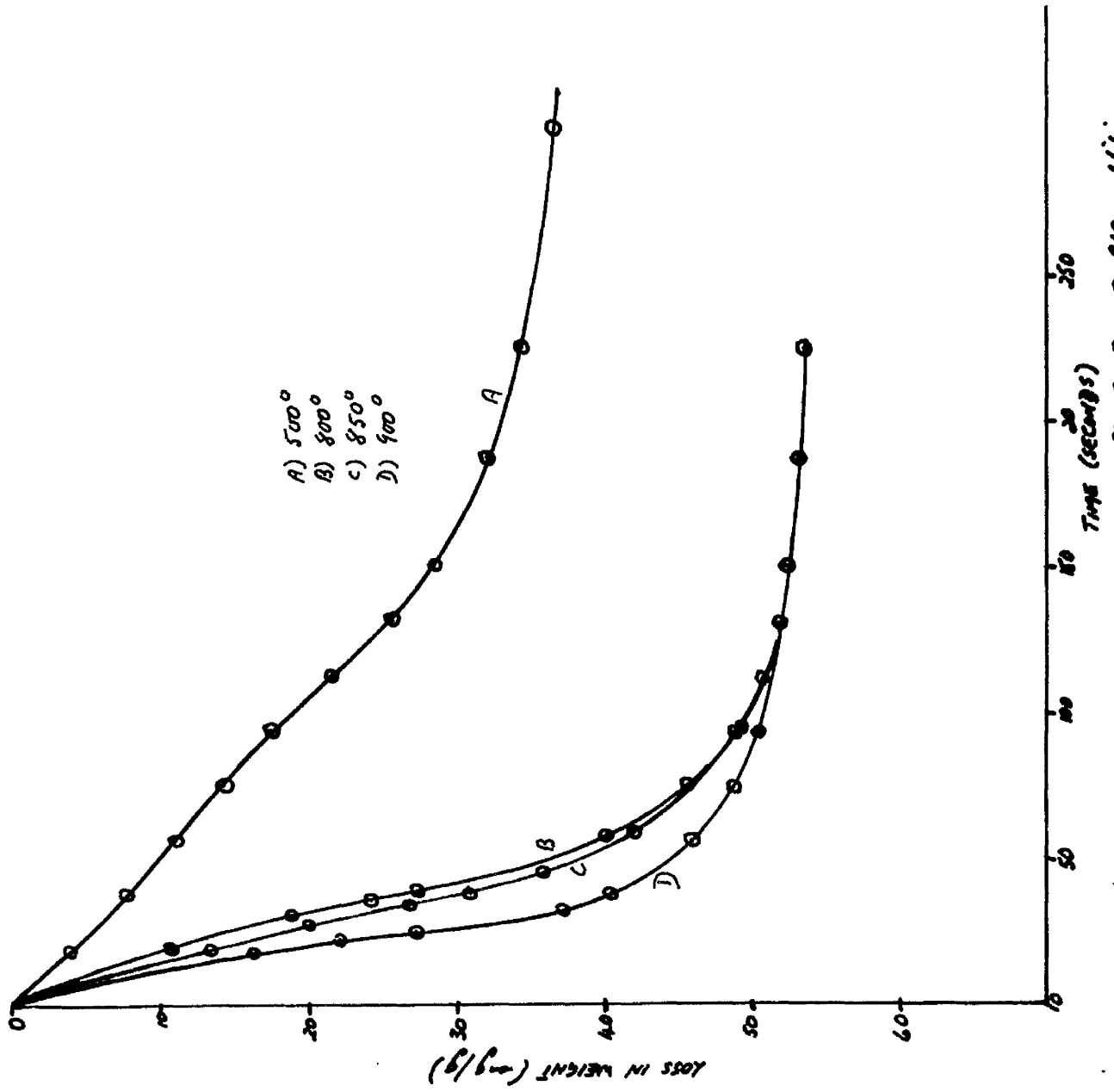


FIG. (3.20) DENATURATION CURVES IN PRESENCE OF CO additive

In this connection it is important to note, that at certain concentrations of additives in other silicate systems, no X-ray pattern has been observed. Milliken et al<sup>50</sup> have shown that in a calcined silica alumina mixture containing 2% alumina, a clear pattern for cristobalite was observed. On increasing the percentage of alumina, the pattern became weaker, and at 15% alumina disappeared completely. Milliken explains this by considering that the stabilising effect which silica exhibits for the alumina structure is dependent on the relative micelle size of the silica and alumina components, and on the amount of alumina present. Increasing the alumina content reduces the relative amount of alumina in contact with silica. Thus, much of the alumina in silica-alumina mixture of high alumina content cannot be influenced by the silica.

#### Silica gel + CdO

The dehydration reaction in the presence of CdO was unique in several aspects, compared to that of the other oxides examined. The weight loss curves

shown in fig.(3.20) illustrate two points. Firstly, the plot for 500° shows that there was a greater amount of dehydration than for any other oxide system examined at this temperature. The second feature shown is that for the higher temperatures, the initial rate of dehydration was in the order 900° > 850° > 800°, but after a relatively short time (ca. 100 seconds), the weight lost reaches the same equilibrium value at each temperature.

The xerogel spheroids which had been in contact with CdO at the higher temperatures were opaque, and there was very little unattacked CdO, if any, left in the reaction vessel at the end of the experiment. [In the other cases, the xerogel spheroids remain clear except for the crystallisation (ca. 10-20%) mentioned previously].

X-ray photographs yield d-values of 4.1090, 2.8117, 3.1420, 2.9582, 2.8560, 2.6993 and 2.4985 from the lines of greatest intensity for the sample heated to 900°. Cadmium oxide was heated alone to 1000° with no perceptible change in the material. It must therefore be concluded that some well-defined

solid-solid interaction was taking place, very soon after the Tamman temperature had been surpassed.

From this short investigation it was not possible to ascribe any definite kinetic data for this system.

Physical properties

Table (3.13) shows the values of surface area and bulk density for the mixed oxide systems.

Table (3.13). Physical measurements of spheroids after oxide additions

<u>Oxide</u>	<u>Temp. (°C)</u>	<u>Surface area (m<sup>2</sup>/g)</u>	<u>Mercury density (g/c.c.)</u>
	500	513	-
CuO	800	447	1.112
	850	400	1.224
	900	256	1.432
Al <sub>2</sub> O <sub>3</sub>	500	578	1.035
	800	443	1.127
	850	338	1.376
ZnO	900	240	1.452
	500	558	1.007
	800	483	1.201
Cr <sub>2</sub> O <sub>3</sub>	850	446	1.308
	900	370	1.416
	500	-	1.140
Cr <sub>2</sub> O <sub>3</sub>	800	459	1.171
	850	338	1.351
	900	287	1.418

Table (3.13). (contd.). Physical measurements of spheroids after oxide additions

<u>Oxide</u>	<u>Temp. (°C)</u>	<u>Surface area (m<sup>2</sup>/g)</u>	<u>Mercury density (g/c.c.)</u>
	500	575	1.057
BeO	800	451	1.129
	850	390	1.305
	900	240	1.348
	500	-	1.203
NiO	800	453	1.238
	850	428	1.239
	900	373	1.415
Gel alone	500	632	1.021
	800	444	1.200
	850	394	1.314
	900	276	1.474
CdO	500	591	1.036
	800	485	1.088
	850	397	1.249
	900	336	1.324

The physical measurements once again showed the expected trend, viz. fall in surface area and increase in bulk density, consistent with bulk movement of the solid around the Tammann temperature.

### Section III

#### Effect of selected halides on the dehydration of silica xerogel.

Previous work,<sup>53</sup> showed that alkaline-earth halides catalysed the dehydration. A brief study was therefore made to investigate the effect of some alkali halides and several transition metal halides on the dehydration.

##### (a) Transition metal halides

When transition metal halides were heated with gel spheroids on the thermal balance, there was a continual loss in weight even after two hours in some cases. It was thus presumed that a large percentage of this weight loss was due to HCl gas and several experiments were conducted with a view to determining this.

##### Examination of Gaseous Reaction Products

The method consisted of heating a mixture of gel plus halide to around 500° in a horizontal furnace. Nitrogen was bubbled over the sample and then through a known volume of standard sodium hydroxide. Volumes of this sodium hydroxide were taken and titrated

with hydrochloric acid and against silver nitrate (after acidification with nitric acid).

A typical calculation is shown for the addition of  $\text{NiCl}_2$  as 5 g. ion %  $\text{Ni}^{2+}$  to gel spheroids:

80 ml. NaOH taken

Wt. of  $\text{NiCl}_2 = 0.29 \text{ g.}$       Wt.  $\text{SiO}_2 = 0.854 \text{ g.}$

(a) 15 ml. NaOH (before heating)  $\equiv 16.2 \text{ ml. } 0.1033\text{N HCl}$   
15 ml. NaOH (after heating)  $\equiv 13.75 \text{ ml. } 0.1033\text{N HCl}$   
Difference (due to absorption of HCl)  $\equiv 2.45 \text{ ml.}$

$$\begin{aligned} \text{.}^\circ \text{. Cl}^- \text{ from HCl evolved} &= \frac{80 \times 2.45 \times 35.5 \times .1033}{15 \times 1000} \\ &\equiv \underline{0.04792 \text{ g.}} \end{aligned}$$

(b) 15 ml. NaOH (neutralised)  $\equiv 2.6 \text{ ml. } 0.1002\text{N AgNO}_3$

$$\begin{aligned} \text{.}^\circ \text{. Cl}^- \text{ from chloride in solution} &= \frac{80 \times 2.6 \times 35.5 \times .1002}{15 \times 1000} \\ &\equiv \underline{0.0493 \text{ g.}} \end{aligned}$$

.°. %  $\text{Cl}^-$  (from original  $\text{NiCl}_2$ ) recovered as HCl

$$\begin{aligned} &= \frac{.04792 \times 100 \times 129.6}{70.91 \times 0.29} \\ &= \underline{30.2\%} \end{aligned}$$

From the other transition metal chlorides added to the gel, the recovery as percentage chloride was as follows:  $\text{CrCl}_3$ , 80.84%;  $\text{CuCl}_2$ , 40.38%; and  $\text{CoCl}_2$ , 24.52%. This type of experiment confirmed

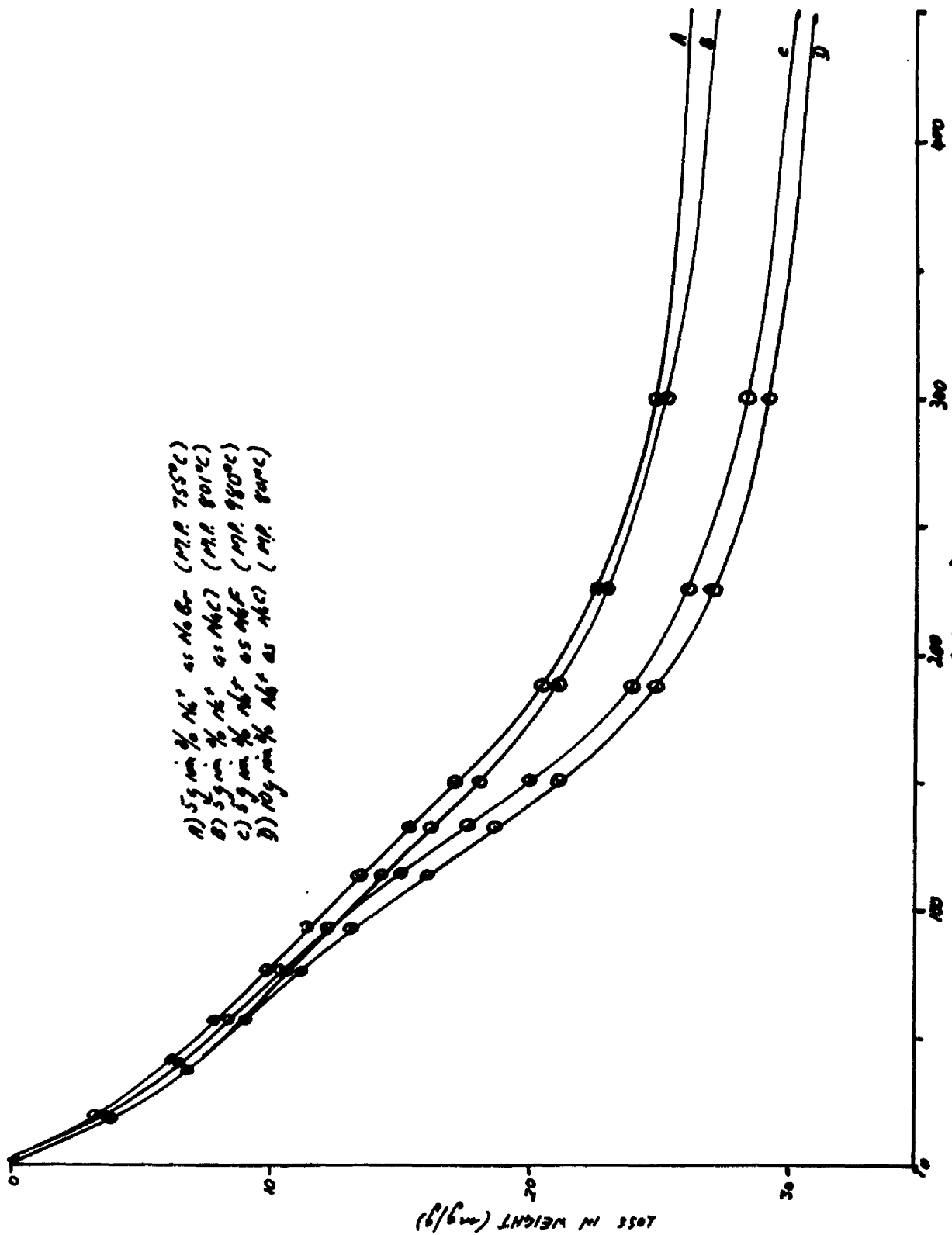


FIG. (3.21) DEHYDRATION CURVES FOR 2000-2500 ÅM SODIUM SALTS IN PRESENCE OF SODIUM CHLORIDE ADDITIVES.

that a large amount of the weight loss was due to the evolution of HCl.

An attempt was made to obtain some structural evidence on the xerogel spheroids heated at 500° in the presence of selected transition metal halides, using infrared, far infrared, and ultraviolet reflectance spectra, but virtually no information was obtained. The ultraviolet was, if anything, the most helpful but merely showed the presence of the metal. However, it was impossible to distinguish whether the metal was present as the chloride, oxide or even a mixture. It was also impossible to determine whether the environment of the metal was tetrahedral or octahedral. The transition metal halides used as additives were NiCl<sub>2</sub> (m.p. 1001°), CuCl<sub>2</sub> (m.p. 498°), CrCl<sub>3</sub> (m.p. 1150°) and CoCl<sub>2</sub> which sublimes at greater than 500°. The conclusion which may be drawn from such systems is that solid solutions are readily formed.

(b) Alkali halides

The sodium halides did not appear to show any great differences in the rates of dehydration as

illustrated in fig.(3.21), though their effect was manifest in the physical properties listed in table (3.14). X-Ray powder photographs did not produce any <sup>NEW</sup> lines from all of the samples examined. On the other hand, lithium halides showed marked differences in the dehydration rate; this difference appearing to be some function of the melting point of the halide (fig.3.22).

In the case of LiBr, the sample was still losing weight when the experiment was terminated. Examination of the spheroids on cooling showed that a large percentage were white, while the rest retained their original glassy appearance.

X-Ray powder photographs on the white spheroids yielded d-values of 4.8086, 3.6637, 3.3580, 2.7393, 2.4215 and 2.3613 from the lines of greatest intensity. These values corresponded to a lithium silicate, the composition of which was unknown. The A.S.T.M. d-values for this lithium silicate were 4.85, 3.39, 2.74, 2.50, 2.35, 2.11.

An attempt to calculate the recovery of  $\text{Br}^-$  similar to the transition metal halides showed only 0.7% of the weight loss was due to evolution of HBr,

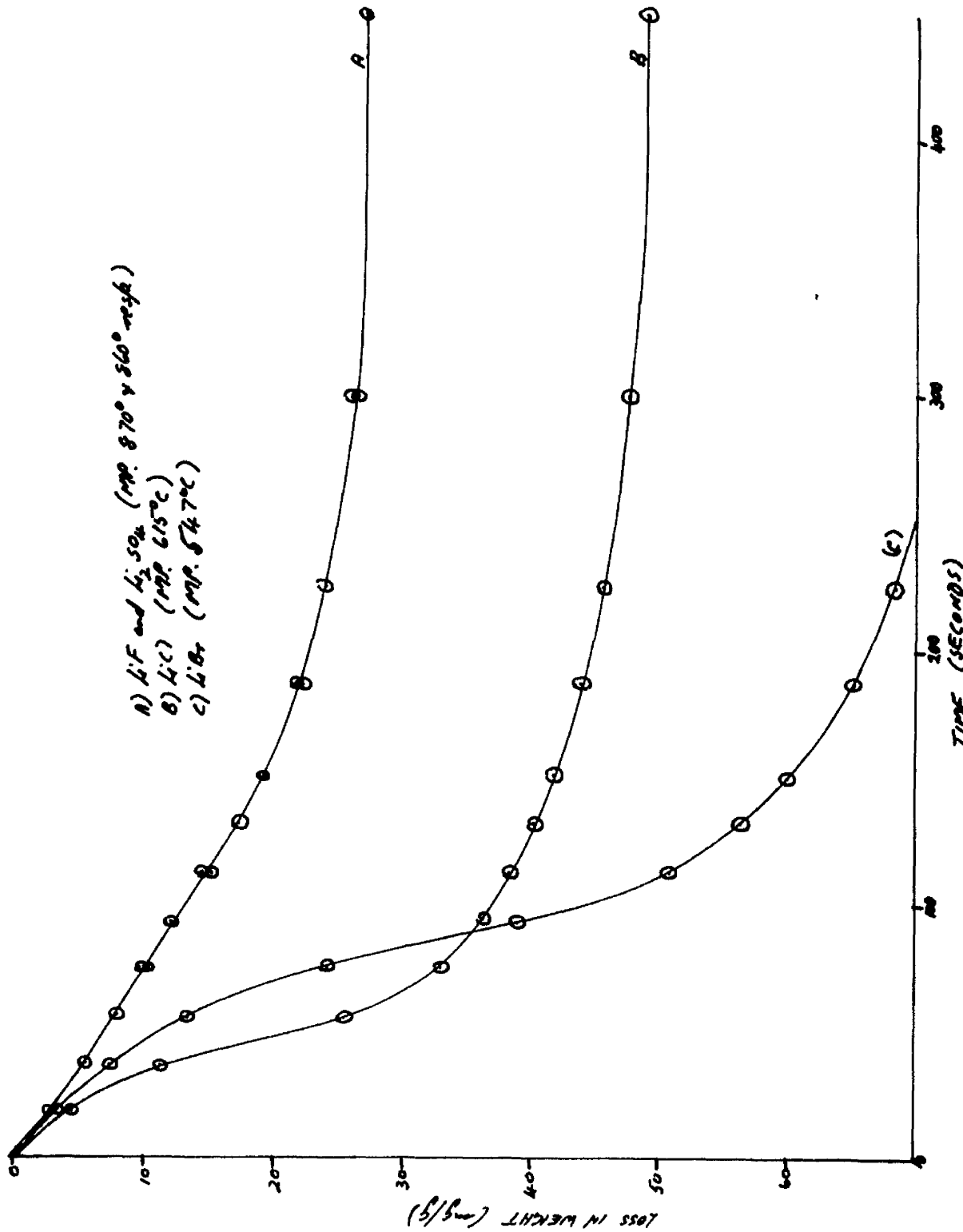


FIG. (3.22) DEHYDRATION CURVES FOR 200-841 $\mu$  SPHEROIDS IN PRESENCE OF LITHIUM HALIDE ADDITIVES.

and that some other mechanism was therefore responsible for the continuing loss in weight.

One possibility may be that the continuous weight loss was due to distillation of LiBr. If this is the case, only part of the weight loss will be due to the normal dehydration process.

The physical properties for the lithium halide experiments are also shown in table (3.14).

Table (3.14). Physical properties of the gel in presence of selected halide additives after treatment at 500°.

<u>Additive</u>	<u>g. ion % metal ion</u>	<u>S.A. (m<sup>2</sup>/g)</u>	<u>Hg. (g/cc)</u>	<u>M.P. (°C)</u>
NaCl	5	562	0.8858	801
NaCl	10	509	0.9120	801
NaBr	5	430, 457	0.8072, 0.8651	755
NaF	5	528	0.8938	980
LiF	5	425	0.8215	870
Li <sub>2</sub> SO <sub>4</sub>	5	466	0.8226	860
LiCl	5	439	0.8581	613
LiBr	5	346	0.8532	547

## CHAPTER IV

### Discussion

The amount of thermal dehydration of silica xerogel achieved by temperature increase is consistent with surface area loss, pore collapse and density increase. Such effects are recognised consequences of sintering processes. Mechanisms of sintering have been suggested by several workers<sup>10-13</sup> and these mechanisms are generally based on a breakdown of the process into several stages. Thus Coble<sup>12</sup> subdivides the process into three stages, viz. (a) initial, (b) intermediate and (c) final (p.2). Photomicrographs (X20, X40 and X100) of xerogel spheroids showed that they had begun to coalesce in runs (with no additive) at around 950-1000°C. Hence a point near the end of the initial stage of sintering had been reached.

In contrast, however, to explanations of the sintering behaviour of metals<sup>10,11</sup> - which can be related purely to change of surface free energy - chemical interaction has to be considered in the case of silica xerogel. Previously, chemical sintering

has been shown to be the preferred process in studies of Berthollide compounds.<sup>59</sup> With zinc oxide an activation energy value of 18.0 k cal.mole<sup>-1</sup> was obtained, and the schematic model for chemical sintering of this oxide led to an equation similar to that of Erofojev<sup>49</sup> and Avrami<sup>50</sup> which fits the experimental data for silica xerogel. At the same time, classical rate laws for chemical elimination reactions fit the xerogel data, also. Rate constants, at various temperatures, calculated from the two equations led in every example to excellent agreement on the value of the activation energy. Thus with 2000-841  $\mu$  spheroidal xerogel the value of  $E_A$  was 9.4 k cal.mole<sup>-1</sup>.

Considering also the low temperature employed here it seems reasonable to expect that most information concerning the sintering should be inferred to be via chemical elimination reactions. This was, of course, confirmed by the thermokinetic experiments and by the obvious link between the degree of surface dehydration of the xerogel and its surface area and bulk density.

Essentially the dehydration may be considered as an elimination of  $H_2O(v)$  from-neighbouring silanol groups.

These could be in adjacent positions on the same particle surface, or at the higher temperature when coalescence sets in, on neighbouring particles.<sup>33</sup>

The dehydration may be represented as:-



In this representation, equation (4.1) denotes the dehydration of a single corpuscle and equation (4.2) that for different corpuscles and/or the situation which allows dehydration across a narrow capillary.

The dotted lines denote bonding of the reacting silicon atoms through a single oxygen atom or through several surface Si-O tetrahedra of the same corpuscle.

This would represent the first complete reaction stage and omits consideration of the formation and possible nature of any intermediate surface complex involving the silanol groups.

In the next step, water has to be desorbed into the vapour phase:-



Reaction such as (4.3) are often found to be rate controlling in many studies of the gas/solid interface. For example, in the decomposition of  $\text{N}_2\text{O}$  on cuprous and other similar oxides, Hauffe<sup>67</sup> has shown that the slow step is the desorption of products from the oxide surface.

This could also be the case in silica xerogel dehydration. It is worth noting that the activation energy for the desorption of water from similar silica xerogel surfaces<sup>61</sup> is 4.5-5.5 k cal.mole<sup>-1</sup>. This is similar to the activation energy of dehydration found for the smallest microspheroids using the Avrami-Erofeyev rate constants (5.6 k cal.mole<sup>-1</sup>). However, particle geometry and contact area cannot be excluded from these considerations. This is emphasised by the differences in the degrees of dehydration obtained at the same temperature for different particle shapes (Table 3.1) and also by the increase of activation energy to 9.4 k cal.mole<sup>-1</sup> with an increase in particle size range from 841-420 $\mu$  to 2000-841 $\mu$ .

A plot of the k values (table 3.2) against temperature for 200-841 $\mu$  and 841-420 $\mu$  xerogels,

cross at around 800°C. This might mean that surface contact effects of the gel are being obscured, and are now playing a minor role to the bulk or body dehydrations. This is a particularly interesting point since it shows up at the Tamman temperature, and thus leads to the conclusion that particle size effects might only be important below 800°C.

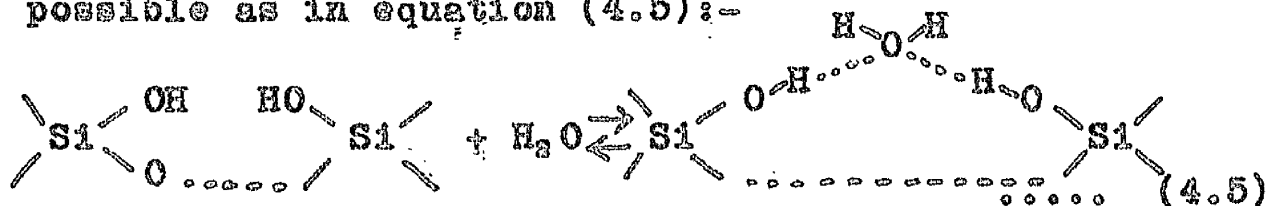
If we note the classical expression:-

$$k = A \exp (-E_A/RT) \quad \dots\dots\dots (4.4)$$

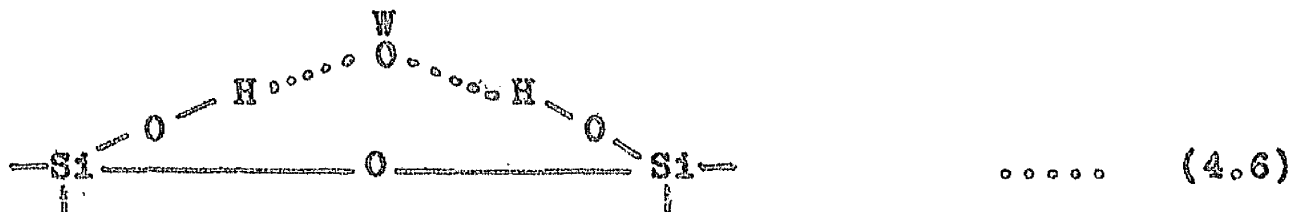
then these curves seem to show a "compensation effect" between  $E_A$  and  $A$  below 800°C, which could well be explained on a "points of contact" theory.  $A$  the frequency factor being related to "points of contact" will have a greater value for the smaller size range, which has the lowest activation energy  $E_A$ . Thus a small  $E_A$  is "compensated" by a high  $A$  and vice versa.

In the experiments in which sodium tungstate was used as an additive, the amount of dehydration of the xerogel at any specific temperature increased, and the activation energy was lowered. That this was primarily a catalytic effect below 800°, was confirmed by the almost 100% recovery of the sodium tungstate in

several selected runs, and to a lesser extent by the X-ray data. Kiselev<sup>62</sup> has shown that for the adsorption of methanol and water, formation of double hydrogen bonds on the surface of the gel is possible as in equation (4.5):-

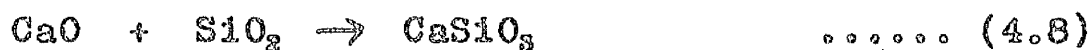


Thus in the tungstate experiments it is feasible to postulate the tungstate being similarly involved in hydrogen bonding giving rise to an intermediate complex structure of the type



It is known that the Si-O-Si distance is 3.28 Å.<sup>63</sup> Hydrogen bonding between the hydroxyl groups of the gel and oxygen atoms of the WO<sub>6</sub><sup>-</sup> octahedron is a possibility since the O-H distance would be well within the limit set by Pauling<sup>60</sup> for such bond formation. Specifically it appears that the dehydration is catalysed by the presence of small amounts of "sodium tungstate vapour", as shown by the vapour experiments. Although the vapour

catalyses the reaction to a much smaller extent than in the solid contact cases, poor vapour mixing with, and penetration through the solid, could account for these differences. Weisz<sup>63</sup> has suggested previously that many so-called solid/solid reactions are in fact controlled by solid/vapour contact much as enunciated here. Examples of note,<sup>15,16,60</sup> in which solid vapour contact has a controlling effect on the reactions between solids are:-



in which the presence of water vapour causes accelerations of 22-fold and 8.5 fold, the effect being manifested on the term  $k_0$  only, in the rate constant  $k = k_0 e^{-E/RT}$ .

Anhydrous sodium tungstate melts at 698° and according to Spitsyn<sup>64</sup>, it is only at around 1200° that it begins partially to decompose. However, dehydration of  $\text{Na}_2\text{WO}_4 \cdot 2\text{H}_2\text{O}$  may give rise to a mixed oxide system  $\text{Na}_2\text{OWO}_3$ . Such a system could act synergetically on the xerogel with the  $\text{Na}_2\text{O}$  acting

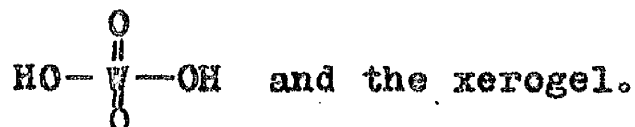
as the principal "water getter". This would explain that at 500°C, the dehydration rate for tungstic oxide additions was 30 mg./g. and for sodium tungstate additions it was 33.5 mg./g. after 300 seconds in both cases.

Tungstic oxide, itself, has a high chemical affinity for water, as shown in the work of Glemser and Wendlandt.<sup>95</sup> Thus, at 1323°K, these workers have shown that the reaction:-



proceeds readily. The amount of  $\text{WO}_3$  transported as the gaseous oxide is high. Polynuclear oxides have been detected in the vapour above solid  $\text{WO}_3$ .

Glemser and Wendlandt state that in the reaction  $\text{WO}_3(\text{s})$  with  $\text{H}_2\text{O}(\text{g})$  it would be possible to have a ring structure with a coordination number 5 for the tungsten atom or a non-linear chain formula with a coordination number 4. They also propose that a coordination number of 4 for all the tungsten atoms is attained in the monomer  $\text{WO}_2(\text{OH})_2$  and this represented the most probable formulation. Hence it would be possible for several intermediate structures to exist involving hydrogen bonding between the monomer



Therefore, it seems entirely possible that sodium tungstate does act synergetically and that intermediate hydrates are formed by both the  $\text{Na}_2\text{O}$  and  $\text{WO}_3$  components. The increase in dehydration rates due to the two components will, of course, be superimposed on each other. The contributions that the components make to the acceleration would be extremely difficult to separate.

The kinetics of the dehydration in the mixed tungstate experiments are best described by a half order relationship. The rates of dehydration are greater than in the absence of tungstate. After 300 seconds at  $500^\circ\text{C}$ , the rate in the presence of tungstate is  $33.5 \text{ mg./g.}$  and in its absence  $20.1 \text{ mg./g.}$  Kinetic relationships such as these could be explained if two adjacent silanol groups were involved in formation of a single intermediate complex with the additive, as suggested by equation (4.6). Thus a terminal  $\text{W-O}$  bond could be involved in hydrogen bridge formation with two adjacent silanols. Similar formations have been suggested to explain

the stoichiometry of tartrato-tungstate complexes,<sup>66</sup> involving hydrogen bonding between carboxyl and terminal W=O groups. Elimination of water across the bridge could then occur by several mechanisms. These would all involve a final water desorption step into the vapour phase. Generally, in solid-solid reactions, the direction and driving force of a reaction are measured by the free energy which can be expressed in terms of the lattice or crystal energy of the constituents.<sup>69</sup> The reactivity will be enhanced by such factors as heat, structure rearrangement at transition temperatures, ionic distortion, solid solutions etc., which will weaken the inter-ionic forces. Thermodynamically for the oxide systems studied, it appears that the lattice energy of the final 'compound' formed between the oxide and the gel is greater than the lattice energy of the gel alone.

It is known<sup>68</sup> in a mixed oxide system, that one possible cause of the activity may be the value of the potential energy of the oxide mixture in relation to that of its products. For such, we do not have a reaction which proceeds discontinuously,

but through intermediate states which are not the original system nor yet the final products.

The activation energies for the oxide additions were

CuO,  $4.8 \pm 0.1$ ; NiO,  $7.2 \pm 0.1$ ;  $\text{Cr}_2\text{O}_3$ ,  $5.8 \pm 0.1$ ;  
BeO,  $5.4 \pm 0.2$ ; ZnO,  $5.2 \pm 0.1$  and  $\text{Al}_2\text{O}_3$ ,  $4.8 \pm 0.1$   
k cal.mole<sup>-1</sup>.

Examination of the activation energies do not in general show any great differences due to valency or to the effects of free d-orbitals. However, the results do lead to another possible explanation based on a classification of the oxides as insulators and semiconductors.

Insulator oxides such as  $\text{Al}_2\text{O}_3$  and BeO appear to owe their activity to their surface acidity.<sup>60</sup> They are usually used as porous particles or as a gel and it appears essential to have a mixture of the oxides for catalytic activity.<sup>70</sup>

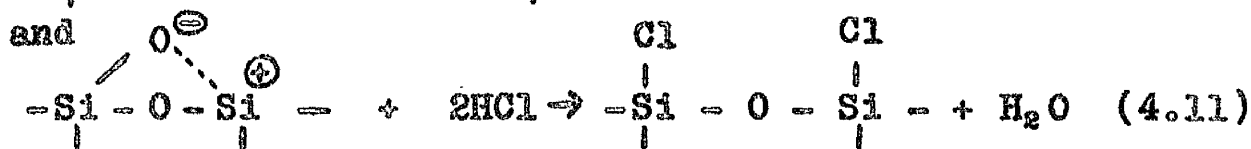
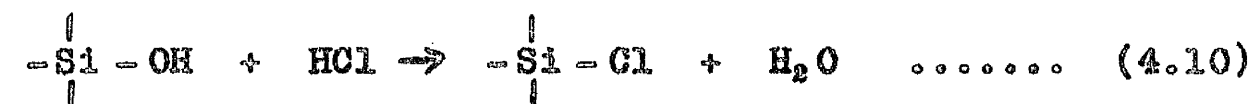
It is known that with semiconductor oxides, molecules are often adsorbed (with or without dissociation) as surface ions.<sup>71</sup> These oxides all have ionic crystals and may be classed as n- or p-type semiconductors. It has been shown by Wagner<sup>72</sup>

for nitrous oxide decompositions, that the least active oxides are all negative hole semiconductors such as ZnO and  $\text{Al}_2\text{O}_3$ , with intrinsic semiconductors such as  $\text{Cr}_2\text{O}_3$ , having approximately the same activity. The present studies have shown that the p-type semiconductor NiO was very ~~much~~ different from the other oxides, and this is ascribed to the presence of certain types of lattice vacancy. This suggestion does not take into account the activation energy ( $4.8 \pm 0.1 \text{ k cal.mole}^{-1}$ ) for the intrinsic semiconductor CuO, especially as Schmid and Keller<sup>73</sup> have shown that the activity of oxides in  $\text{N}_2\text{O}$  decomposition is in the order  $\text{CuO} > \text{NiO} > \text{Al}_2\text{O}_3 > \text{ZnO}$ . However, this discrepancy in the present results may be due to the presence of very small amounts of cuprous oxide on the cupric oxide surface which would greatly affect the activity. This becomes apparent from the work of Dell et al<sup>74</sup> on the carbon monoxide/oxygen oxidation reaction.

The present work has shown that CdO additions are most active in attacking the xerogel. Apart from  $\text{Cu}^{2+}$ , the  $\text{Cd}^{2+}$  ion is the largest of all the cations used. CdO is a defect lattice which

crystallises in the sodium chloride structure. It is also oxygen deficient, i.e. an n-type semiconductor. Thus it may act as a reducing agent on the gel; stripping oxygen from  $\text{Si(O)}_n$  groups into vacant anion sites in the CdO lattice, while  $\text{Si}^{4+}$  ions could also be accommodated in interstitial positions. This would be expected to happen at the surface of the gel spheroids giving a cadmium oxide rich layer on the spheroid surface. This is a possible explanation of the anomalous results obtained using CdO additions. Some of the difficulty in interpreting the present results may be due to impurity levels in raw materials. Roberts<sup>75</sup> et al have already shown that because of such impurities, the observed effects of additives on sintering rates cannot be consistently interpreted in terms of changes of defect structure according to the valence of the additive.

Examination of the gaseous products using the horizontal furnace showed that HCl was liberated in the reactions of transition metal chlorides with the gel spheroids. As shown by Bavarez's<sup>76</sup> experiments with anhydrous HCl on outgassed silica gel there are two possible simultaneous mechanisms, viz.,



At first the acid will react with all the accessible hydroxyl groups on the surface, and then will attack the 'double oxygen bridges'. Bavarez<sup>76</sup> showed that the hydrogen chloride attacked the hydroxyl groups more readily than the oxygen bridges. However, as siloxane bridges will be formed during the heat treatment (4.1), then reaction (4.11) takes over from (4.10). Thus the combination of both reactions probably accounts for the greater and continued loss in weight which was observed with the transition metal halide additives. This suggested mechanism is unlike the one proposed earlier for alkaline-earth halides above 800°,<sup>33</sup> and in fact, X-ray powder photographs showed a variety of diffuse lines but did not give a clear mechanistic picture. For the cupric chloride additive, X-rays showed that there tended to be cuprous chloride present in the spheroids.

As stated previously, the sodium halide additives did not show any great differences in their rates of dehydration. However, with the smaller cation Li<sup>+</sup>

(0.60 Å as compared to Na<sup>+</sup> 0.95 Å), the rate of dehydration appeared to show that the lower the melting point of the halide, the greater was the amount and rate of dehydration. The fact that the smaller molecule will more readily reach accessible sites of adjacent silanol groups, combined with the greater mobility of the lithium halides from LiF to LiCl to LiBr accounts for the dehydration increasing in the order LiBr > LiCl > LiF.

The results of the lithium bromide experiments are not totally explained by the above suggestions or the proposals put forward for the transition metal halide additives. The main reason for those hypotheses being unsuitable, is that X-ray photographs show that a lithium silicate is clearly formed as low as 500°. For some reason it appears that it is much easier for the lithium ion from lithium bromide to enter the coordination sphere of silicon in the gel.

The difficulties in this type of work are observed from the results of several workers<sup>77,78,79</sup> as well as the present investigation. The types of processes involved seem to depend on the 'affinities' which the reactants (particularly the oxides) have for

each other, this being purely an experimental observation. Many such catalytic reactions involve dissociative adsorption of the reactants and it would be of interest to determine the extent of such a step in similar systems. A suitable set of experiments for this type of determination would include oxidations taking place upon oxide surfaces. Dissociative adsorption could then be followed using isotopes to follow any exchange of oxygen between the reactants. At the same time, investigations of the mode of dehydration of similar gelatinous oxide systems, e.g. alumina and titania, would add further information to the present data obtained with silica xerogel. Such studies should yield patterns of additive activity which might be expected to clarify some of the less tractable phenomena observed in this work.

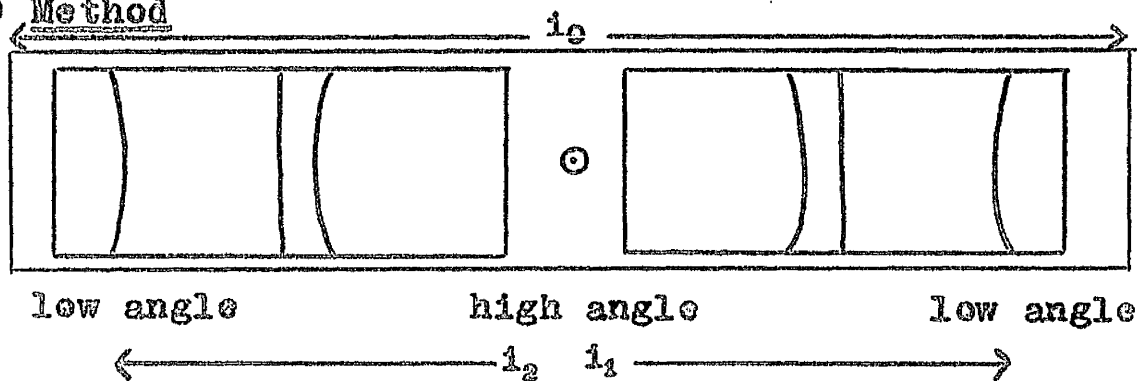
APPENDIX

I. Programme 1.

Data from X-ray photographs computed on Ferranti-Sirius COMPUTER

Values of  $\theta$ ,  $\sin^2 \theta$ , d-spacing and  $\sin \frac{\theta}{\lambda}$  are calculated from line position measurements taken from Debye powder photographs obtained using a Van Arkel type camera. It is possible to suppress the printing of  $\sin \frac{\theta}{\lambda}$  if this is not required.

(1) Method



The programme calculates the data by reading in measurements for each line one at a time. If  $\phi$  is the camera constant,  $\lambda$  the X-ray wavelength,  $i_0$  the distance between the knife edges,  $i_1$  and  $i_2$  the left and right hand line readings respectively ( $i_2 > i_1$ ), then

$$\theta = [\pi - (i_2 - i_1) \times \phi / i_0] \times 57.295 \text{ degrees}$$

$$d = \lambda / 2 \sin \theta$$

(2) Data required

The programme requires the following data, in order:

- (i) camera constant: one quarter of the angular distance in radians between the knife edges of the camera (i.e. about 1.5).
- (ii) X-ray wavelength: to be used in calculating d-spacings.
- (iii) Knife edge readings: smaller reading first
- (iv) Line data: an integral estimate of the line intensity followed by two line position readings are needed for each line. The intensity can be any integer from 0 to 9999. The line position readings must have the smaller one first for each line, and it is necessary to measure from low to high angle systematically.
- (v) End of data: the last line measurement must be followed by the warning character L, and the last set of data by Z.

(3) Output

The results are printed out in tabular form under the following headings:

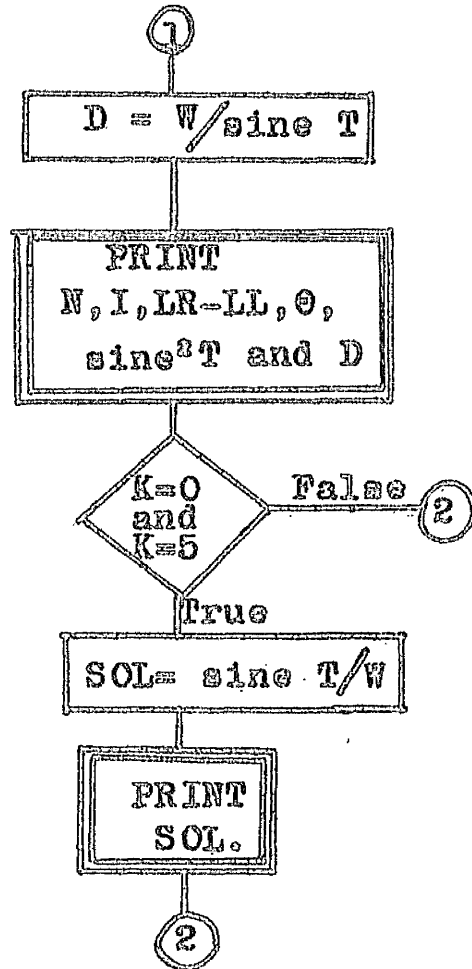
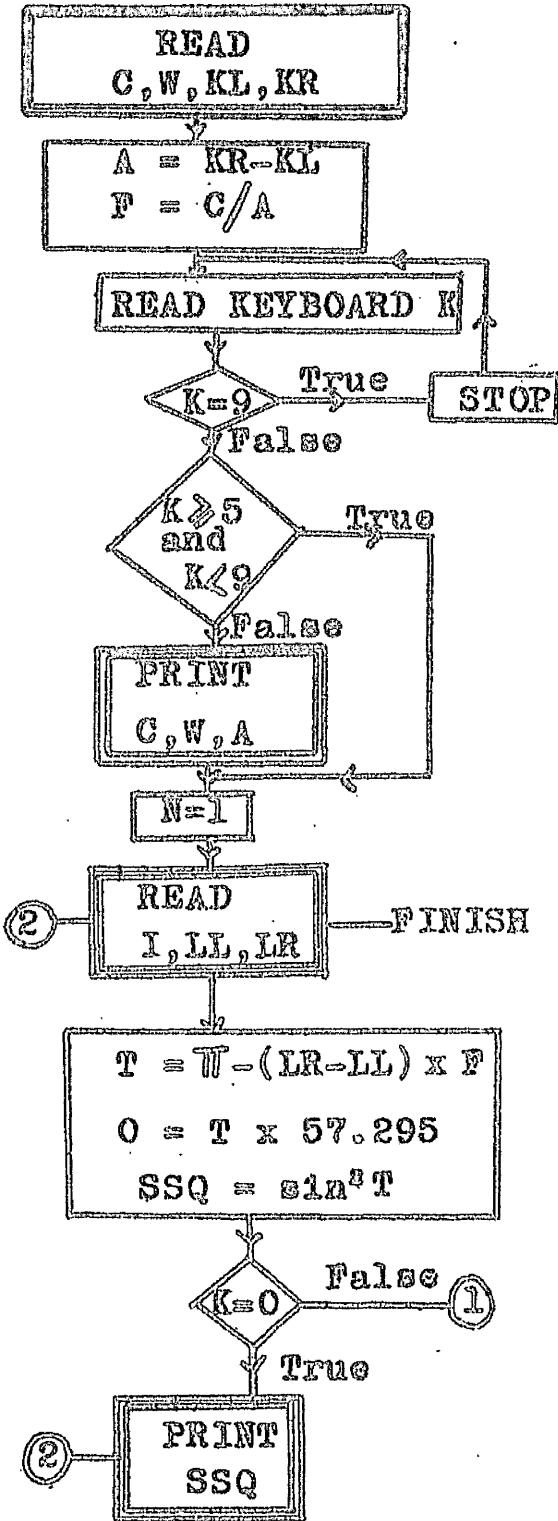
LINE	lines are numbered in order.
INT.	copied directly from the input tape.
DIFF.	distance between lines of diffraction cone, to 3 decimal places.
THETA	Bragg angle to 3 decimal places in degrees.
SIN TH.SQ.	$\sin^2 \theta$ to 5 decimal places.
D-VAL.	d-spacing to 4 decimal places in the same units as $\lambda$ .
SIN TH. L	$\sin \theta / \lambda$ to 3 decimal places.

The most significant digit ( $D_0$ ) of the keyboard may be set to have the following effect:

$D_0$	Effect
0	All data is punched out
2	$\sin \theta / \lambda$ is suppressed
5	All printing except $\sin^2 \theta$ is suppressed.
9	Computer stops and proceeds on resetting keyboard and pressing continue.

In the case of  $D_0 = 5$ , the  $\sin^2 \theta$  values are preceded by 6 inches of blank tape, and followed by L and three erases.

Flow Diagram for Programme 1



C = Camera constant

KL, KR = L.H. and R.H. knife edge readings

W = X-ray wavelength

I = intensity

LL, LR = L.H. and R.H. line readings.

II. Tables of constants used in the determination of Pore structures from Nitrogen Adsorption Isotherms.

The following tables give the constants used in equation (2.5).

Table 1

Values of  $P/P_0$ ,  $R_{12}$  and  $k_{12}$  for Standard Increments of Pore Diameter.

Pore diameter				Pore diameter			
A	$P/P_0$	$k_{12}$	$R_{12}$	A	$P/P_0$	$k_{12}$	$R_{12}$
300	0.931					1.19	1.478
			1.212	110	0.809		
290	0.929					1.30	1.518
		0.50	1.219	100	0.787		
280	0.926					1.44	1.565
		0.52	1.226	90	0.764		
270	0.924					1.60	1.624
		0.54	1.233	80	0.734		
260	0.921					1.80	1.696
		0.56	1.241	70	0.696		
250	0.918					2.08	1.791
		0.58	1.249	60	0.646		
240	0.915					2.44	1.917
		0.60	1.258	50	0.578		
230	0.911					1.40	2.070
		0.62	1.268	45	0.535		
220	0.907					1.56	2.180
		0.65	1.279	40	0.484		

Pore diameter				Pore diameter			
$\Delta$	$P/P_0$	$k_{12}$	$R_{12}$	$\Delta$	$P/P_0$	$K_{12}$	$R_{12}$
210	0.902					1.76	2.315
		0.68	1.291	35	0.423		
200	0.897					2.00	2.495
		0.71	1.304	30	0.350		
190	0.891					2.34	2.740
		0.75	1.318	25	0.265		
180	0.885					2.86	3.060
		0.79	1.333	20	0.168		
170	0.879					1.34	3.380
		0.84	1.350	18	0.130		
160	0.871					1.49	3.580
		0.89	1.369	16	0.090		
150	0.861					1.68	3.710
		0.95	1.391	14	0.058		
140	0.850					1.93	3.690
		1.02	1.416	12	0.035		
130	0.838					2.26	3.300
		1.10	1.445	10	0.016		
120	0.824						

Programme 2.

Data from adsorption isotherms computed on KDF9.

Value of pore volume, surface area, cumulative surface area, specific pore volume, and the derivative  $\Delta v / \Delta d$  are calculated using equation (2.5) and the constants tabulated previously.



(1) Data required

$R_{12}$ ,  $k_{12}$ ,  $(d-2t)/d^2$ , and A values given in tables I and II, corresponding to decreases in the pore diameter of 300, 290 ..... 50, 45 ..... 20, 18 ..... 10 in Å. Values of  $V/m$  from the adsorption isotherms corresponding to  $P/P_0$  values in table I.

(2) Output

The results are printed out in tabular form under the following headings:

PORE VOLUME ( $V_{12}$ )

This is the pore volume in ml.(N.T.P.)/g. corresponding to pore diameters (A) given in table I.

SURFACE AREA ( $S_{12}$ )

The values of surface area in  $m^2/g.$  are obtained by converting the values of  $V_{12}$  using the relationship

$$S_{12} = \frac{4a V_{12}}{d'} \times 10^4$$

where  $a = 1.584 \times 10^{-3}$ , the ratio of the density of gaseous nitrogen at N.T.P. to that of liquid nitrogen.  $d'$  is the mean diameter of the increment A.

CUM. S.A. ( $m^2/g$ )

This is the cumulative surface area obtained by accumulating the values  $S_{12}$ .

SP. PORE VOL. ( $V'$ )

The specific pore volume is obtained by multiplying  $V_{12}$  by 'a' ( $1.584 \times 10^{-3}$ ).

PORE DIAM.(A) Copied directly from input  
tape.

DERIVATIVE ( $\Delta v / \Delta d$ ) This is simply the specific  
pore volume divided by the  
pore diameter.

Detail of programme in algol language

```
begin array R,D,K,d,c[1:36]; integer i,j,k,h;open(30);  
open(20);  
for i:= 1 step 1 until 36 do R[i] := read(20);  
for i:= 1 step 1 until 36 do D[i] := read(20);  
for i:= 1 step 1 until 36 do K[i] := read(20);  
for i:= 1 step 1 until 36 do d[i] := read(20)  
for h:= 1 step 1 until 33 do  
begin  
begin array y,x,a,b[1:37];  
write text(30,[[ccc 15s]Tableh]);write(30,format  
([ndc]),h);  
for i:= 1 step 1 until 37 do y[i]:= read (20);  
for i:= 1 step 1 until 36 do y[i]:= y[i+1]-y[i];  
x[1]:= 0;  
for j:= 1 step 1 until 36 do  
begin a[j]:= x[j] x K[j];  
b[j]:= -y[j] - a[j];
```

```
if b[j]<0 then begin k:=j ; goto L end  
  c[j]:= b[j] x R[j];  
  x[j+1]:= x[j] + c[j] x D[j];  
  k:= j;
```

```
end;
```

```
end;
```

```
L:begin array s,v [0:36] ; real a,b ; integer Fl;  
  a:= 63.36;  s[0] := 0;  
  Fl := format([+ndd.dddsssssss]);  
  for i:= 1 step 1 until k-1 do  
    begin v[i]:= a x c[i]/d[i];  
      s[i]:= s[i-1] + v[i];  
      write(30, Fl, c[i]);  
      write(30, Fl, v[i]);  
      write(30, Fl, s[i]);  
      b:=if i<26 then 310-10xi else if i< 32 then  
        50-(i-26)x5  
        else20-(i-32)x2;  
      write(30,format([nddsssssss]), b);  
      write(30,format([d.ddd10+ndc]),(c[i]x  
        0.001584) b);  
    end;  
  end;  
  close(20);  close(30);  
  end;  
end
```

REFERENCES

1. Goodman, J.F. and Gregg, S.J., J. Chem. Soc., 1959, 694.
2. Hausner, H.H. and Dedrick, J.H., Physics of Powder Metallurgy, New York, 1951, 320.
3. Kingston, W.E. and Huttig, G.F., Physics of Powder Metallurgy, New York, 1951, 1.
4. Huttig, G.F., Kolloid Z., 1942, 98, 6; 1942, 98, 263.
5. Jones, W.D., Metal Treatment, 1946, 13, 265.
6. Clark, P.W. and White, J., Trans. Brit. Ceram. Soc., 1950, 49, 305; 1953, 52, 1.
7. Marshall, P.A., Enright, D.P. and Weyl, W.A.  
Proceedings of the International Symposium of the Reactivity of Solids, Gothenburg, 1954, 1952, 273.
8. Shaler, A.J., J. Metals, 1949, 1, 796.
9. Roberts, J.P., Metallurgia, 1950, 42, 123.
10. Kingery, W.D. and Berg, M., J. Appl. Phys., 1955, 26(10), 1205.
11. Kuczynski, G.C., Trans. A.I.M.E., 1949, 185, 169.
12. Coble, R.L., G.E. Research Lab. Reports, Nos. 60-RL-2595M and 60-RL-2594M (1960).
13. Coble, R.L., J. Am. Ceram. Soc., 1958, 41, 55.
14. Barrer, R.M., Disc. Far. Soc., 1949, 5, 326.
15. Taylor, W.W., J. Am. Ceram. Soc., 1934, 17, 155.
16. Cohn, G., Chem. Rev., 1948, 42, 527.
17. Barrer, R.M., J. Chem. Soc., 1948, 127.
18. Morey, W. and Penner, C.N., J. Am. Chem. Soc., 1917, 39, 1173.

19. Vail, J.G., Soluble Silicates (New York: Reinhold Publishing Corporation, 1952), I, 175.
20. Signer, R. and Egli, H., Rec. trav. Chim., 1950, 69, 45.
21. Iler, R.K., J. Phys. Chem., 1953, 57, 604.
22. Shapiro, I. and Kolthoff, I.M., J. Am. Chem. Soc., 1950, 72, 776.
23. Plank, C.J. and Drake, L.C., J. Colloid Sci., 1947, 2, 399.
24. Carman, P.C., Trans. Far. Soc., 1940, 36, 964.
25. Gibbs, R.E., Proc. Roy. Soc., 1925, A109, 405; 1926, 110, 443; 1927, 113, 351.
26. Ries, H.E., Advances in Catalysis, 1952, 4, 87.
27. Milligan, W.O. and Rachford, H.H., J. Phys. Coll. Chem., 1947, 51, 330.
28. van Nordstrand, R.A., Kreger, W.E. and Ries, H.E., J. Phys. Coll. Chem., 1951, 55, 621.
29. Bastick, J., Bull. Soc. Chim., 1953, 437.
30. Gregg, S.J., J. Chem. Soc., 1953, 3940.
31. Gregg, S.J., Packer, R.K. and Wheatley, K.H., J. Chem. Soc., 1955, 46.
32. Gregg, S.J. and Packer, R.K., J. Chem. Soc., 1955, 55.
33. Henry, W. and Ross, R.A., J. Chem. Soc., 1962, 4265.
34. Marisic, M.M., U.S. Patent, 2,384,217, 1945.
35. Langmuir, I., J. Am. Chem. Soc., 1918, 40, 1361.
36. Brunauer, S., Emmett, P.H. and Teller, E., J. Am. Chem. Soc., 1938, 60, 309.

37. Emmett, P.H., Advances in Colloid Science, 1942, 1, 1.
38. Hill, T.L., Advances in Catalysis, 1952, 4, 211.
39. Hill, T.L., Structures and Properties of Solid Surfaces, 1953, 384.
40. Emmett, P.H., Structures and Properties of Solid Surfaces, 1953, 415.
41. Livingston, H.K., J. Coll. Sci., 1949, 4, 450.
42. Wheeler, A., discussed at American Association for the Advancement of Science Conference on Catalysis, Gibson Island, 1945.
43. Shull, C.G., J. Am. Chem. Soc., 1948, 70, 1405.
44. Carman, P.C., Proc. Roy. Soc., 1951, A209, 69.
45. Barrett, E.P., Joyner, L.G. and Halenda, P.P., J. Am. Chem. Soc., 1951, 73, 373.
46. Cranston, R.W. and Inkley, F.A., Advances in Catalysis, 1957, IX, 143.
47. Joyner, L.G., Scientific and Industrial Glassblowing, 1944, 257.
48. Jepson, W.B., J. Sci. Inst., 1959, 36, 319.
49. Erofeyev, B.V., Compt. rend. acad. Sci. U.R.S.S., 1946, 52, 511.
50. Avrami, M., J. Chem. Phys., 1941, 9, 177.
51. Erofeyev, B.V., Proceedings of the 4th International Symposium on the Reactivity of Solids, Amsterdam, 1960, 273.
52. Jacobs, P.W.M. and Tariq Kureishy, A.R., Proceedings of the 4th International Symposium on the Reactivity of Solids, Amsterdam, 1960, 352.

53. Peyronel, G., Z. Krist., 1936, 95, 274.
54. Encyclopedia of Chemical Technology, 1954, 12, 270.
55. Huttig, G.F., Far. Soc. Disc., 1950, 8, 215.
56. Taylor, H.S., Far. Soc. Disc., 1950, 8, 1.
57. Goodman, J.F. and Gregg, S.J., J. Chem. Soc., 1956, 3612.
58. Milliken, T.H., Mills, G.A. and Oblad, A.G., Far. Soc. Disc., 1950, 8, 279.
59. Parravano, G., Proceedings of the 4th International Symposium on the Reactivity of Solids, Amsterdam, 1960, 83.
60. Jander, W. and Stamm, W., Z. anorg. Chem., 1930, 190, 65.
61. Ross, R.A. and Darlow, B.B., Nature, 1963, 198, 988.
62. Kiselev, A.V., Symposium of Colston Research Soc., 1958, 195.
63. Weisz, J., Advances in Catalysis, 1962, 13, 137.
64. Spitsyn, V.I., Zhur. Obschei Khim., 1950, 20, 550.
65. Glemser, O. and Wendlandt, H.G., Advances in Inorganic Chemistry and Radiochemistry, 1963, 5, 215.
66. Baillie, M.J. and Brown, D.H., J. Chem. Soc., 1961, 3691.
67. Hauffe, K., Advances in Catalysis, 1955, 7, 213.
68. Chemical Society special publication, London, 1958, 11.
69. Taylor, N.W., J. Am. Ceram. Soc., 1934, 17, 155.
70. Ryland, L.B., Tamele, M.W. and Wilson, J.N., Catalysis, 1960, 7, Ch.1, Ed. P.H. Emmett, Reinhold, New York.

71. Trapnell, B.M.W., Chemisorption, Butterworth, London, 1955.
72. Wagner, C., J. Chem. Phys., 1950, 18, 69.
73. Schmid, G. and Keller, N., Naturwissenschaften, 1950, 37, 42.
74. Dell, R.M., Stone, F.S. and Tiley, P.F., Trans. Far. Soc., 1953, 49, 201.
75. Roberts, J.P., Hutchings, J. and Wheeler, C., Trans. Brit. Ceram. Soc., 1956, 55, 75.
76. Bavarez, M., Bull. Soc. chim. Fr., 1964, 6, 1298.
77. Scwab, G.M. and Keratzas, A., J. Physic. Chem., 1948, 52, 1053.
78. Hedvall, J.A., Chalmers tekn. Hogskolas Handl., 1942, No.4.
79. Scwab, G.M. and Scwab-Agallidis, Kemisk Tidskrift, 1946, 58, 161.
80. Pauling, L., The Nature of the Chemical Bond., Cornell University Press, New York, 1948.

PART II

### Introduction

As modern research expands, the use of non-aqueous solvents is becoming more important in the examination of inorganic species in solution, and in the preparation of otherwise unobtainable anhydrous compounds. Many new compounds, which cannot exist in aqueous solution, are readily obtainable in a stabilised form in the absence of water. One difficulty in the crystallisation of inorganic compounds from organic solvents is that the compound formed very often contains solvent of crystallisation which is extremely difficult to remove if decomposition of the parent compound is to be avoided.

Non-aqueous solvents containing atoms with an unshared pair of electrons possess remarkable solvent properties despite having a low dielectric constant. It is well known that many salts are soluble in ether, e.g. covalent mercuric chloride and bromide; and that etherates such as  $MgX_2 \cdot 2Et_2O$  where X = Cl or Br are readily formed. Sidgwick<sup>1</sup> lists many compounds which dissolve in ether and form etherates, thus establishing the donor properties

of ether.

The solubility of salts in ether must be due to the solvation of the ions by the ether, coordination arising from the lone pair of electrons on the oxygen atom of the ether.

Silver salts are rather unique in that relatively few complexes containing a metal-oxygen bond exist. Examples of this type of metal-oxygen bond are illustrated in the work of Sharp and Sharpe<sup>2</sup> on complexes of fluoro acids and perchlorates in ether solution. Using copper powder for the displacement of silver, these authors were able to prepare cuprous fluoroborate and hexafluorophosphate. Schwarzenbach<sup>3</sup> has reported that nickel perchlorate may be obtained in solution by neutralising a suspension of nickel ammonium perchlorate in ether using anhydrous perchloric acid.

In the present work, solutions of perchlorates and tetrafluoroborates of some first row transition metals have been prepared in ether. These solutions were prepared by reacting an ether solution of the appropriate anhydrous silver salt with excess metal halide or by using stoichiometric quantities of each salt. The solutions thus obtained were then reacted

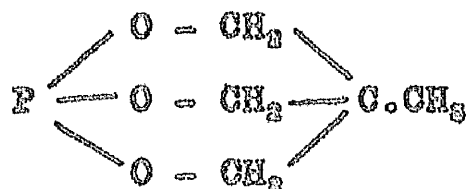
with the following series of ligands, viz. triphenylphosphine, triphenylarsine, triphenylstibine, triphenylbismuthine, trimethylphosphite, triethylphosphite, triphenylphosphite, triethylamine and 4-methyl-2,6,7-trioxa-1-phosphabicyclo[2,2,2]octane (hereafter referred to as M.T.P.).

The formation of complexes between triaryl derivatives of Group V elements and metal ions is well established,<sup>4</sup> the ease of formation being in the order  $\text{PPh}_3 > \text{AsPh}_3 > \text{SbPh}_3$ . Little work appears to have been done on transition metal complexes with  $\text{BiPh}_3$ , although Nuttall<sup>5</sup> et al have claimed that well-defined complexes such as  $\text{AgClO}_4 \cdot \text{Ph}_3\text{Bi}$  are readily formed from ether solution. There are two possible sources which can give rise to coordination in trialkyl derivatives, viz. (a) the Group V element, and (b) the  $\pi$ -electron system of the aromatic ring. Since Sharp and Sharpe<sup>6</sup> have shown that aromatic systems give rise only to weak complexes with copper and silver, it is therefore expected that the most important contribution to complex formation will arise from the Group V elements.

A recent review article by Booth<sup>7</sup> discusses the present knowledge of phosphine complexes. Tertiary phosphines show a marked tendency to form non-ionic complexes which are readily soluble in organic solvents. Phosphines, in general are particularly useful and versatile ligands, in that they form compounds containing both the highest and lowest valency states of transition metals. Phosphorus has empty 3d orbitals capable of accepting  $\pi$ -electrons, and in addition, they have a lone pair of electrons capable of forming a  $\sigma$  bond. Thus phosphines are strong bases, and combine strong sigma bond donor functions, such as are found in amines, with strong  $\pi$ -bond acceptor properties. The importance of d-orbitals in covalent bonding has been a subject of much discussion since Pauling's<sup>8</sup> paper on the hybridisation of atomic orbitals in molecule formation. The effects of  $\pi$ -bonding involving d-orbitals on the properties of transition metal compounds including some complexes formed by tertiary phosphines, arsines and stibines, have been explained by several authors.<sup>9,10</sup>

The above effects are also evident in phosphites. However, previous attempts to prepare complexes with trialkyl phosphites have met with only limited success. The reaction of first row transition metals such as Co(II) and Ni(II) invariably yield only oils though some reaction is indicated by colour changes.<sup>11</sup> Arbuzov<sup>12</sup> et al have prepared complexes with trialkyl phosphites and heavy transition metals such as Pt(II) and a few of the post-transition metals such as Hg(II). The difficulty in forming complexes of transition metals and alkylphosphites appears to be a steric effect, since a new alkyl phosphite (M.T.P.) first prepared by Verkade and Reynolds<sup>13</sup> has shown remarkable complexing powers.<sup>14,15</sup> The ability of M.T.P. to form stable complexes in contrast to trialkyl phosphites, arises from its low steric hindrance and stronger sigma- and  $\pi$ -bonding abilities. The alkyl part of the molecule is a ring system which is essentially strainless. Studies by nuclear magnetic resonance spectroscopy<sup>14</sup> show the molecule to have the structure depicted in Fig.(1.1).

FIG. (1.1)



The most notable aspect of Verkade's work<sup>16</sup> is that the maximum coordination number for transition metal perchlorates was achieved with only M.T.P. molecules in the first coordination sphere, which is strong evidence for a reduction of ligand-ligand steric repulsion. However, work by Cotton and Goodgame<sup>17</sup> on perchlorates of Ag(I) and Cu(I) has shown that complexes are formed in which 4 PPh<sub>3</sub> molecules were found in the coordination sphere of the metal although the anion could also have been coordinated.

Bonding in triethylamine complexes with transition metals will differ from the other Group V elements already discussed in two aspects. Brown<sup>18</sup> has shown the existence of back strain in trialkylamines produced by packing three alkyl groups round the relatively small nitrogen atom as compared to the phosphorus atom. Thus there is a decrease in basicity due to steric factors. The other difference arises since NEt<sub>3</sub> has no orbitals available for

feedback and must therefore be considered as a pure sigma donor.

The complexes formed in the present work were investigated using infrared, far infrared and ultraviolet reflectance spectroscopy.

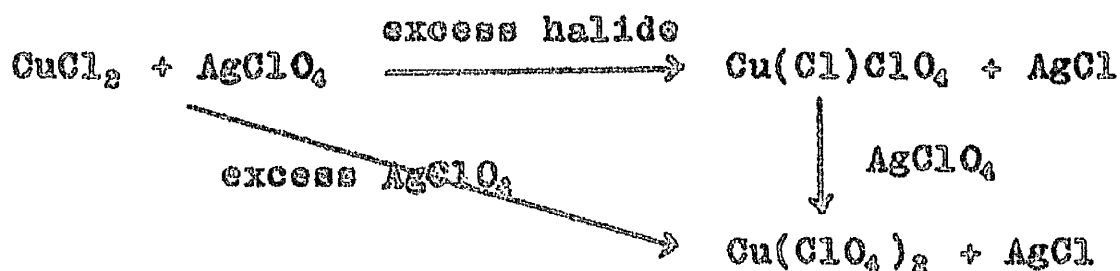
Discussion

The most interesting feature of the ether solutions of transition metal perchlorates and tetrafluoroborates has been the discovery of a new type of compound.<sup>10</sup> It was found that on addition of anhydrous cupric chloride to silver perchlorate in ether solution, an immediate colouration was observed. This was blue but on prolonged shaking the colour changed to green. Baillie et al<sup>20</sup> investigated this colour change by ultraviolet spectroscopy and conductivity measurements. The conclusions which were drawn were that two species existed in solution corresponding to the formula



where X represented the strong acid anion.

Solution (I) may be converted to II by titrating with silver perchlorate dissolved in ether, and the reactions formulated as



As far as the solution formed using silver tetrafluoroborate and copper(II) chloride was concerned, it appeared that the yellow-green solution was exclusively of type I, viz.  $\text{Cu}(\text{Cl})\text{BF}_4$ . Details of the preparation and properties of the other solutions are given in the experimental section.

The above types of solution when reacted with the ligands listed in Chapter I gave a series of complexes which were of the general formula  $\text{MX}_3\text{L}_2$ ,  $\text{MX}_2\text{L}_4$ ,  $\text{MX}_2\text{L}_3$ ,  $\text{MXL}_2$ ,  $\text{MXL}_3$ ,  $\text{MXL}_4$ ,  $\text{M}(\text{Cl})\text{XL}_2$  and  $\text{M}(\text{Cl})\text{XL}_4$  where X = perchlorate or tetrafluoroborate. The stereochemistry of the cobalt and nickel complexes was investigated by measuring the ultraviolet reflectance spectra [Tables (3.1), (3.2) and (3.3)] and are discussed, where appropriate, in the section dealing with the infrared spectrum of a particular complex.

In general, the yield of complex obtained was not very large. The analysis for the stable complexes prepared are given in the experimental section.

(A) Monosubstituted phenyl ligands

The infrared spectra of the ligands used in this study,  $\text{PPh}_3$ ,  $\text{AsPh}_3$ ,  $\text{SbPh}_3$  and  $\text{BiPh}_3$  are quite similar to one another.<sup>21</sup> However, the infrared spectra of the complexes formed are quite complicated due to the masking effect of the perchlorate and tetrafluoroborate anions. Consequently nothing can be said about ligand vibrations in the regions  $1200\text{--}950\text{ cm.}^{-1}$  and  $630\text{--}520\text{ cm.}^{-1}$ . Such variations in ligand vibrations as are observed are confined to the peaks in the regions  $740\text{--}720$ ,  $700\text{--}680$ ,  $500\text{--}450$  and the region below  $300\text{ cm.}^{-1}$  [Tables (2.1), (2.2), (2.3) and (2.4)].

Table (2.1)

<u>Complex</u>	<u>Absorption frequency (cm.<sup>-1</sup>)</u>			
AsPh <sub>3</sub>	310	467 475	690	732
Zn(ClO <sub>4</sub> ) <sub>2</sub> (AsPh <sub>3</sub> ) <sub>2</sub>	314 329 <sup>≠</sup>	467	693	735
Cu(ClO <sub>4</sub> ) <sub>2</sub> (AsPh <sub>3</sub> ) <sub>4</sub>	323	470	692	735
Co(ClO <sub>4</sub> ) <sub>2</sub> (AsPh <sub>3</sub> ) <sub>4</sub>	320	462 472	689	735 740 <sup>≠</sup>
Ni(ClO <sub>4</sub> ) <sub>2</sub> (AsPh <sub>3</sub> ) <sub>4</sub>	320	470	695	735
Zn(BF <sub>4</sub> ) <sub>2</sub> (AsPh <sub>3</sub> ) <sub>4</sub>	313(w)	460	684	741 750 <sup>≠</sup>
CuClBF <sub>4</sub> (AsPh <sub>3</sub> ) <sub>4</sub>	325	452 <sup>*</sup> 461	692	727 735 <sup>≠</sup>
CuClBF <sub>4</sub> (AsPh <sub>3</sub> ) <sub>2</sub>	326	455 463 <sup>≠</sup>	691	725 735 <sup>≠</sup>
CoClBF <sub>4</sub> /AsPh <sub>3</sub>	-	460	685	743 750 <sup>≠</sup>

Table (2.2)

<u>Complex</u>	<u>Absorption frequency (cm.<sup>-1</sup>)</u>			
SbPh <sub>3</sub>	253 267	450 455	693	729
Ni(ClO <sub>4</sub> ) <sub>2</sub> (SbPh <sub>3</sub> ) <sub>2</sub>	240	455	690	730(sh) 745(sh) 760(s) <sup>≠</sup>
Co(ClO <sub>4</sub> ) <sub>2</sub> (SbPh <sub>3</sub> ) <sub>2</sub>	240 <sup>≠</sup> 267	455	687	730 <sup>≠</sup> 758
CuClO <sub>4</sub> (SbPh <sub>3</sub> ) <sub>2</sub>	267	455 453 458 <sup>≠</sup>	693	729

Table (2.2)

<u>Complex</u>	<u>Absorption frequency (cm.<sup>-1</sup>)</u>			
$\text{CuClO}_4 (\text{SbPh}_3)_4$	267	454	693	729
$\text{Zn}(\text{ClO}_4)_2 / \text{SbPh}_3$	240	455	690	735 750(sh) $\equiv$
$\text{CuClBF}_4 (\text{SbPh}_3)_4$	267	445 452 $\equiv$ 457	692	728
$\text{Zn}(\text{BF}_4)_2 / \text{SbPh}_3$	-	435 (w) 450	687 $\equiv$ 694 $\equiv$	727 $\equiv$ 736 $\equiv$

Table (2.3)

<u>Complex</u>	<u>Absorption frequency (cm.<sup>-1</sup>)</u>		
$\text{PPh}_3$	490 496 510	690	740
$\text{Zn}(\text{ClO}_4)_2 (\text{PPh}_3)_2$	493 497 510	695	741* 747
$\text{Co}(\text{ClO}_4)_2 (\text{PPh}_3)_4$	491 510	692	726* 740
$\text{CuClO}_4 (\text{PPh}_3)_2$	500 515	695	720 745 $\equiv$ 755(sh)
$\text{Ni}(\text{ClO}_4)_2 (\text{PPh}_3)_4$	490(sh) 500(s) 510(sh)	693	720 745 $\equiv$ 755
$\text{Zn}(\text{BF}_4)_2 / \text{PPh}_3$	507	687	733
$\text{CoClBF}_4 / \text{PPh}_3$	500(w)	692	722(s) 750(w) $\equiv$
$\text{CuClBF}_4 (\text{PPh}_3)_2$	503(w)	680	721(s) 745(m) $\equiv$

Table (2.4)

<u>Complex</u>					
$\text{BiPh}_3$	232(m)	450	694	723	
$\text{Co}(\text{ClO}_4)_2(\text{BiPh}_3)_2$	238	444	680	720	*
				730	*
$\text{Ni}(\text{ClO}_4)_2/\text{BiPh}_3$	234(w)	444	690(w)	732	
$\text{CuClClO}_4/\text{BiPh}_3$	232(w)	437(sh)	690(w)	723	(m)
				733	
$\text{Cu}(\text{ClO}_4)_2/\text{BiPh}_3$	234(w)	443(w)	685(w)	732	
$\text{Zn}(\text{BF}_4)_2/\text{BiPh}_3$	241	431 (m)	683	732	
		444 *			
$\text{CuClBF}_4/\text{BiPh}_3$	236(w)	458	695	723	

(s)  $\equiv$  strong    (m)  $\equiv$  medium    (w)  $\equiv$  weak    (sh)  $\equiv$  shoulder

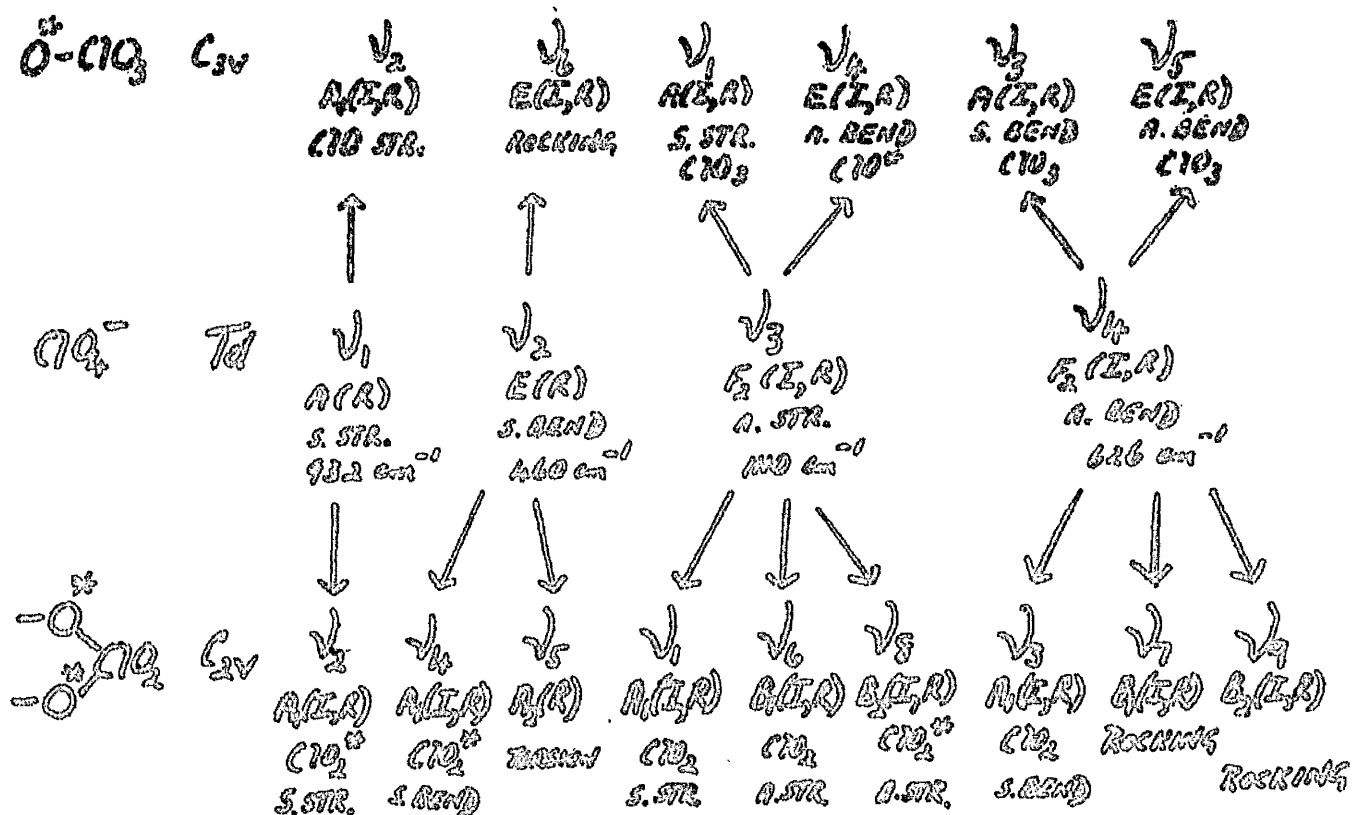
Unless designated otherwise, the absorptions given in the above tables are strong. Tables (2.1), (2.2) (2.3) and (2.4) show that any alteration in the position of the ligand vibrations appears to be entirely random. First impressions given by the absorptions marked with an asterisk, were that the observed splitting was a crystal field effect. However, closer examination of coordinated complexes revealed that some of these peaks may in fact be due to the anion being either monodentate or bidentate. This will be dealt with later on in the discussion.

Table (2.4) in which some of the strong ligand absorptions are reduced to medium or weak peaks on complexing, supports the view obtained from analysis, that with  $\text{BiPh}_3$  there is dephenylation taking place.

### (B) Anion Absorptions

The principal absorptions which were of interest in the present investigations were those due to perchlorate and tetrafluoroborate ions. The infrared<sup>22,23,24,25</sup> and Raman<sup>26,27</sup> spectra of perchlorates have been studied and assignments made.<sup>28</sup> The unperturbed perchlorate ion has a regular tetrahedral structure, and possesses nine modes of vibration giving four fundamental modes. Hatheway and Underhill<sup>29</sup> have tabulated the nature, symmetry and approximate typical frequencies of the observed modes for the tetrahedral ion as well as the effects of coordination through one or both oxygen atoms of the perchlorate group [Table (2.5)].

TABLE (2.5)



A and B, non-degenerate; E, doubly degenerate;  
 F, triply degenerate; I, infrared active;  
 R, Raman active; s, symmetric; a, asymmetric;  
 O<sup>x</sup> refers to coordinated oxygen.

In general, the triply degenerate modes  $\nu_3$  and  $\nu_6$  are infrared active in ionic perchlorates,  $\nu_3$  as a strong, broad absorption with a poorly defined maximum, which is occasionally split.<sup>25</sup>

The non-degenerate mode  $\nu_1$ , which is theoretically forbidden in the infrared usually occurs very weakly at 930 cm.<sup>-1</sup> This absorption becomes weakly

allowed owing to distortion of the ion in a crystal field of lower symmetry than itself.

Similar arguments apply equally well to other tetrahedral systems such as  $\text{BF}_4^-$ , though not a great deal has been published in this direction. Several authors<sup>50,51</sup> have quoted values of ca. 1020 and 530  $\text{cm.}^{-1}$  ( $\nu_3$  and  $\nu_4$ ) for the infrared active modes of the tetrafluoroborate ion.

The fundamental frequencies for a perchlorate or tetrafluoroborate group with  $\text{C}_{3v}$  symmetry are not accurately predictable. However, the infrared active frequencies for other  $\text{C}_{3v}$  symmetrical compounds, e.g. perchloric acid<sup>52</sup> and perchloryl fluoride<sup>53</sup> have been reported and may be taken as a guide.

	$\nu_1$	$\nu_2$	$\nu_3$	$\nu_4$	$\nu_5$	$\nu_6$	( $\text{cm.}^{-1}$ )
$\text{HClO}_4$	1032	739	574	1312	585	426	
$\text{ClO}_3\text{F}$	1061	715	549	1315	589	405	

In the case of two oxygen atoms being involved in covalent bonding, i.e. a bidentate perchlorate group, the symmetry is lowered to  $\text{C}_{2v}$ . A similar type of guide to the frequencies may be obtained from studies

of the bidentate sulphate ion<sup>34</sup> and sulphuryl fluoride.<sup>35</sup>

	$\nu_1$	$\nu_2$	$\nu_3$	$\nu_4$	$\nu_5$	$\nu_6$	$\nu_7$	$\nu_8$	$\nu_9$
$\text{SO}_4^{2-}$	1055	995	641	462	-	1105	610	1176	571
$\text{SO}_2\text{F}_2$	1269	848	544	300	-	1502	553	885	539

$\nu_8$  is only Raman active, the rest being observed in the infrared.

The absorption frequencies listed in tables (2.6), (2.7), (2.8) and (2.9) are those due to the anion, plus absorptions which cannot be related to simple ligand vibrations.

The absorptions marked with an asterisk are difficult to assign. These absorptions may be due to a crystal field effect or to the anion being coordinated but will be considered in the discussion of the complexes where this occurs.

Table (2.6) Triphenylarsine Complexes

<u>Complex</u>	<u>Absorption Frequency (cm.<sup>-1</sup>)</u>				
Zn(ClO <sub>4</sub> ) <sub>2</sub> (AsPh <sub>3</sub> ) <sub>2</sub>	357(m)	620* 647	800(m) 855	929	1007, 1080, 1150
Cu(ClO <sub>4</sub> ) <sub>2</sub> (AsPh <sub>3</sub> ) <sub>4</sub>		621 635(sh)		910(m)	1020, 1085, 1117
Co(ClO <sub>4</sub> ) <sub>2</sub> (AsPh <sub>3</sub> ) <sub>4</sub>		620	735 740	860	1080
Ni(ClO <sub>4</sub> ) <sub>2</sub> (AsPh <sub>3</sub> ) <sub>4</sub>		625			1080
Zn(BF <sub>4</sub> ) <sub>2</sub> (AsPh <sub>3</sub> ) <sub>4</sub>	351(m)	510(m) 560(m)	741 750	930	1085, 1120
CuClBF <sub>4</sub> (AsPh <sub>3</sub> ) <sub>4</sub>	263 265(sh)	452 461	727 735		1087
CuClBF <sub>4</sub> (AsPh <sub>3</sub> ) <sub>2</sub>	260 267	455 463	727 735		1085
CoClBF <sub>4</sub> /AsPh <sub>3</sub>		512(w) 563(w)	743 750	920	1085

Table (2.7) Triphenylstibine Complexes

<u>Complex</u>	<u>Absorption Frequency (cm.<sup>-1</sup>)</u>		
$\text{Ni}(\text{ClO}_4)_2 (\text{SbPh}_3)_2$	625	730(sh) 745(sh) $\equiv$ 760	870(m) 1010, 1090, 1140
$\text{Co}(\text{ClO}_4)_2 (\text{SbPh}_3)_2$	240 267 $\equiv$	521(m) 533(m)	625 730 $\equiv$ 758 $\equiv$ 935 1075, 1130
$\text{CuClO}_4 (\text{SbPh}_3)_2$	445 453 $\equiv$ 458 $\equiv$	622	930(w) 1090
$\text{CuClO}_4 (\text{SbPh}_3)_4$		624	1085
$\text{Zn}(\text{ClO}_4)_2 / \text{SbPh}_3$	298	625 735 635 750(sh) $\equiv$	1090, 1140(w) broad
$\text{CuClHF}_4 (\text{SbPh}_3)_4$	282 290	445 452 * 451 $\equiv$	747 742 (w) 731
$\text{Zn}(\text{BF}_4)_2 / \text{SbPh}_3$		687 694 $\equiv$	727 736 $\equiv$ 1085 broad with lots of shoulders

Table (2.8) Triphenylphosphine Complexes

Absorption Frequency (cm.<sup>-1</sup>)

Complex	442	527	625	741	865	1011, 1085, 1150
Zn(ClO <sub>4</sub> ) <sub>2</sub> (PPh <sub>3</sub> ) <sub>2</sub>				741 <sup>m</sup> 747	865 <sup>m</sup> 885	
Co(ClO <sub>4</sub> ) <sub>2</sub> (PPh <sub>3</sub> ) <sub>4</sub>	429	520	623	726 <sup>m</sup> 740 <sup>m</sup>	832	1025(sh), 1085, 1135 (sh) broad
CuClO(PPh <sub>3</sub> ) <sub>2</sub>	429	540	625	720		1090 broad
		543(sh)		745 <sup>m</sup> 755(sh)		
Ni(ClO <sub>4</sub> ) <sub>2</sub> (PPh <sub>3</sub> ) <sub>4</sub>	427	547	620	720	890(w)	1090, 1140(w) 1163(w) broad
				745 <sup>m</sup> 755		
Zn(BF <sub>4</sub> ) <sub>2</sub> /PPh <sub>3</sub>	239	388				
		523		751	880	1082, 1117
		541				
		570				926(m) broad
CoClBF <sub>4</sub> /PPh <sub>3</sub>	540			722 <sup>m</sup> 750		922(w) 1085, 1115, 1145
CuClBF <sub>4</sub> (PPh <sub>3</sub> ) <sub>2</sub>	540			721 <sup>m</sup> 745(m)		1065(w), 1094(w), 1117(s), 1150(w) broad

Table (2.9) Triphenylbismuthine Complexes

<u>Complex</u>	<u>Absorption Frequency (cm.<sup>-1</sup>)</u>			
Co(ClO <sub>4</sub> ) <sub>2</sub> / B1Ph <sub>3</sub> ) <sub>2</sub>	260 (m)	285 (m)	625	720
	268	291		730
Ni(ClO <sub>4</sub> ) <sub>2</sub> / B1Ph <sub>3</sub>			625	870(m)
				1087
CuClClO <sub>4</sub> / B1Ph <sub>3</sub>	292(m)		625	1085
	broad			broad
Cu(ClO <sub>4</sub> ) <sub>2</sub> / B1Ph <sub>3</sub>	285(m)		623	1100
	broad		575 (m)	broad
½n(BF <sub>4</sub> ) <sub>2</sub> / B1Ph <sub>3</sub>	431		515 (w)	1050, 1090
	444 (m)			1189
CuClBF <sub>4</sub> / B1Ph <sub>3</sub>			522(m)	1080

The ultraviolet reflectance spectrum of the blue complex  $\text{Co}(\text{ClO}_4)_2(\text{AsPh}_3)_4$  has shown the cobalt to be in a tetrahedral environment. Table (2.6) shows this complex to be ionic though the absorption at  $860 \text{ cm.}^{-1}$  may be due to some covalent character. Although the infrared spectrum of  $\text{Ni}(\text{ClO}_4)_2(\text{AsPh}_3)_4$  seems to show the complex as ionic, the reflectance spectrum indicates a complex of octahedral symmetry. This means that for octahedral symmetry the perchlorate must be coordinated in a symmetrical fashion and therefore does not manifest itself by splitting. Using the values of Hathaway et al.<sup>36</sup> and Wickenden and Krause<sup>37</sup> for coordinated perchlorates as a guide, it appears that  $\text{Zn}(\text{ClO}_4)_2(\text{AsPh}_3)_2$  is coordinated through two of the oxygen atoms of each perchlorate group ( $\text{C}_{2v}$ ). The peaks at 620 and 647  $\text{cm.}^{-1}$  in the zinc complex could be assigned to the non-degenerate rocking frequency  $\nu_7$  and the non-degenerate  $\text{ClO}_2$  symmetrical bending frequency  $\nu_3$  respectively. This is in contrast to the two peaks at 735 and 740  $\text{cm.}^{-1}$  in the cobalt complex which must be due to a crystal field effect. In the case of

$\text{Cu}(\text{ClO}_4)_2(\text{AsPh}_3)_4$ , the perchlorate is monodentate ( $\text{C}_{3v}$ ).

A white complex analysing to  $\text{CuClO}_4(\text{SbPh}_3)_2$  was prepared from copper(II)bisperchlorate, whereas copper(II)chloroperchlorate yielded another white solid but this analysed to  $\text{CuClO}_4(\text{SbPh}_3)_4$ , both of which appear ionic from their infrared spectra. Similar to other copper(I) complexes these might be expected to be tetrahedral, though this would mean that the perchlorate in the former would have to be coordinated. The triplet around  $450 \text{ cm.}^{-1}$  and the weak peak at  $930 \text{ cm.}^{-1}$  may be interpreted as evidence of covalency for  $\text{CuClO}_4(\text{SbPh}_3)_2$ .

The ultraviolet reflectance spectrum of  $\text{Ni}(\text{ClO}_4)_2(\text{SbPh}_3)_2$  suggests that this complex is octahedral, and the infrared spectrum indicates coordination of the perchlorate group.  $\text{Co}(\text{ClO}_4)_2(\text{SbPh}_3)_2$  is shown from table (2.7) to have a bidentate perchlorate group. One of the peaks at  $730$  and  $758 \text{ cm.}^{-1}$ , probably the latter is due to coordination though the doublet at  $240$  and  $267 \text{ cm.}^{-1}$  is too low for this type of assignment, and appears

to be either a slight shift in the ligand vibration [see table (2.2)] or a metal-oxygen vibration.

The complex formed between  $\text{Zn}(\text{ClO}_4)_2$  and triphenylstibine, although not characterised by analysis appears from its infrared spectrum to contain a weakly coordinated perchlorate group.

Of the complexes formed between triphenylphosphine and the various perchlorate solutions,  $\text{CuClO}_4(\text{PPh}_3)_2$  appears to be ionic [table (2.8)] but it is difficult to put forward a definite structure for this complex if copper has a sensible coordination number of four.  $\text{Zn}(\text{ClO}_4)_2(\text{PPh}_3)_2$

similar to  $\text{Zn}(\text{ClO}_4)_2(\text{AsPh}_3)_2$ , is shown to contain a bidentate perchlorate group of  $\text{C}_{2v}$  symmetry.

The spectrophotometric measurements of  $\text{Co}(\text{ClO}_4)_2(\text{PPh}_3)_4$  are somewhat anomalous in that the ultraviolet reflectance spectrum shows tetrahedral symmetry, whereas the infrared spectrum appears to show the anion to be strongly coordinated. The complex  $\text{Ni}(\text{ClO}_4)_2(\text{PPh}_3)_4$  yielded a poor reflectance spectrum which did not help to elucidate the symmetry, and the infrared spectrum suggested only weak coordination of the anion.

The perchlorate-triphenylbismuthine complexes appear from table (2.9) to be ionic, though some doubt exists about the  $\text{Co}(\text{ClO}_4)_2(\text{BiPh}_3)_2$  complex which was the only one to fit satisfactory analysis figures. Both  $\text{Cu}(\text{ClO}_4)_2$  and  $\text{Cu}(\text{Cl})\text{ClO}_4$  ether solutions gave green solids on addition of triphenylbismuthine. These complexes appeared to dephenylate, though table (2.9) shows the presence of ionic perchlorate from the absorptions at ca.  $625 \text{ cm.}^{-1}$  and the broad peaks around  $1100 \text{ cm.}^{-1}$ . However, the peaks around  $290 \text{ cm.}^{-1}$  might be taken as indicating metal-halogen bridging similar to the distorted octahedral complexes suggested by Clark et al.<sup>36</sup> for copper-halide complexes of pyridine.

The infrared spectra of  $\text{CuClBF}_4(\text{AsPh}_3)_2$  and  $\text{CuClBF}_4(\text{AsPh}_3)_4$  shown in table (2.6) suggest that these complexes are ionic. The absorptions around  $260 \text{ cm.}^{-1}$  for these complexes approximately corresponds to values observed for copper-halogen vibrations observed by Clark and Williams<sup>36</sup> for distorted polymeric octahedral compounds. Using this assumption, fig. (2.1) indicates a possible structure

for  $\text{CuClBF}_4(\text{AsPh}_3)_2$  in which the copper is six-coordinate, involving chlorine bridging with the tetrafluoroborate being ionic and held in interstices in the lattice.

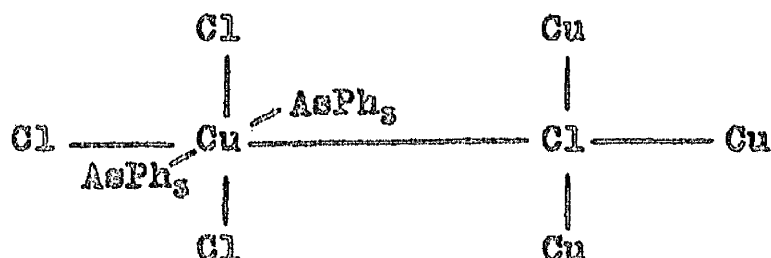


Fig. (2.1)

In general the infrared data for the tetrafluoroborate complexes are more difficult to interpret than the corresponding perchlorate complexes. The main reasons are that very little prominence has been given to coordination through the fluorine atoms of tetrafluoroborate, and in several cases the resolution of the infrared peaks was poor. Such poor resolution may be due in part to the existence of  $B^{10}-F$  stretching modes which often appear in the 900-1300  $\text{cm.}^{-1}$  region as shoulders on a broad absorption due to  $B^{11}-F$  modes.

Hathaway and Webster,<sup>88</sup> and Clark and O'Brien<sup>89</sup> have studied coordination of the tetrafluoroborate group in trimethyltin tetrafluoroborate.

The assignments which they give to the seven infrared active bands are due to (a) the triply degenerate asymmetric B-F stretch ( $\nu_3$ ) being resolved into three strong bands at 930, 1070 and 1170  $\text{cm.}^{-1}$ , (b) symmetric B-F stretch ( $\nu_1$ ) at 746  $\text{cm.}^{-1}$ , (c) the  $\nu_4$  doublet due to an asymmetric bend around 525 and (d) a broad band at 446  $\text{cm.}^{-1}$

arising from splitting of  $\nu_4$  mode, and may be either a rocking mode or a symmetrical bending mode of the  $\text{BF}_4$  group with  $\text{C}_{2v}$  symmetry. Using these values as a guide it is evident the complex formed between  $\text{Zn}(\text{BF}_4)_2$  and triphenylphosphine, although not characterized by analysis, has the anion present as a bidentate group. Using published frequencies of the vibrations of perchlorate anion with  $\text{C}_{3v}$  symmetry, analogy shows the complex  $\text{Zn}(\text{BF}_4)_2(\text{AsPh}_3)_4$  to contain a monodentate ion. The  $\text{Zn}(\text{BF}_4)_2\text{-SbPh}_3$  complex shows one strong peak at 1085  $\text{cm.}^{-1}$  and thus appears to be ionic, though the peaks at 687, 694, 727 and 736  $\text{cm.}^{-1}$  suggest that either some

covalent character exists or that the symmetry of the tetrafluoroborate group is affected by its position in the crystal lattice, but this would tend to be a minor effect. The absorptions shown in table (2.7) for  $\text{CuClBF}_4(\text{SbPh}_3)_2$  show that coordination of the anion is present, and the peaks at 282 and 290  $\text{cm.}^{-1}$  are strong evidence for copper-chlorine bridging. The complex  $\text{CuClBF}_4(\text{PPh}_3)_2$  might be expected to exhibit coordination of the  $\text{BF}_4$  group and metal-halogen bridging if copper is to have a reasonable coordination number. These observations are not evident from the infrared spectrum.

Ultraviolet reflectance spectra and analysis were not obtained for the  $\text{CoClBF}_4\text{-AsPh}_3$  and  $\text{CoClBF}_4\text{-PPh}_3$  complexes since only poor yields of blue solid were obtained. Both of these complexes show strong coordination of the  $\text{BF}_4$  group and it might be anticipated that had a far infrared spectrum been obtained there would have been peaks around 230  $\text{cm.}^{-1}$  for cobalt-chlorine bridging similar to the values obtained for the distorted polymeric octahedral compound  $\text{CoCl}_2(\text{pyridine})_2$ .<sup>30</sup>

Table (2.9) shows that the complex  $Zn(BF_4)_2 \cdot BiPh_3$  contains coordinated  $BF_4$  ions whereas the  $CuClBF_4 \cdot BiPh_3$  complex appears to be purely ionic.

### (C) Phosphite Ligands

Generally it might be expected that tertiary phosphites would show approximately the same coordinating affinity as triphenylphosphine, with the phosphorus acting as a sigma-bond donor and a  $\pi$ -bond acceptor, the vacant 3d orbitals of the phosphorus being capable of interaction with filled non-bonding d-orbitals of a transition metal.

Specifically it might be expected that triphenylphosphite would exhibit stronger bonding properties than triphenylphosphine, by virtue of the fact that conjugation between the lone pair of electrons on the phosphorus atom and the aromatic ring, could be expected to be hindered by the interposition of the oxygen atom, thus rendering the phosphorus lone pair more available for sigma-bond formation.

The argument appears to be substantiated in several cases in which triphenylphosphine is displaced by  $(PhO)_3P$  in metathetical reactions.<sup>40, 41</sup> Reactions of the above type have usually been carried out using

the heavier transition metals such as platinum and palladium. The complexes formed are of the type  $\text{Pt}[(\text{PhO})_3\text{P}]_3$  and they have also been formed by the addition of triphenylphosphite to an ethanolic KOH solution of  $\text{K}_2\text{PtCl}_4$ .<sup>40</sup> There does not appear to be much reported for triphenylphosphite complexes of the 1st row transition metals though Heck<sup>42</sup> has prepared complexes of the type  $\text{AcCo}(\text{CO})_2(\text{PPh}_3)[\text{P}(\text{OMe})_3]_3$ . In the present study, no solid complexes were obtained using triphenylphosphite as a ligand, though in a few cases, a change was observed in the colour of the solution.

Several cases<sup>11, 22</sup> in which trialkylphosphites yielded intractable oils with transition metals have been reported, and it is only recently that Huttemann<sup>43</sup> has mentioned well-defined complexes with this system. Some of the difficulty experienced in attempts to prepare complexes of trialkylphosphites must be ascribed to steric hindrance. This effect has been studied by Brown and Sujishi.<sup>44</sup> They compared quinuclidine and triethylamine as bases towards  $\text{BF}_3$  and found that quinuclidine [fig.(2.2)] formed a more stable adduct with  $\text{BF}_3$  than did

triethylamine (fig. 2.3). The former is a bicyclic analogue of the latter and may be compared to 4-methyl-2,6,7-trioxa-1-phosphabicyclo[2,2,2]octane (fig. 1.1) and a trialkylphosphite respectively.

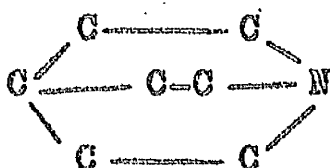


fig. (2.2)

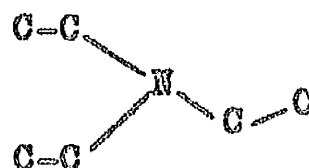


fig. (2.3)

In the present investigations, several transition metal-trialkylphosphite complexes formed readily from ether solution, though in other attempts the failure to obtain a solid complex was put down to solubility effects. The complexes which were obtained are  $\text{Co}(\text{ClO}_4)_2 [(\text{MeO})_3\text{P}]_3$ ,  $\text{Co}(\text{ClO}_4)_2 [(\text{EtO})_3\text{P}]_3$ ,  $\text{Ni}(\text{ClO}_4)_2 [(\text{MeO})_3\text{P}]_3$ , and  $\text{Ni}(\text{ClO}_4)_2 [(\text{EtO})_3\text{P}]_3$ . The complexes  $\text{CuClO}_4 [(\text{MeO})_3\text{P}]_4$  and  $\text{CuClO}_4 [(\text{EtO})_3\text{P}]_4$  were obtained from  $\text{Cu}(\text{Cl})\text{ClO}_4$  solution, and  $\text{CuClO}_4 [(\text{MeO})_3\text{P}]_3$  and  $\text{CuClO}_4 [(\text{EtO})_3\text{P}]_3$  from  $\text{Cu}(\text{ClO}_4)_2$  solution. The ether solution of  $\text{CuClBF}_4$  yielded a complex which analysed to  $\text{CuBF}_4 [(\text{MeO})_3\text{P}]_4$ .

The other phosphite which was used with great effect was the caged phosphite M.T.P., the structure of which is illustrated in fig.(1.1).

Tables (2.10), (2.11) and (2.12) list the infrared absorptions for the range of complexes prepared. The spectra of the alkylphosphites were run as liquid films whereas M.T.P. and all the complexes were studied as Nujol mulls. Unless otherwise indicated, the absorptions shown in the tables are observed as strong peaks.

Before discussing the infrared spectra of the cobalt and nickel trialkylphosphite complexes, it must be mentioned that except for  $\text{Ni}(\text{ClO}_4)_2 [(\text{MeO})_3\text{P}]_6$  no information could be gathered regarding the structure of the complexes from the ultraviolet reflectance spectra. Both of the cobalt complexes decomposed without showing any absorptions, while  $\text{Ni}(\text{ClO}_4)_2 [(\text{EtO})_3\text{P}]_6$  tended to decompose continuously, giving a very odd spectrum which rose to a maximum at  $22,720 \text{ cm.}^{-1}$  and then levelled out very quickly on the low frequency side.  $\text{Ni}(\text{ClO}_4)_2 [(\text{MeO})_3\text{P}]_6$  which was a bright yellow solid was shown to be octahedral having peaks at  $1300$  and  $2400 \text{ cm.}^{-1}$  and

Table (2.11) (MeO)<sub>2</sub>P Complexes

Complex	Absorption Frequency (cm <sup>-1</sup> )			
(MeO) <sub>2</sub> P	365(m)	512(m)	730	816(w) 1012 1180(m)
	385(s)		765(sh)	1055(sh)
	400(m)			
Co(ClO <sub>4</sub> ) <sub>2</sub> [(MeO) <sub>2</sub> P] <sub>2</sub>	386(w)	540	625	705(w) 975 to 1110 1180
	400(w)			broad
			727(w)	
			790(sh)	
			820	
Ni(ClO <sub>4</sub> ) <sub>2</sub> [(MeO) <sub>2</sub> P] <sub>2</sub>	388(w)	550	620	725 800 980 to 1140 1170
	392(m)			broad
CuClO <sub>4</sub> [(MeO) <sub>2</sub> P] <sub>2</sub>	364(sh)	502	625	764 920(w) 1080 1180
	388	530 (w)	635(sh)	broad
	400(sh)	548		
			789	
			833	
Cu(ClO <sub>4</sub> ) <sub>2</sub> [(MeO) <sub>2</sub> P] <sub>2</sub>	360(sh)	523 (m)	627	745 1070 1180(sh)
	388(w)	535	635(sh)	broad
	400(w)			
CuBF <sub>4</sub> [(MeO) <sub>2</sub> P] <sub>2</sub>	362(sh)	521		735 960 to 1160
	386			broad
	427(m)		790(m)	

Table (2.12) (EtO)<sub>2</sub>P Complexes

<u>Complex</u>	<u>Absorption frequency (cm<sup>-1</sup>)</u>				
(EtO) <sub>2</sub> P	450(m)	530	740	920, 1023, 1165, 1265	
Co(ClO <sub>4</sub> ) <sub>2</sub> [(EtO) <sub>2</sub> P] <sub>2</sub>	452(m)	560	720	950-1030-1090, 1140(sh)	1220(w)
			775	broad	
Ni(ClO <sub>4</sub> ) <sub>2</sub> [(EtO) <sub>2</sub> P] <sub>2</sub>	450(w)	555	720	950-1010-1100	
			775	broad	
CuClO <sub>4</sub> [(EtO) <sub>2</sub> P] <sub>2</sub>		535	765	950-1020-1100	1267(m)
		550	795 (b)	broad	
CuClO <sub>4</sub> [(EtO) <sub>2</sub> P] <sub>2</sub>		545	770 (b)	968-1030-1090	1265(m)
				broad	

Table(2.13) MFP: Complexes.

M.T.P.	Cu(ClO <sub>4</sub> ) <sub>2</sub> (MFP) <sub>4</sub>	Ni(ClO <sub>4</sub> ) <sub>2</sub> (MFP) <sub>4</sub>	Cu(ClO <sub>4</sub> ) <sub>2</sub> (MFP) <sub>4</sub>	CuClO <sub>4</sub> (MFP) <sub>4</sub>	Zn(ClO <sub>4</sub> ) <sub>2</sub> (MFP) <sub>4</sub>	CuClBF <sub>4</sub> (MFP) <sub>4</sub>
262	267 262	276	267	268	-	-
342	328(m)	330	361	362	-	-
402	386(m) 430 494	377 422 460(w)	410 460	411 457	460(w)	407 459(m)
493(m) 503	515	510	492(w) 507	490(w) 505	505(w)	492(w) 507
649(m)	625 649	622 645	620 647	620 647	623	647
726	720(w)	722(w)	720(w)	730(sh)	725(m)	720(w)
800(w) 845(sh) 860	790 803 850.	783 820 835 855	777(w) 800 855 865(sh)	775(w) 795 855 865(sh)	800(w) 859(m)	777(w) 800 855
921(w)	930	932	930	927		930
	1005	992	1005	1000	1025(sh) 1040(sh)	1000
1040 1172(w)	1090 1170(sh)	1092 1172(m)	1097 1171	1092 1172(w)	1080 1180(sh)	1095 1175(m)

a shoulder around  $1600\text{ cm.}^{-1}$ . The close resemblance in the colour of these complexes (i.e. orange-yellow) taken in conjunction with the similarity observed in their infrared spectra for anion and ligand vibrations suggests they are all octahedral.

Table (2.12) indicates that the nickel and cobalt complexes are ionic, as far as perchlorate and tetrafluoroborate is concerned, the doublet at  $720$  and  $775\text{ cm.}^{-1}$  being assigned to the splitting of the ligand vibration at  $740\text{ cm.}^{-1}$  due to a crystal field effect. Table (2.11) shows two new peaks in the cobalt and nickel complexes which cannot simply be assigned to anion vibrations, viz. the bands at ca.  $550\text{ cm.}^{-1}$  and the strong doublet at ca.  $725$  and  $800\text{ cm.}^{-1}$ . There are several possibilities which could give rise to this phenomena viz. (1) bonding taking place through the oxygen atoms of the phosphite instead of the phosphorus, (2) infrared inactive bands in the liquid film which become active on complexing and (3) crystal field effects. The most likely of these is the effect of crystal field in the solid complex, but it is impossible to verify this at present.

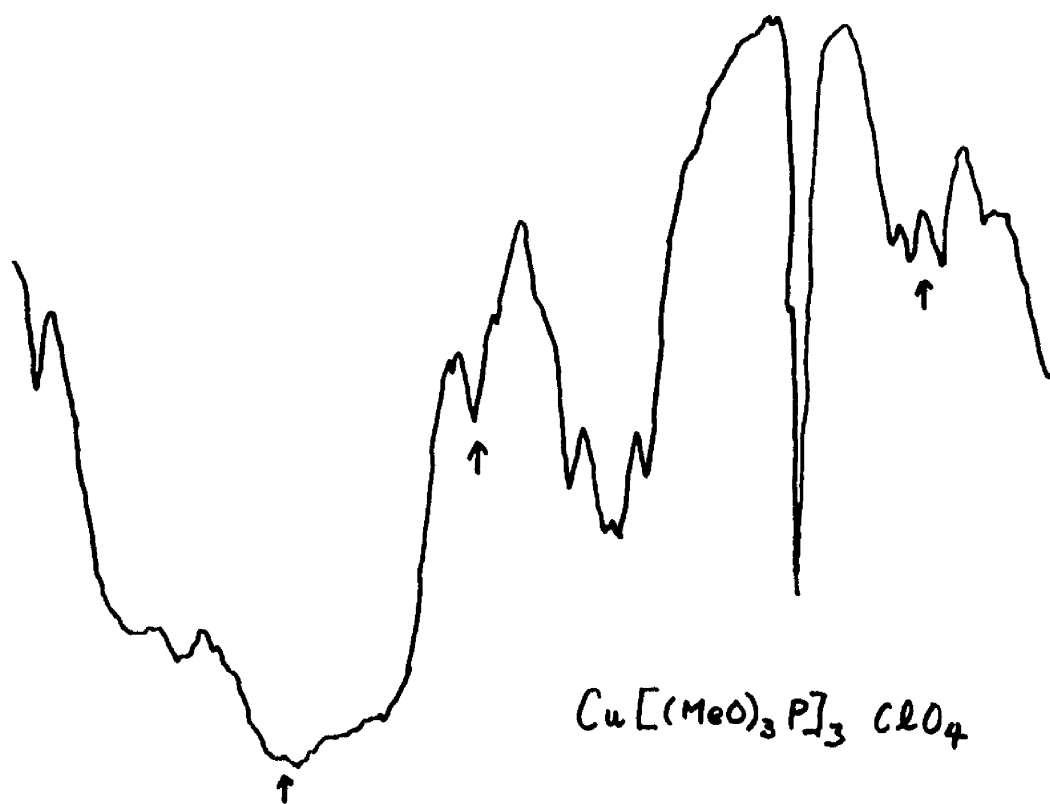
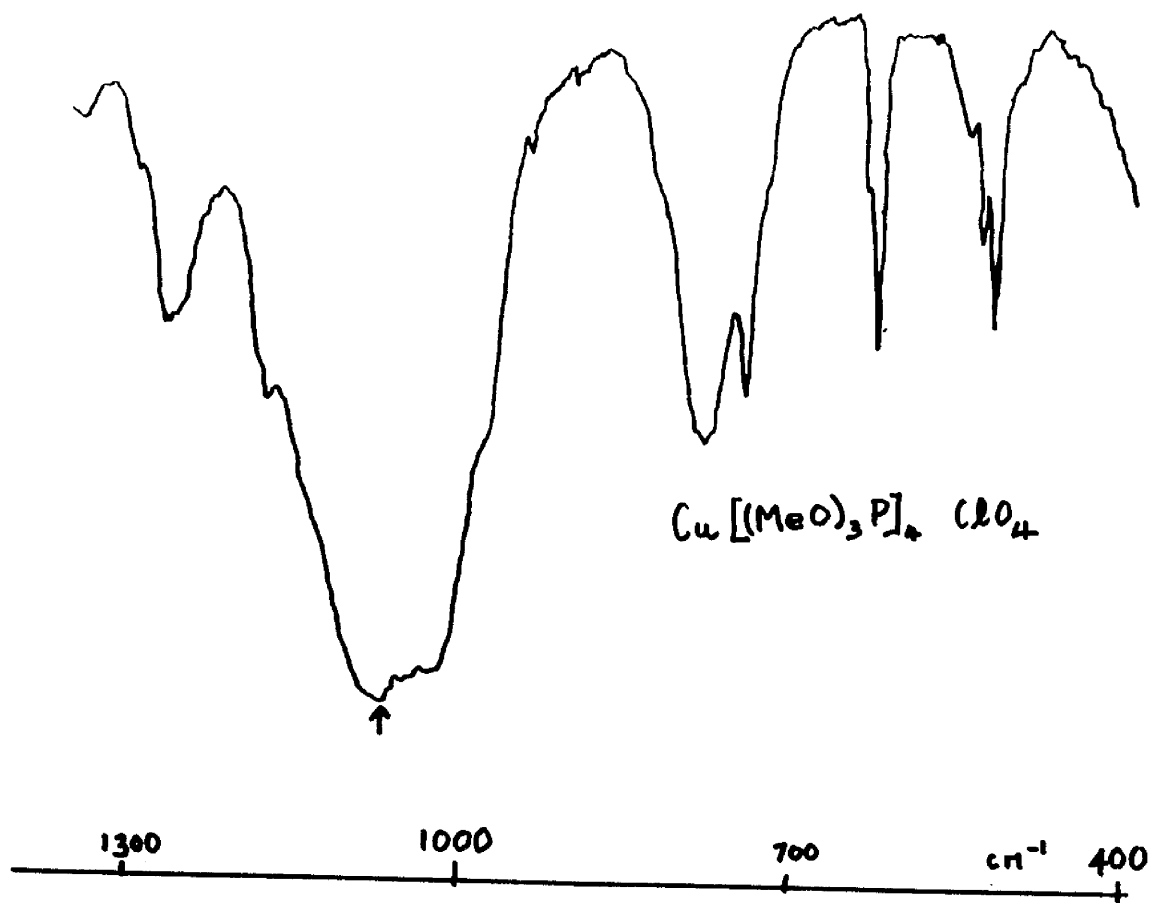


FIG (2.4)

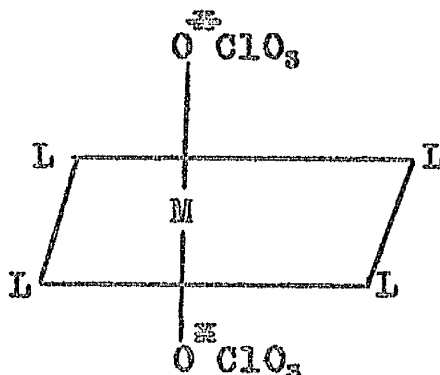
Fig. (2.4) illustrates in detail the spectra of  $\text{CuClO}_4[(\text{MeO})_3\text{P}]_3$  which was obtained from copper(II) bisperchlorate solution and  $\text{CuClO}_4[(\text{MeO})_3\text{P}]_4$  which was derived from the green copper(II)chloro-perchlorate solution. Complexing of an ether solution of  $\text{Cu}(\text{ClO}_4)_2$  with trimethylphosphite results in reduction of the copper(II) to copper(I) giving a complex of formula  $\text{CuClO}_4[(\text{MeO})_3\text{P}]_3$ . When the parent solution is  $\text{Cu}(\text{Cl})\text{ClO}_4$ , complexing with trimethylphosphite again gives reduction of copper(II) to copper(I), but in this case a tetra-ligand complex  $\text{CuClO}_4[(\text{MeO})_3\text{P}]_4$  is formed. Both of these reductions presumably must involve electron transfer from the ligand, but with the present information it is impossible to elucidate the true nature of the mechanisms. Most copper(I) complexes are tetrahedral. If this is so with both these complexes, then the perchlorate group in  $\text{CuClO}_4[(\text{MeO})_3\text{P}]_3$  must be monodentate, and in  $\text{CuClO}_4[(\text{MeO})_3\text{P}]_4$  the perchlorate will be ionic. These postulates are substantiated by fig. (2.4) which shows that there is less splitting in the infrared around the  $500$  and  $750 \text{ cm.}^{-1}$  region for

$\text{CuClO}_4[(\text{MeO})_3\text{P}]_4$  than for the complex  $\text{CuClO}_4[(\text{MeO})_3\text{P}]_3$ .

The same phenomena are apparent in the triethylphosphite complexes [table (2.12)] indicating similar mechanisms.

Table (2.11) shows the infrared absorptions for the complex  $\text{CuBF}_4[(\text{MeO})_3\text{P}]_4$ . Once again symmetry requirements may be satisfied without coordination of the anion, and a similar mechanism as for  $\text{CuClO}_4[(\text{MeO})_3\text{P}]_4$  is probably involved. Addition of triethylphosphite to copper(II)chlorotetrafluoroborate yielded a brown solution which turned colourless. The failure to prepare a solid complex with triethylphosphite similar to the trimethylphosphite complex is possibly due to a solubility effect. Table (2.13) is a clear indication that the complex  $\text{Zn}(\text{ClO}_4)_2(\text{MTP})_4$  is ionic. The other four caged phosphite complexes, viz.  $\text{Co}(\text{ClO}_4)_2(\text{MTP})_4$ ,  $\text{Ni}(\text{ClO}_4)_2(\text{MTP})_4$ ,  $\text{Cu}(\text{ClO}_4)_2(\text{MTP})_4$  and  $\text{Cu}(\text{Cl})\text{ClO}_4(\text{MTP})_4$  are extremely good examples of coordination taking place through the anion. Both the nickel and cobalt complexes have been shown from ultraviolet reflectance spectra to be octahedral. This fact taken in conjunction with the infrared spectra

which show that the anion has assumed  $C_{3v}$  symmetry means that the structure for these complexes is probably as shown in fig. (2.5).



Although ultraviolet spectra have not been measured for either of the copper(II) complexes, the infrared spectra indicate that the complexes have similar structures as for nickel and cobalt. The infrared spectrum of the complex  $Cu(Cl)ClO_4(MTP)_4$  shows that the perchlorate anion is monodentate.

For octahedral symmetry coordination through  $Cl^-$  must also be present.

Several anomalies are observed in the present investigations as compared with the results obtained by Verkade. Verkade et al<sup>16</sup> found that cobalt(II) bisperchlorate hexahydrate when reacted with M.T.P., disproportionated to give (a) a yellow cobalt(I)

complex, viz.  $[\text{Co}(\text{MTP})_3]\text{ClO}_4$  and (b) colourless  $[\text{Co}(\text{MTP})_3](\text{ClO}_4)_3$ . Another complex prepared by Verkade et al.<sup>15</sup> was  $[\text{Ni}(\text{MTP})_3\text{H}_2\text{O}]\text{ClO}_4$  in which he found it impossible to remove the water molecule from the inner coordination sphere of the nickel atom. These examples, along with the fact that he did not manage to prepare a complex using zinc(II)bisperchlorate hydrate, compared to the present work must be due to the fact that he worked with hydrated systems, whereas the present investigations were carried out under strictly anhydrous conditions.

The spectrum of  $\text{CuClBF}_4(\text{MTP})_3$  again suggest that the strong acid anion has assumed  $C_{3v}$  symmetry, and implies coordination both through the chlorine atom and one of the fluorine atoms of the tetra-fluoroborate group.

#### (D) Triethylamine Complexes

The relative affinities of ligand atoms or molecules of Group Vb elements for acceptor molecules or ions is discussed by Ahrland et al.<sup>4</sup>, and mainly depends on the acceptor concerned. Two regular features are apparent, viz. (1) there is a great difference between the coordinating affinities of

nitrogen donors from donors of the other elements in this group, and (2) there are two classes of acceptors. Acceptors designated class (b) are those which form their most stable complexes with the second or subsequent atom in a group.

Class (b) acceptors, with a few exceptions, appear to be confined to the transition metals, character type depending on the availability of electrons from the lower d-orbitals of the metal for  $\pi$ -bonding.

Cobalt, nickel and copper in their normal oxidation states are of class (b) type, i.e. the coordinating affinities of the donor atom being in the order

$N < P > As > Sb > Bi$ . These metals form stable phosphine complexes, less stable arsines and much less stable stibine complexes. With class (b) acceptors, nitrogen can be placed in the

$P > As > Sb > Bi$  sequence, the position of nitrogen in the sequence giving a measure of class (b)

character. Coordinating affinities of Group Vb elements have been studied for a number of class (b) acceptors.<sup>45,46,47,48,49</sup> Several authors<sup>50,51,52</sup>

have stated that tertiary alkylamines have virtually

no tendency to coordinate to metal salts unless stabilised by chelation.<sup>53</sup> On the other hand, Hatfield and Yoke<sup>54</sup> give a number of references to authors who have prepared complexes of trimethylamine and/or triethylamine with a series of metal halides though there is no mention of infrared measurements. The literature does not appear to assign absorptions of triethylamine complexes, probably due to the fact that tertiary amines are difficult to identify spectroscopically.<sup>55</sup> Table (14) lists the observed frequencies for the infrared absorptions of the triethylamine complexes studied in the present investigations.

Table (14).      Triethylamine complexes

<u>NEt<sub>3</sub></u>	<u>Co(ClO<sub>4</sub>)<sub>2</sub> (NEt<sub>3</sub>)<sub>2</sub></u>	<u>Ni(ClO<sub>4</sub>)<sub>2</sub> (NEt<sub>3</sub>)<sub>2</sub></u>	<u>Cu(ClO<sub>4</sub>)<sub>2</sub> (NEt<sub>3</sub>)<sub>2</sub></u>	<u>CuClClO<sub>4</sub> /NEt<sub>3</sub></u>
625(s)	627(s)	625(s)	624(s)	623(s)
735(m)	723(m)	740(w)	720(m)	720(w)
780(w)		793(w)	795(w)	792(w)
800(w)	800(w) 840(w)	815(w) 840(w)	810(w) 839(w)	835(w)
900(w)				895(w)
920(w)	930(w)	930(w)	925(w)	925(w)
940(w)		940(w)		

Table (14).      Triethylamine complexes

<u>NEt<sub>3</sub></u>	<u>Co(ClO<sub>4</sub>)<sub>2</sub> (NEt<sub>3</sub>)<sub>2</sub></u>	<u>Ni(ClO<sub>4</sub>)<sub>2</sub> (NEt<sub>3</sub>)<sub>2</sub></u>	<u>Cu(ClO<sub>4</sub>)<sub>2</sub> (NEt<sub>3</sub>)<sub>2</sub></u>	<u>CuClClO<sub>4</sub> /NEt<sub>3</sub></u>
997(w) 1020(w)				
1087 1130(sh)	1085(s, b)	1100(s, b)	1095(s, b)	1095(s, b)
1300(m)	1300(w)	1290(w)	1300(w)	1290(w)

Although there is a strong absorption at 1080 cm.<sup>-1</sup> in the ligand itself, the absorption in this region for the complex is much broader due to the presence of the perchlorate group. Ultraviolet reflectance spectra have shown that the metal atoms in Co(ClO<sub>4</sub>)<sub>2</sub>(NEt<sub>3</sub>)<sub>2</sub> and Ni(ClO<sub>4</sub>)<sub>2</sub>(NEt<sub>3</sub>)<sub>2</sub> are in an octahedral environment. It is not considered that definite structural conclusions may be drawn from the infrared spectra of these compounds at this juncture. There are two possibilities which have to be considered. The first is that the perchlorate is essentially ionic in a symmetrical site and secondly, the perchlorate group may be coordinated in a symmetrical tetrahedral manner.

The similarity of the infrared spectra of  $\text{Cu}(\text{ClO}_4)_2(\text{NEt}_3)_2$  and  $\text{Cu}(\text{Cl})\text{ClO}_4/\text{NEt}_3$  suggest that the same arguments apply as for the nickel and cobalt complexes.

### Experimental

All the solutions prepared were made up in a dry box using anhydrous solvents and salts. The solutions were prepared in 100 ml. flasks and the ground glass stoppers sealed in the flasks using P.T.F.E. sleeves. As an added precaution the stoppers were wired on to the flask. Shaking was carried out on a mechanical shaker, reaction being completed in times varying from a few days to one month. The solutions were filtered in the dry box using a porosity 4 sintered funnel and a hand bulb connected to a Buchner flask. In some cases, repeated filtration was required and in other instances where separation was impossible by filtration, clear solutions were obtained by decantation.

The solutions were stored in the dry box and the ligands added either as a liquid or as an ether solution of the solid ligand. When complex formation took place, the precipitate was filtered in the dry box and then dried under vacuum.

The infrared spectra of the solid compounds were recorded as nujol mulls using a Perkin-Elmer 125 grating spectrophotometer.

The far infrared spectra were recorded as nujol mulls using a Grubb-Parsons double-beam spectrophotometer, Type DM2 (200-667  $\text{cm.}^{-1}$ ). The mulls were supported between plates which are transparent in the spectral region under study, e.g. potassium bromide or polythene.

A Hilger Uvispek photoelectric spectrophotometer H700.307 fitted with a reflectance unit was used for measuring the ultraviolet spectra of the complexes in the range 200-1000  $\text{m}\mu$ .

#### Preparation and analysis

Solvent: Ether was dried over sodium wire and then stored over molecular sieves. The ether was kept in a dry box which was kept free from moisture by means of open trays of  $\text{P}_2\text{O}_5$ .

Silver perchlorate: Anhydrous silver perchlorate was obtained from B.D.H. but was further dehydrated by continuous pumping at 50-70°C. The perchlorate was then left under vacuum in the dry box.

Silver tetrafluoroborate: The method of Sharpe<sup>2</sup> was used for the preparation. Dry silver borate

was prepared by precipitation from silver nitrate and boric acid. The borate (1.5 g.) was placed in a silica bottle fitted with a B14 cone.

Bromine (5 ml.) was added to act as a moderator in the reaction. Bromine trifluoride was added, drop by drop, through a copper funnel. When excess  $\text{BrF}_3$  had been added, the  $\text{Br}_2$  and remaining  $\text{BrF}_3$  were removed under vacuum on a normal vacuum line fitted with a silica trap. The last traces of  $\text{BrF}_3$  were removed by heating at  $130^\circ\text{C}$  for two hours.

### Ligands

With the exception of M.T.P., which was prepared by the method of Verkade and Reynolds,<sup>13</sup> the ligands were all commercial samples.

#### (A) Copper

Copper(II) chloride. Copper(II) chloride was prepared by partial dehydration of the dihydrate under vacuum at  $100^\circ\text{C}$ . The halide was then treated with freshly distilled thionyl chloride.

When reaction ceased the thionyl chloride was distilled off under partial vacuum using a dry nitrogen

bleed. The product was washed several times with dry carbon disulphide and finally heated at 100° under vacuum to remove the remaining carbon disulphide. A yellow brown powder was obtained.

Analysis: Theory Cl, 52.8

Found Cl, 52.6

The absence of hydroxyl peaks in the near infrared was taken to mean that anhydrous halide had been obtained.

Copper(II)chloroperchlorate: Metathesis in this case had to be carried out for approximately 7 days before the reaction was complete. The green solution obtained was analysed to confirm that the solution was 100% copper(II)chloroperchlorate.

Analysis: Theory Cu, 31.8; Cl, 17.9.

Found Cu, 31.5; Cl, 17.7.

Tetrakis(triphenylstibine)copper(I)perchlorate:  
white powder.

Analysis: Theory C, 54.9; H, 3.8; Cl, 2.2; O, 4.1.

Found C, 55.2; H, 3.9; Cl, 2.1; O, 4.5.

Tetrakis(trimethylphosphite)copper(I)perchlorate:  
white crystals - very hygroscopic.

Analysis: Theory C, 21.9; H, 5.5; Cl, 5.3; P, 18.8.

Found C, 21.6; H, 5.6; Cl, 5.6; P, 18.2.

Tetrakis(triethylphosphite)copper(I)perchlorate:

white crystals - very hygroscopic.

Analysis: Theory C, 34.9; H, 7.3; Cl, 4.2; P, 15.0.

Found C, 34.6; H, 7.2; Cl, 4.0; P, 14.5.

Tetrakis(4-methyl-2,6,7-trioxo-1-phospha-bicyclo

[2,2,2]octane)copper(II)perchlorate: off-white powder.

Analysis: Theory C, 30.4; H, 4.6; Cl, 9.0; P, 15.7.

Found C, 30.1; H, 4.7; Cl, 8.7; P, 15.5.

Bis(triphenylphosphine)copper(I)perchlorate:

white powder.

Analysis: Theory C, 63.0; H, 4.4; Cl, 5.1; P, 9.0.

Found C, 62.7; H, 4.7; Cl, 4.9; P, 9.0.

Reaction with triphenylbismuthine: Addition of an ether solution of BiPh<sub>3</sub> to copper(II)chloroperchlorate gave a green colloidal solution which settled out on standing to a dull green precipitate. The colour suggested the formation of a copper(II) complex but analysis did not correspond to any reasonable formulation. Infrared spectra showed the presence of a perchlorate.

Reaction with triphenylarsine: An immediate precipitation of a flocculent white powder was obtained. Analysis did not show the presence of either copper or oxygen. A similar reaction and analysis were obtained in several cases in which  $\text{AsPh}_3$  was added to copper(II)bisperchlorate.

Copper(II)bisperchlorate: A blue solution of copper(II)bisperchlorate was obtained by titrating a solution of copper(II)chloroperchlorate with an ether solution of silver perchlorate.

Bis(triphenylstibine)copper(I)perchlorate:

white powder.

Analysis: Theory C, 49.8; H, 3.5; Cl, 4.0; O, 7.4.  
Found C, 51.0; H, 3.6; Cl, 3.9; O, 7.3.

Tetrakis(triphenylarsine)copper(II)perchlorate:

yellow powder.

Analysis: Theory C, 58.1; H, 4.0; Cl, 4.8; As, 20.2.  
Found C, 58.2; H, 4.2; Cl, 4.6; As, 20.4.

As mentioned previously, a white powder was formed on several occasions which did not contain copper or oxygen.

Tris(trimethylphosphite)copper(I)perchlorate:

hygroscopic white crystals.

Analysis: Theory C, 20.2; H, 5.1; Cl, 6.6; P, 17.4.

Found C, 20.1; H, 5.3; Cl, 6.5; P, 17.4.

Tris(triethylphosphite)copper(I)perchlorate:

hygroscopic white crystals.

Analysis: Theory C, 32.7; H, 6.8; Cl, 5.4; P, 14.1.

Found C, 29.5; H, 6.5; Cl, 5.4; P, 14.3.

Tetrakis(M.T.P.)copper(II)perchlorate: very pale

pink powder.

Analysis: Theory C, 28.0; H, 4.2; Cl, 8.3; P, 14.5.

Found C, 28.0; H, 4.4; Cl, 8.2; P, 14.2.

Bis(triethylamine)copper(II)perchlorate: green solid.

Analysis: Theory C, 31.0; H, 6.5; Cl, 15.3; N, 6.0;

O, 27.6; Cu, 13.6.

Found C, 29.7; H, 6.6; Cl, 15.0; N, 5.3;

O, 27.6; Cu, 13.9.

Other reactions with copper(II)bisperchlorate:

An identical complex was formed using  $PPh_3$  as a ligand as in the case of copper(II)chloroperchlorate.

$BiPh_3$  again yielded a green complex which did not analyse to any reasonable formulation.



Bis(triphenylarsine)copper(II)chlorotetrafluoro-  
borate: colourless needles.

Analysis: Theory C, 54.2; H, 3.8; Cl, 4.5; F, 9.5;  
As, 18.8.

Found C, 54.5; H, 3.9; Cl, 4.5; F, 9.2;  
As, 18.5.

Tetrakis(triphenylarsine)copper(II)chlorotetra-  
fluoroborate: white powder.

Analysis: Theory C, 61.3; H, 4.3; Cl, 2.5; B, 0.8;  
F, 5.4; As, 21.3.

Found C, 61.1; H, 4.3; Cl, 2.4; B, 0.8;  
F, 5.4; As, 21.8.

Tetrakis(M. T. P. copper(II)chlorotetrafluoroborate:  
yellow solid.

Analysis: Theory C, 30.9; H, 4.6; Cl, 4.5; B, 1.4;  
F, 9.8; P, 16.0.

Found C, 30.8; H, 4.8; Cl, 4.0; B, 1.2;  
F, 9.8; P, 16.5.

Tetrakis(trimethylphosphite)copper(I)tetrafluoro-  
borate: white crystals - very hygroscopic.

Analysis: Theory C, 22.3; H, 5.6; P, 19.2; F, 11.8.  
Found C, 22.3; H, 5.6; P, 19.1; F, 11.8.

Bis(triethylamine)copper(II)chlorotetrafluoroborate:

yellow-green solid.

Analysis: Theory C, 37.2; H, 7.7; N, 7.2; B, 2.8;

Cl, 9.0.

Found C, 36.6; H, 7.1; N, 6.9; B, 2.7;

Cl, 8.8.

Other reactions

Once again a green precipitate was obtained using  $\text{BiPh}_3$ . The analysis did not yield a suitable formulation, the ratio of C : H : Cl : B : F being 20.5 : 24.7 : 2.8 : 1 : 2.7. Both  $(\text{EtO})_3\text{P}$  and  $(\text{PhO})_3\text{P}$  gave brown solutions which then turned colourless and did not yield a solid.

(B) Nickel

Nickel(II)chloride: The preparation was carried out using the hexahydrate as for copper(II)chloride.

A straw coloured powder was obtained.

Analysis: Theory Cl, 54.8; Found Cl, 54.6.

Nickel(II)bisperchlorate

In this case metathesis was continued for 20-30 days before reaction had been completed. A yellow solution

was obtained which was shown by analysis to be a mixture of the chloroperchlorate and bisperchlorate. Attempts to prepare a solution which was entirely chloroperchlorate were unsuccessful. Titration of the mixed solution with an ether solution of silver perchlorate produced a yellow solution of nickel(II)bisperchlorate.

A nickel solution of silver tetrafluoroborate in ether could not be prepared.

Tetrakis(triphenylphosphine)nickel(II)perchlorate:

light brown solid.

Analysis: Theory C,66.1; H,4.6; Cl,5.4; P,9.5;

Ni,4.6

Found C,60.0; H,4.6; Cl,5.4; P,9.6;

Ni,4.7.

Tetrakis(triphenylarsine)nickel(II)perchlorate:

pale yellow. This reaction seemed to be temperamental - sometimes a small yield of precipitate was obtained, other occasions did not produce any complex.

Analysis: Theory C,58.3; H,4.1; Cl,4.8; As,20.2.

Found C,58.4; H,4.3; Cl,4.4; As,20.1.

Bis(triphenylstibine)nickel(II)perchlorate:

white powder.

Analysis: Theory C, 44.8; H, 3.1; Cl, 7.4.

Found C, 44.6; H, 3.6; Cl, 7.3.

Hexakis(trimethylphosphite)nickel(II)perchlorate:

deep orange powder - very hygroscopic.

Analysis: Theory C, 21.6; H, 5.4; Cl, 7.1; P, 18.6.

Found C, 20.7; H, 5.1; Cl, 7.0; P, 18.9.

Hexakis(triethylphosphite)nickel(II)perchlorate:

orange solid - very hygroscopic.

Analysis: Theory C, 34.4; H, 7.2; Cl, 5.7; P, 14.8.

Found C, 31.3; H, 6.8; Cl, 5.5; P, 14.2.

Bis(triethylamine)nickel(II)perchlorate:

pale yellow solid - hygroscopic.

Analysis: Theory C, 31.3; H, 6.5; Cl, 15.4; N, 6.1.

Found C, 31.0; H, 6.3; Cl, 15.0; N, 6.2.

Other reactions

(PhO)<sub>3</sub>P simply yielded an intractable oil.

Reaction of BiPh<sub>3</sub> produced a dull yellow solid in which the ratio of C : H : Cl was 10.7 : 10 : 1.

Tetrakis(MTP)nickel(II)perchlorate: yellow solid.

Analysis: Theory C, 28.3; H, 4.2; Cl, 8.3; P, 14.6.

Found C, 28.1; H, 4.4; Cl, 8.2; P, 14.2.

(C) Cobalt

Cobalt(II)chloride: The preparation was carried out using the hexahydrate as for copper(II)chloride. A blue powder was obtained.

Analysis: Theory Cl, 54.7; Found Cl, 54.6.

Cobalt(II)bisperchlorate: Reaction was complete in approximately 7 days. A purple solution was obtained which was a mixture of chloroperchlorate and bisperchlorate, as in the case of the corresponding nickel solution. Attempts to prepare the chloroperchlorate in 100% yield were unsuccessful.

The red cobalt(II)bisperchlorate was obtained by titrating the mixed solution with silver perchlorate in ether.

Tetrakis(triphenylphosphine)cobalt(II)perchlorate:  
blue crystals.

Analysis: Theory C, 66.1; H, 4.6; Cl, 5.4; P, 9.5.  
Found C, 65.6; H, 4.7; Cl, 4.8; P, 9.4.

Tetrakis(triphenylarsine)cobalt(II)perchlorate:  
blue crystals.

Analysis: Theory C, 58.3; H, 4.1; Cl, 4.8; As, 20.2.  
Found C, 58.2; H, 4.2; Cl, 4.8; As, 20.3.

Bis(triphenylstibine)cobalt(II)perchlorate:

off-white solid.

Analysis: Theory C, 44.8; H, 3.1; Cl, 7.4.

Found C, 44.2; H, 3.2; Cl, 7.3.

Bis(triphenylbismuthine)cobalt(II)perchlorate:

brown solid.

Analysis: Theory C, 37.9; H, 2.6; Cl, 6.2.

Found C, 36.9; H, 2.7; Cl, 6.0.

Hexakis(trimethylphosphite)cobalt(II)perchlorate:

orange solid.

Analysis: Theory C, 21.6; H, 5.4; Cl, 7.1; P, 18.6.

Found C, 21.5; H, 5.4; Cl, 7.2; P, 18.6.

Hexakis(triethylphosphite)cobalt(II)perchlorate:

orange solid - very hygroscopic.

Analysis: Theory C, 34.4; H, 7.2; Cl, 5.7; P, 14.8.

Found C, 30.0; H, 6.9; Cl, 5.6; P, 14.6.

Tetrakis(M. T. P.)cobalt(II)perchlorate: yellow solid.

Analysis: Theory C, 28.3; H, 4.2; Cl, 8.3; P, 14.6.

Found C, 28.6; H, 4.2; Cl, 8.0; P, 14.4.

Bis(triethylamine)cobalt(II)perchlorate: purple solid

which tends to turn brown very quickly.

Analysis: Theory C, 31.3; H, 6.6; Cl, 15.4; N, 6.1; Co, 12.8;

Found C, 31.5; H, 6.5; Cl, 14.8; N, 5.5; Co, 12.5.

Cobalt(II)chlorotetrafluoroborate: Metathesis

yielded a colourless solution which turned blue on standing over a prolonged period.

Analysis: Theory Co, 32.5; Cl, 19.5.

Found Co, 32.1; Cl, 19.3.

Reactions: Blue precipitates were formed on addition of  $\text{PPh}_3$  and  $\text{AsPh}_3$ , and a very pale pink complex with  $\text{SbPh}_3$ . In each case it was only possible to obtain enough sample for infrared analysis. Various attempts failed to improve the yield.

(D) Zinc

Zinc(II)chloride: Zinc(II)chloride was prepared from the hydrate as for copper(II)chloride.

A white powder was obtained and since it was extremely hygroscopic, it was used immediately after preparation.

Analysis: Theory Cl, 52.1; Found Cl, 51.8.

Zinc(II)perchlorate: Stoichiometric amounts of zinc(II)chloride and silver perchlorate were shaken together in ether. An immediate white flocculent

precipitate of silver chloride was formed.

The reaction went to completion within 30 minutes giving a colourless solution. In order to obtain complete separation of the halide from the solution, repeated filtrations and/or decantation was necessary.

Bis(triphenylphosphine)zinc(II)perchlorate:

white powder.

Analysis: Theory C, 54.8; H, 3.8; P, 7.9; Cl, 9.0;

Zn, 8.2.

Found C, 54.1; H, 4.0; P, 7.6; Cl, 8.7;

Zn, 8.0.

Bis(triphenylarsine)zinc(II)perchlorate: white solid.

Analysis: Theory C, 49.3; H, 3.4; Cl, 8.1; As, 17.1.

Found C, 49.3; H, 3.7; Cl, 7.9; As, 17.6.

Tetrakis(triethylamine)zinc(II)perchlorate:

Addition of triethylamine resulted in the formation of a white colloidal solution which deposited a white precipitate. Very quickly this precipitate yielded a yellow oil which solidified when a vacuum was applied. The tacky yellow solid analysed as follows:

Theory C, 30.9; H, 6.4; Cl, 15.2; N, 6.0.

Found C, 29.8; H, 6.8; Cl, 14.8; N, 5.6.

Other reactions:  $\text{SbPh}_3$  yielded a white precipitate which analysed in the ratio C : H : Cl : O as 12 : 13 : 1 : 6. Similarly it was not possible to assign a formula to the brown needles formed on the addition of  $\text{BiPh}_3$  to the parent solution. The ratio of C : H : Cl : O for the brown needles was 6.1 : 8.2 : 1 : 4.8. The remaining phosphites yielded intractable yellow oils.

Zinc(II)bistetrafluoroborate: The colourless solution of zinc(II)bistetrafluoroborate was prepared in an identical manner to the bisperchlorate solution.

Tetrakis(triphenylarsine)zinc(II)tetrafluoroborate: white needles.

Analysis: Theory C, 59.1; H, 4.1; B, 1.5; F, 10.4;  
As, 20.5.  
Found C, 58.5; H, 4.1; B, 1.6; F, 10.2;  
As, 19.7.

Other reactions: Using the ligands  $\text{SbPh}_3$ ,  $\text{BiPh}_3$  white solids were obtained but could not be characterised. A small yield of white needles was obtained with M.T.P. but there was not enough sample

to characterise this complex either.

Bis(triphenylphosphine)zinc(II)tetrafluoroborate:

Analysis: Theory C, 56.6; H, 3.9; B, 2.9; F, 19.9;  
P, 8.1.

Found C, 53.8; H, 4.6; B, 2.9; F, 19.8;  
P, 8.5.

Ultraviolet spectra.

The ground state for octahedral nickel(II) complexes is  $^3A_{2g}$ . Table (3.1) indicates the transitions observed, the frequency of the maxima being given in wave numbers  $\times 10^{-3}$ .

Table (3.1). Octahedral nickel(II) complexes.

	Colour	$\rightarrow ^3T_{2g}(F)$	$\rightarrow ^3T_{1g}(F)$
$Ni(ClO_4)_2(ArPh_3)_4$	pale yellow	13.7	24.7
$Ni(ClO_4)_2(SbPh_3)_2$	white	13.7	25.0
$Ni(ClO_4)_2/BiPh_3$	dull yellow	14.2	23.2
$Ni(ClO_4)_2[(MeO)_3P]_2$	orange	13.0	23.9
$Ni(ClO_4)_2[(EtO)_3P]_2$	orange	-	22.7 <sup>±</sup>
$Ni(ClO_4)_2[MTP]_2$	yellow	13.3	24.4(gh)
$Ni(ClO_4)_2(NEt_3)_2$	yellow	14.0	24.4

The light brown complex  $Ni(ClO_4)_2(PPh_3)_4$  did not give a satisfactory reflectance spectrum. The complex

$\text{Ni}(\text{ClO}_4)_2 \cdot [(\text{EtO})_3\text{P}]_3$  tended to decompose and the spectrum is therefore not very conclusive.

Table (3.2) shows the transitions from the ground state  ${}^4\text{T}_{1g}$  for octahedral cobalt(II) complexes.

Table (3.2).                      Octahedral cobalt(II) complexes.

<u>Complex</u>	<u>Colour</u>	$\rightarrow {}^4\text{A}_2\text{g}(\text{F})$	$\rightarrow {}^4\text{T}_{1g}(\text{P})$
$\text{Co}(\text{ClO}_4)_2(\text{MTP})_4$	yellow	15.9	17.6
$\text{Co}(\text{ClO}_4)_2(\text{NEt}_3)_3$	purple	15.8	17.0

The bands [Table (3.3)] observed in the visible region for tetrahedrally coordinated cobalt(II) complexes arise from transitions from the ground state  ${}^4\text{A}_2$  to  ${}^4\text{T}_1$ ,  ${}^2\text{E}$ ,  ${}^2\text{T}_1$ .

<u>Complex</u>	<u>Colour</u>	$\rightarrow {}^4\text{T}_1$ , ${}^2\text{E}$ , ${}^2\text{T}_1$
$\text{Co}(\text{ClO}_4)_2(\text{PPh}_3)_4$	blue	14.9 to 16.4
$\text{Co}(\text{ClO}_4)_2(\text{AsPh}_3)_4$	blue	14.5 to 16.5

References

1. Sidgwick, N.V., The Chemical Elements and their Compounds, Oxford University Press, 1950.
2. Sharpe, A.G. J.C.S., 1952, 4538.  
Sharp, D.W.A., Thesis, Cambridge, 1957.
3. Schwarzenbach, G., see Fairbrother, F., Proc. Int. Conf. on Coord. Chem., Amsterdam, 1955.
4. Ahrland, S., Chatt, J., and Davies, N.R., Quart. Revs., 1958, XII, 265.
5. Nuttall, R.H., Roberts, E.R., and Sharp, D.W.A., J.C.S., 1962, 2854.
6. Sharp, D.W.A. and Sharpe, A.G., J.C.S., 1956, 1855, 1858.
7. Booth, G., Advances in Inorganic Chemistry and Radiochemistry, 1964, 6, 1.
8. Pauling, L., J. Amer. Chem. Soc., 1931, 53, 1367.
9. Chatt, J., J.C.S., 1952, 4300.
10. Nyholm, R.S., J.C.S., 1951, 3245.  
idem, ibid, 1951, 2602.  
idem, ibid, 1950, 2061.
11. Arbuzov, A.E., and Zoroastreva, V., Dokl. Acad. Nauk S.S.S.R., 1952, 84, 503.
12. Idem, Izv. Akad. Nauk S.S.S.R., Otd. Khim. Nauk, 1952, 809, 818, 826.  
Idem, Chem. Abs., 1953, 47, 9898h.
13. Verkade, J.G., and Reynolds, L.T., J. Org. Chem., 1960, 25, 683.

14. Verkade, J.G., McCarley, R.E., Hendricker, D.G.,  
and King, Roy W., Inorg. Chem.,  
1965, 4, 228.
15. Verkade, J.G., and Piper, T.S., Inorg. Chem.,  
1963, 2, 944.
16. idem, ibid, 1962, 1, 453.
17. Cotton, F.A. and Goodgame, D.M.L., J.C.S., 1960, 5267.
18. Brown, H.C., J. Amer. Chem. Soc., 1945, 67, 503.
19. Baillie, M.J.B., Thesis, Glasgow, 1965.
20. Baillie, M.J.B., Brown, D.H., Moss, K.C. and  
Sharp, D.W.A., Chem. Comm.,  
1965, 5, 921.
21. Harrah, L.A., Ryan, M.T. and Tamborski;  
Spectrochim. Acta, 1962, 18, 21.
22. Taylor, A.M., Trans. Far. Soc., 1929, 25, 856.
23. Schaeffer, C. and Schubert, M., Ann. Physik,  
1916, 50, 283.
24. Idem, Z. Physik, 1921, 7, 297.
25. Miller, F.A. and Wilkins, C.H., Anal. Chem.,  
1952, 25, 1253.
26. Goubeau, J. Z. Physik. Chem. (Leipzig), 1937, B36, 45.
27. Woodward, L.A., Trans. Far. Soc., 1958, 54, 1271.
28. Herzberg, G., Infrared and Raman Spectra of  
Polyatomic Molecules,  
Van Nostrand, New York, 1945.
29. Hathaway, B.J. and Underhill, A.E., J.C.S., 1961, 3091.
30. Goubeau J. and Beus, W., Z. anorg. Chem., 1952, 268, 221.
31. Greenwood, W.N., J.C.S., 1959, 3811.

32. Landolt-Bornstein, "Zahlenwerte und Funktion", Springer-Verlag, Berlin 1951, I Band, 2-Teil, Molekeln, p. 152, 259.
33. Lide, D.R. and Mann, D.E., J. Chem. Phys., 1956, 25, 1128.
34. Nakamoto, K., Fujita, J. and Kobayashi, M., J. Amer. Chem. Soc., 1957, 79, 4904.
35. Perkins, W.D. and Wilson, M.K., J. Chem. Phys., 1952, 20, 1792.
36. Clark, R.J.H. and Williams, C.S., Inorg. Chem., 1965, 4, 350.
37. Wickenden, A.E. and Krause, R.A., Inorg. Chem., 1965, 4, 404.
38. Hathaway, B.J. and Webster, D.E., Proc. Chem. Soc., 1963, 14.
39. Clark, H.C. and O'Brien, R.J., Inorg. Chem., 1963, 2, 1020.
40. Malatesta, L., and Cariello, J.C.S., 1958, 2323.
41. McAvoy, J., Moss, K.C. and Sharp, D.W.A., J.C.S., 1965, 1376.
42. Heck, R.F., J. Amer. Chem. Soc., 1963, 85, 1220.
43. Huttemann, T.J. Jr., Foxman, B.M., Sperati, C.R. and Verkade, J.G., Inorg. Chem., 1965, 4, 950.
44. Brown, H.C. and Sujishi, S., J. Amer. Chem. Soc., 1948, 70, 2878.
45. Graham, W.A.G. and Stone, F.G.A., J. Inorg. Nucl. Chem., 1956, 3, 164.
46. Coates, G.E. and Whitcombe, R.A., J.C.S., 1956, 3351.

47. Meddings, B. and Burkin, A.R., J.C.S., 1956, 1115.
48. Arhland, S., Chatt, J., Davies, N.R., and Williams, A.A., J.C.S., 1958, 276.
49. Idem, ibid, 1958, 1403.
50. Bailar, J.C. and Busch, D.H., "Chemistry of the Coordination Compounds", Reinhold. Pub. Co., New York, N.Y. 1956.
51. Chatt, J. and Gamlen, G.A., J.C.S., 1956, 2371.
52. Fairbrother, F., Robinson, D. and Taylor, J.B., J.C.S., 1958, 2074.
53. Mann, F.G. and Watson, H.R., J.C.S., 1958, 2772.
54. Hatfield, W.E. and Yoke, J.T., Inorg. Chem., 1962, 1, 463.
55. Bellamy, L.J., "The Infrared Spectra of Complex Molecules", Methuen and Co. Ltd., London, 1958.